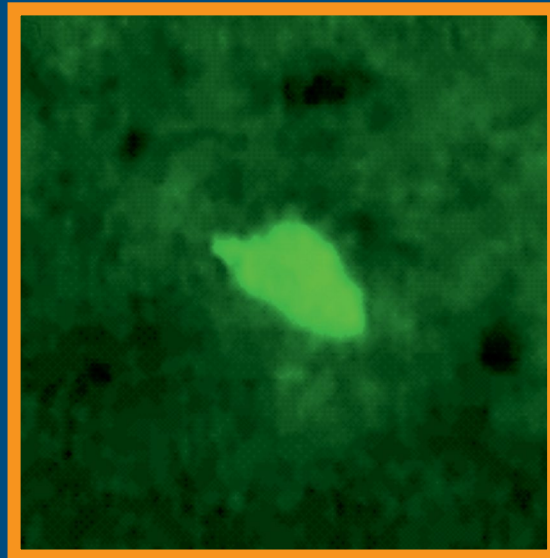


Folia Histochemica et Cytobiologica

Scientific quarterly devoted to problems of histochemistry,
cytochemistry and cell & tissue biology

www.fhc.viamedica.pl



Vol. 57

No. 2

2019

ISSN 0239-8508



VIA MEDICA

Folia Histochemica et Cytobiologica

Scientific quarterly devoted to problems of histochemistry,
cytochemistry and cell & tissue biology

www.fhc.viamedica.pl

EDITOR-IN CHIEF:

Z. Kmiec (Gdansk, Poland)

EDITORS:

M. Piasecka (Szczecin, Poland)

M.Z. Ratajczak (Louisville, USA)

J. Thekkiniath (New Haven, USA)

EDITORIAL BOARD:

C.E. Alpers (Seattle, USA)

B. Bilinska (Cracow, Poland)

I.-D. Caruntu (Iassi, Romania)

M. Dietel (Berlin, Germany)

P. Dziegiel (Wroclaw, Poland)

T. Fujimoto (Nagoya, Japan)

J. Kawiak (Warsaw, Poland)

J.Z. Kubiak (Rennes, France)

J.A. Litwin (Cracow, Poland)

C. Lucini (Naples, Italy)

A. Lukaszuk (Poznan, Poland)

Z. Mackiewicz (Vilnius, Lithuania)

A. Mazur (Clermont-Ferrand, France)

I. Petersen (Jena, Germany)

A.T. Slominski (Memphis, USA)

C.J.F. van Noordan (Amsterdam, Netherlands)

Y. Wegrowski (Reims, France)

S. Wolczynski (Bialystok, Poland)

M. Zabel (Poznan, Poland)

V. Zinchuk (Kochi, Japan)

M. J. Zeromski (Poznan, Poland)

M.A. Zmijewski (Gdansk, Poland)

MANAGING EDITOR:

C. Kobierzycki (Wroclaw, Poland)

PUBLISHER EDITOR:

I. Hallmann (Gdansk, Poland)

EDITORIAL OFFICE:

Department of Histology

Medical University of Gdansk

Debinki St. 1, 80–210 Gdansk, Poland

tel.: + 48 58 349 14 37

fax: + 48 58 349 14 19

e-mail: zkmiec@gumed.edu.pl

<http://www.fhc.viamedica.pl>

Folia Histochemica et Cytobiologica (pISSN 0239–8508, eISSN 1897–5631) is published quarterly, one volume a year, by the Polish Society for Histochemistry and Cytochemistry at VM Media sp. z.o.o VM Group sp.k., Gdansk.

Indexed in: Index Medicus/MEDLINE, Excerpta Medica/EMBASE, Chemical Abstracts/CAS, SCI Expanded, SciSearch, Biochemistry & Biophysics Citation Index, ISI Alerting Services, Biosis Previews Index Copernicus, Biological Abstracts, SCOPUS, Research Alert, ProQuest, EBSCO, DOAJ, Ulrich's Periodicals Directory.

POLISH SOCIETY FOR HISTOCHEMISTRY AND CYTOCHEMISTRY STATEMENT OF FOLIA HISTOCHEMICA ET CYTOBIOLOGICA EDITORIAL POLICY

Folia Histochemica et Cytobiologica is an international, English-language journal devoted to the rapidly developing fields of histochemistry, cytochemistry, cell and tissue biology.

The Folia Histochemica et Cytobiologica publishes papers that meet the needs and intellectual interests of medical professionals, basic scientists, college and university teachers and students. Prospective authors should read most recent issues of FHC to determine the appropriateness of a possible contribution. However, such an examination does not provide an infallible guide because editorial policy is always under review. Technical correctness is necessary, but it is not the only condition for acceptance. Clarity of exposition and potential interest of the readers are important considerations; it is the reader, not the author, who must receive the benefit of the doubt.

Folia Histochemica et Cytobiologica publishes review articles, original articles, short communications and proceedings of scientific congresses/symposia. Fields of particular interests include development and application of modern techniques in histochemistry and cell biology, cell biology and pathology, cell-microenvironment interactions, tissue organization and pathology.

Manuscripts announcing new theoretical or experimental results, or manuscripts questioning well-established and successful theories, are highly desirable and are a subject for evaluation by specialists. Manuscripts describing original research that clarifies past misunderstandings or allows a broader view of a subject are acceptable. Manuscripts that demonstrate new relations between apparently unrelated areas of fields of interests are appropriate. Manuscripts that show new ways of understanding, demonstrating, or deriving familiar results are also acceptable. Such manuscripts must provide some original cytobiological insight and not just a clever derivation.

Regularly, review or tutorial articles are published, often of a length greater than that of the average article. Most of these articles are a subject of a review; authors planning such articles are asked to consult with the editors at an early stage.

Most readers of a particular article will be specialists in the subject matter presented; the context within which the paper is presented should be established in the order given in Instructions for Authors. Manuscripts must be technically correct and must take proper cognizance of previous work on the same subject regardless of where it may have appeared. Such referencing is especially important for reminders of once well known ideas, proofs, or techniques that may have again become useful to readers. It is the responsibility of the author to provide adequate references; editors and referees will not do the literature search that should have been done by the authors. The references are a matter of review though.

Contributions considered include: Regular Articles (Papers), Short Communications, Review Articles, Conference Proceeding, Book Reviews and Technical Notes, which describe new laboratory methods or substantial improvements of the existing techniques. Regular articles should be about five journal pages or less in length. Short communications are usually confined to the discussion of a single concept and should be about two journal pages in length. Review articles are confined to a broad discussion and should contain the most recent knowledge about the subject.

Instructions concerning the preparation of manuscripts are given in the Information for Authors. Care in following those instructions will permit editors and referees to devote more time to thoughtful evaluation of contributions and will ultimately lead to a better, more interesting Journal.

Copying information, in part or in whole by any means is prohibited without a written permission from the owner.

SUBSCRIPTION

Folia Histochemica et Cytobiologica is available for paper subscription (print on demand).

To read and download articles for free as pdf document, visit <http://czasopisma.viamedica.pl/fhc>

Publisher: VM Media sp. z o.o. VM Group sp.k., Swietokrzyska St. 73, 80–180 Gdansk, <http://www.viamedica.pl>, wap.viamedica.pl

Illustration on the cover: *Gallbladder interstitial Cajal-like cells and gallbladder contractility in patients with cholelithiasis: a prospective study* (see: Runyu Ding *et al.*, pp. 94–100)

Legal note: <http://czasopisma.viamedica.pl/fhc/about/legalNote>

© Polish Society for Histochemistry and Cytochemistry



18-0228.002.001

Folia Histochemica et Cytobiologica

Scientific quarterly devoted to problems of histochemistry,
cytochemistry and cell & tissue biology
www.fhc.viamedica.pl

Vol. 57
No. 2
2019

Official Journal of the Polish Society for Histochemistry and Cytochemistry

REVIEW

**MPP1-based mechanism of resting state raft organization in the plasma membrane.
Is it a general or specialized mechanism in erythroid cells?**

Magdalena Trybus, Lukasz Niemiec, Agnieszka Biernatowska,
Anita Hryniewicz-Jankowska, Aleksander F. Sikorski 43

ORIGINAL PAPERS

L1-ORF1p and Ago2 are involved in a siRNA-mediated regulation for promoter activity of L1-5'UTR

Liu Shi, Huanhuan Shi, Liangliang Lou, Xiaoning Yuan, Yunfeng Zhu 56

The miR-1204 regulates apoptosis in NSCLC cells by targeting DEK

Zhen Qian, Juan Yang, Huanhuan Liu, Yue Yin, Lingling Hou, Honggang Hu 64

The immunoreactivity of TGF- β 1 in non-alcoholic fatty liver disease

Radoslaw Kempinski, Katarzyna Neubauer, Elzbieta Poniewierka, Maciej Kaczorowski, Agnieszka Halon 74

WNT5A gene and protein expression in endometrial cancer

Tomasz Wasniewski, Jacek Kiezun, Bartłomiej E. Krazinski Anna E. Kowalczyk,
Blazej Szostak, Piotr M. Wierzbicki, Jolanta Kiewisz 84

**Gallbladder interstitial Cajal-like cells and gallbladder contractility in patients with cholelithiasis:
a prospective study**

Runyu Ding, Junmin Wei, Jingyong Xu 94

MPP1-based mechanism of resting state raft organization in the plasma membrane. Is it a general or specialized mechanism in erythroid cells?

Magdalena Trybus, Lukasz Niemiec, Agnieszka Biernatowska,
Anita Hryniewicz-Jankowska, Aleksander F. Sikorski

Department of Cytochemistry, Faculty of Biotechnology, University of Wrocław

Abstract

Biological membranes are organized in various microdomains, one of the best known being called membrane rafts. The major function of these is thought to organize signaling partners into functional complexes. An important protein found in membrane raft microdomains of erythroid and other blood cells is MPP1 (membrane palmitoylated protein 1)/p55. MPP1 (p55) belongs to the MAGUK (membrane-associated guanylate kinase homolog) family and it is a major target of palmitoylation in the red blood cells (RBCs) membrane. The well-known function of this protein is to participate in formation of the junctional complex of the erythrocyte membrane skeleton. However, its function as a “raft organizer” is not well understood. In this review we focus on recent reports concerning MPP1 participation in membrane rafts organization in erythroid cells, including its role in signal transduction. Currently it is not known whether MPP1 could have a similar role in cell types other than erythroid lineage. We present also preliminary data regarding the expression level of *MPP1* gene in several non-erythroid cell lines. (*Folia Histochemica et Cytobiologica* 2019, Vol. 57, No. 2, 43–55)

Key words: membrane palmitoylated protein 1 (MPP1); resting state rafts; lateral membrane organization; raft-associated proteins

Introduction

The red cell membrane comprises a lipid bilayer with integral membrane proteins embedded in it and a membrane skeleton. During its 120 days life in the circulation the red blood cell undergoes cyclic mechanical shear and deforming stresses in the blood stream, in particular during passages through capillary vessels, which often are four times smaller in diameter than the larger diameter of the erythrocyte. As the lipid bilayer is essentially devoid of extensibility and mechanical resistance (but characterized by high linear elasticity), which results in rapid vesiculation under even mild shear stress, an essential role in

maintaining erythrocyte membrane mechanical properties plays membrane skeleton, whose structure and function have been a subject of many studies and reviews [1–3]. The erythrocyte membrane bilayer is not homogeneous; it is characterized by relatively high cholesterol content (> 20% lipids by weight) and a set of lipids including sphingolipids (sphingomyelin (SM) and glycolipids) which participate in the generation of membrane lateral heterogeneity by forming domains among which lipid or membrane rafts have been attracting the attention of many laboratories. Literature up to 2014 was surveyed in the previous review [4]. The question remains whether membrane rafts are functional or just remnants of the early stages of nucleated cells. Despite several years of research, there is no great progress towards answering this question. For example, as was mentioned previously [4] there have been several raft-dependent signaling pathways found in red blood cells, e.g. Gs α -protein coupled β -adrenergic receptors cAMP-kinase A leading to the phosphorylation of adducin [5, 6]. Still the

Correspondence address: Aleksander F. Sikorski, Professor
Department of Cytochemistry,
Faculty of Biotechnology,
University of Wrocław,
F. Joliot-Curie 14a, 50–383 Wrocław, Poland
e-mail: aleksander.sikorski@uwr.edu.pl

erythrocyte membrane remains an interesting object of the study of lateral membrane organization and its function. An example of interesting studies concerns binding of amyloid beta by erythrocyte membrane and its connection with Alzheimer's disease. A fluorescence correlation spectroscopy (FCS)-based study [7] revealed that fluorescently labeled amyloid peptide (A β 1-42) localizes to erythrocyte membrane nanodomains which were suggested to be caveolin-rich.

Due to its relative simplicity, erythrocyte membrane still remains a very attractive object to study lateral membrane heterogeneity, *i.e.* organization of nanodomains. Despite long-term studies we still do not know the molecular mechanisms of how they are organized or even an apparently simpler question, *i.e.* whether we are dealing with single or multiple kinds of domains in this simple membrane. This issue was addressed by Leonard *et al.* [8], who *via* Laurdan-general polarization (GP) studies detected separate nanodomains enriched in SM present in the red blood cell membrane regions of low curvature and cholesterol enriched in the regions of high curvature. Our studies described below focused on one possible mechanism of lateral membrane organization regulation in which peripheral membrane palmitoylated protein 1 (MPP1) was found to play a crucial role, so the considerations presented below concern presentation of the model of this mechanism and address the question of how specific the presented mechanism is, and whether it operates only in blood/erythroid cells or is common in mammals.

Membrane raft concept

Spatiotemporal organization of biological membranes is characterized by dynamic lateral heterogeneity, as proven by many biophysical and biochemical observations. One of the best known and most acknowledged forms of this heterogeneity is the existence of lateral subcompartments, called membrane rafts (lipid rafts) — a concept formulated by Simons and Ikonen in 1997 [9] which has been the subject of detailed current reviews [10–12].

The basic assemblies, which for clarity in this text will be called resting state rafts, are domains which are highly dynamic ($t_{1/2} \sim 1$ s and ~ 20 nm in diameter), formed by lo phase lipid and a set of characteristic proteins some of which are permanent residents of these domains (*e.g.* stomatin and flotillins) while other are temporarily associated with these domains (*e.g.* growth factor receptors, H-Ras protein, GPI-anchored proteins), which is connected with their activation or resting state. The lipid component of vertebrate cell membrane rafts, enriched

in sphingolipids and cholesterol together with other membrane phospholipids which contain long-chain, mostly saturated alkyl residues, is in the so-called liquid ordered phase. Although the molecular basis of lateral phase separation in model membranes seems relatively well understood, available data concerning biological mechanism(s) controlling Ld (liquid disordered) — (liquid ordered) phase separation and formation of rafts in natural membranes are rather scarce and permit only general hypotheses. Lateral interactions of cholesterol with membrane raft-specific lipids seem to be crucial for maintaining these microdomains in the 'lo', liquid-ordered state, which is characterized by decreased conformational (trans-gauche) freedom and, consequently, reduced "fluidity", compared to the bulk, containing less cholesterol, membrane, which exists in the 'ld' (liquid disordered) state. However, unlike the gel phase in artificial lipid systems they are characterized by similar (within the same range) lateral (translational) mobility to the lo membrane phase, as was measured by FRAP technique on plasma membranes [13–15].

The detergent-resistant membrane (DRM) fraction is defined as a low-density, insoluble in cold non-ionic detergent solution membrane fraction floating at 5/30% sucrose step gradient. It was suggested to be useful in assigning potential raft association when changes in the composition are induced by physiologically meaningful events. However, it is possible that DRMs may represent an artificial coalescence of raft proteins and lipids into a residue that does not exist in living cells. Therefore, although there is no simple relationship between DRM and membrane rafts, DRM isolation and characterization is still considered a useful tool, providing some insight into their lateral organization [16, 17].

The molecular basis of Chol:SM complex formation is the hydrogen bond between the amide group of sphingolipid and the hydroxyl group of cholesterol and also the interaction of cholesterol with saturated alkyl chains. Cholesterol is thought to interact with saturated long alkyl chains of other phospholipids. It should be noted that data on lipidomics of the DRMs reveal that, in addition to the abundance of sphingolipids (mostly sphingomyelin), cholesterol and glycolipids, they contain other phospholipids, including some species of PE and PS that mostly contain fully saturated or monounsaturated acyl chains. Predominant among these are the phosphatidylethanolamine glycerophospholipids and plasmalogens [18]. Phosphatidylserine, which is a relatively minor membrane component, is three times more prevalent in the DRM than in the bulk volume of the plasma membrane, while phosphatidylinositols are rather diminished

within the DRM, as are phosphatidylcholine species. PEs occur in the membrane predominantly as sn-1 saturated, sn-2 unsaturated glycerophospholipids, and experimental data show that some DRM preparations are enriched in 1-stearoyl-2-linoleoyl-sn-glycero-3-phosphoethanolamine (SLPE), regardless of the method of isolation [18]. Our own data indicate that this PE interacts with cholesterol comparably to SM, while dipalmitoyl-PE does not bind cholesterol [19]. This suggests the importance of the structure of acyl chains of particular phospholipids (not all of which are saturated) and also explains the background of the mechanism by which inner-layer phospholipids participate in membrane rafts.

Membrane rafts contain several specific sets of membrane proteins [20], which include membrane proteins belonging to the SPFH family (stomatin/prohibitin/flotillin/HflK), such as raft scaffold proteins flotillin-1 and -2, and stomatin or stomatin-like protein. These proteins share a common feature in that they associate with raft domains, possibly through cholesterol binding or oligomerization [21]. Apart from these proteins, and other palmitoylated and transmembrane proteins, membrane rafts also include GPI-anchored proteins and integral and peripheral proteins involved in signal transduction.

Many of the raft proteins are modified with saturated acyl (palmitoyl) chains, or with cholesterol, which is thought to facilitate interactions with lo-domains [22]. The mechanism(s) by which the proteins partition into membrane rafts may involve preferred solubility in the ordered domains and/or chemical affinity for raft lipids, as exemplified by the above-mentioned cholesterol-binding properties of some of the proteins [23]. Other examples include a structural protein motif recognizing sphingolipids or specific glycolipids such as ganglioside [24].

It has long been known that rafts are engaged in cellular signal transmission pathways by hosting a number of receptors and their associated adapter proteins, and also facilitate signaling switches during activation of the respective pathways. These proteins include receptor tyrosine kinases (EGF-R, IGF-1 receptor), non-receptor kinases (*e.g.* src kinases: Src, Lck, Hck, Fyn, Blk, Lyn, Fgr, Yes, and Yrk [25]), serpentine (G-protein-linked seven transmembrane domain) receptors [26], sigma receptors [27] and the growth factor receptor c-kit, as well as heterotrimeric and monomeric G-proteins and other adaptor proteins. Also endothelial nitric oxide synthase, hedgehog protein and pro- or anti-apoptotic signaling elements have been found in raft domains, as was reviewed [28]. Of particular interest are the potential roles of membrane rafts as signaling platforms in neoplasia

[29] and their possible use as targets for anticancer drugs [28].

The catalogue of physiological functions of rafts involves several important biological processes, and some of them have been shortly described below.

1. Immune signaling involving several innate and adaptive immune responses. These processes have been studied for more than 20 years, beginning with the discovery of involvement of rafts in IgE signaling [30]. Many components of the immune reactions such as Fc ϵ R1, T cell receptor and B cell receptor move from non-raft (detergent sensitive membrane) to the raft (DRM) upon activation. The DRM fraction was also found to be enriched in signal transduction machinery which includes LCK and FYN kinases and LAT protein and also GPI anchored proteins such as CD14 or THY1 (CD90) [31]. Formation of the so-called immune synapse is considered an example of a “raft signaling platform”, a relatively stable structure in diameter in the micrometer range.
2. Host-pathogen interactions. For example, the raft domain is suggested to be a site for HIV budding, binding [32] and stabilization of rafts by cholera toxin (Ctx) and Shiga toxin (Stx) [33, 34]. Also VacA, a vacuolating toxin of *H. pylori*, predominantly associates with the raft phase; however, this binding was found to be independent of oligomerization and pore-forming activity [10, 35]. For example, an interesting observation was published recently indicating that *H. pylori* expression of the *cgt* gene encoding cholesterol- α -glucosyltransferase reduces cholesterol levels in infected gastric epithelial cells, which disrupts membrane rafts, blocking in turn IFN γ signaling, allowing bacteria to escape the host inflammatory response [36].
3. In cancer cells, as mentioned above, a considerable number of receptors and adapter proteins involved in signaling pathways engaged in proliferation were found in the DRM fraction, suggesting the crucial role of these structures for signaling of these aberrant cells' development. The literature reviewing various aspects of this subject is particularly rich [27–29]. Some of the signaling pathways and processes could become a target for cancer treatment by using raft domain disrupting agents, as was reviewed previously [28].
4. Involvement in other pathologies. In atherosclerosis, transition of macrophages into foam cells following uptake of ox-LDL is raft dependent as ox-LDL receptors localize to raft domains [37, 38]. Other data [39] suggest that lipid-free apoA-I mediates beneficial effects through attenuation of immune cell membrane raft cholesterol content,

which affects numerous types of signal transduction pathways that rely on microdomain integrity for assembly and activation. On the other hand, it was found [40] that 7-dehydrocholesterol, but not cholesterol or other sterols, promotes lipid raft/caveolae formation, leading to suppression of canonical TGF- β signaling and atherogenesis.

An important and mostly unresolved question is how the raft domains are organized. In a sense, it predominantly concerns domains corresponding to “resting state rafts” defined by Hancock [41], *i.e.* functional, more stable domains, > 20 nm in diameter. The model proposed by Hancock assumes that in cell membranes the smallest nanocomplexes of the so-called membrane rafts precursors, which are built of several protein molecules and lipids, are unstable structures and they disintegrate in milliseconds, but when they are connected in larger structures of approximately 20 nm, they become more stable and functional microdomains and so-called ‘resting rafts’ [42]. These microdomains can be further associated in structures through protein-protein [43] and protein-lipid interactions with a diameter larger than 100 nm, called signaling platforms. In their stabilization, the membrane or cell skeleton is involved. Recent hypotheses concerning membrane raft organization/regulation presented in several reviews [10, 41, 44, 45] include:

1. Lipid–lipid interactions, which include preferential cholesterol binding with sphingolipids [46] and possibly other lipids such as gangliosides [47] or saturated/di- or more unsaturated amino phospholipids [19];
2. Lipid–protein interactions, such as proteins modified by cholesterol [48], *e.g.* PSD95 [49], MPP1 [4] discussed herein, or by sphingolipid-binding [50] motifs. There are even suggestions that proteins which are secreted from the cells binding α 2-3-sialyllactose common in the glycans of monosialogangliosides regulate lateral membrane organization. According to Dalton *et al.* [51], soluble klotho binding of gangliosides reduces the propensity of membrane to form large ordered domains for endocytosis, which downregulates PI3K signaling.
3. We should add protein-protein interactions, an example of which is MPP1-flotillins and/or possibly other raft residing proteins such as ABCC4 reported recently by Pitre *et al.* [52];
4. Hydrophobic match or mismatch; it is hypothetically possible that integral proteins of longer transmembrane domain (TMD) would segregate into lipid domains containing longer fatty acid chains. A solidifying effect of transmembrane

peptides of longer TMD and a liquifying effect of shorter TMD peptides were reported previously by Killian *et al.* [53];

5. Actin-skeleton-driven mechanisms. Cortical actin skeleton is widely considered to affect lateral membrane organization since it has been shown to affect molecular diffusion (hop and trapped diffusion) and supramolecular arrangements in the membrane [54, 55]. Stabilization of nanometer sized domains by an actin filament meshwork was suggested by several groups [56, 57]. Also an interesting approach is a technique of giant plasma membrane vesicles (GPMVs) which provides a model of membrane devoid of membrane/or cortical actin skeleton. This membrane shows phase separation at the micrometer scale [58–60]. Also in the case of erythroid cells liquid-liquid phase separation in the plasma membrane devoid of spectrin-actin skeleton either *via* extraction with alkaline solution or treatment with latrunculin takes place [61], which somewhat contradicts the statements presented at the beginning of this paragraph. Certainly, keeping the raft domain small (~20 nm) in most of the resting state cells may be connected with the presence of membrane/cortical actin skeleton, which might be in agreement with the picket-fence model.

In general, involvement of single or multiple protein-protein and or protein-lipid interactions in the organization and regulation of membrane rafts would imply the possibility of regulation at the cellular and/or tissue level. Knowledge of such interactions and their regulation may lead to understanding the molecular mechanism of raft domain organization and regulation and, moreover, may provide ways for manipulation of such processes which would be useful in therapeutic approaches. At this moment, the number of possible proteins engaged in the process of raft domain organization is limited and in the PubMed database we can find only about 6–7 proteins/genes which are suspected to be involved in “flat” (non-caveolae) raft domain organization. These are flotillin-1 and -2, annexin A2, C-type lectin domain family 2 member (Clec2i), epithelial membrane protein-2 (Emp2), Pacsin2 (protein kinase C and casein kinase substrate in neurons 2), raftlin (Rftn1) and calpactin (S100a10).

Membrane palmitoylated protein 1

Our previous studies [61] on red blood cell rafts led us to the hypothesis that MPP1 and its palmitoylation play a crucial role in lateral membrane organization in erythroid cells. Membrane palmitoylated



Figure 1. Domain structure of the membrane palmitoylated protein 1 (MPP1). PDZ — postsynaptic density-95 /discs large/zonula occludens-1 domain; SH3 — src Homology 3 Domain; D5 — domain contains the binding site for the FERM domain of protein 4.1R; GUK — catalytically inactive guanylate kinase (GuK) domain. Based on data presented in [61, 66].

protein 1 (MPP1/p55) encoded by the *MPP1* gene belongs to the MAGUK family (membrane associated guanylate kinase homologs) [62, 63]. MPP1 (p55), a MAGUK family member, was first cloned by Ruff *et al.* [64] and identified as a major target of palmitoylation in red blood cell membrane. It partially fulfills the criteria for scaffolding protein, in that it contains several functional domains which are potentially responsible for simultaneous binding of regulatory and skeletal proteins and is, therefore, an important protein of the membrane skeleton ternary complex (for review see Machnicka *et al.* [1]). MPP1 shares single GUK, SH3 and PDZ domains and contains a D5/Hook/I3 domain which is responsible for protein 4.1R binding (Fig. 1) [65]. MPP1 has the ability to stabilize mechanical properties of red blood cell membrane by the formation of a tripartite complex with protein 4.1 and glycoporphin C linking the spectrin-based membrane skeleton to the membrane bilayer, which is the best known role of MPP1. In this role, the PDZ domain of MPP1 interacts with the cytoplasmic domain of glycoporphin C, while the central region (D5- domain) is responsible for interaction with protein 4.1R [65, 66]. This interaction markedly strengthens protein 4.1-glycoporphin C binding [67].

MPP1 is involved in resting state raft formation in erythroid cells

The functional role of MPP1 palmitoylation is currently not well understood but it is believed that MPP1 palmitoylation is a crucial event involved in raft formation, which might be linked to pathology [4, 28, 61]. Studies performed on erythroid precursor cell line HEL cells revealed that following inhibition of palmitoylation by treatment with the potent protein acetyltransferase (PAT) inhibitor 2-BrP (2-bromo palmitate), the amount of DRM fraction was markedly decreased. When a stable HEL cell-line with silenced expression of the *MPP1* gene was used for experiments, the same effect was observed. Moreover,

fluorescence lifetime imaging microscopy (FLIM) experiments using di-4 probe performed on normal and 2-BrP-treated HEL cells and HEL cells with stably silenced *MPP1* expression demonstrated a significant decrease in membrane order upon inhibition of palmitoylation, or a decrease in cellular MPP1 level [61, 68]. The key role of MPP1 protein in the lateral membrane organization has also been demonstrated in model systems which are GPMV vesicles derived from living cells. As a model GPMVs were used, obtained from HEL cells (control and MPP1 KnD) [68]. Numerous studies indicate that the biochemical composition of GPMVs to a significant degree represents their original membranes [58, 69] and also reflects the native membrane structure. The results from the research on giant plasma membrane, performed by using several advanced microscopic methods using order-sensing probes, such as C-Laurdan and di-4, showed that, in erythroid cell-membrane derived vesicles, MPP1 plays an important role in maintaining proper order of the membrane [68]. Moreover, the presence of this protein stabilizes the liquid-ordered phase, as observed in the higher miscibility transition temperature of separated vesicles.

In conclusion, changes in membrane fluidity are caused by MPP1, in the absence of major changes in membrane lipid composition, as the fluidity of pure lipids extracted from GPMV membranes remained unchanged and MPP1 recovery in KnD cells leads to the re-establishment of plasma membrane organization [68]. Furthermore, *MPP1* knockdown significantly affects the activation of MAP-kinase signaling *via* raft-dependent tyrosine kinase receptors, indicating the importance of MPP1 for lateral membrane organization [61]. Further studies showed that, in HEL cells with *MPP1* knock-down, the changes in the plasma membrane led to the disruption of signaling cascades from the activated insulin receptor. The signal inhibition occurs at the level of H-Ras, as we did not observe GDP-to-GTP exchange upon insulin treatment [70]. FLIM-FRET microscopy studies revealed impaired interaction of H-Ras with its effector molecule, Raf, in insulin-treated MPP1-knockdowned cells, confirmed by changes in H-Ras lateral diffusion revealed by FRET analysis (Fig. 2). Moreover, in these cells its lateral mobility was not sensitive to insulin treatment. Taken together, our data suggest a relationship between MPP1-dependent plasma-membrane organization and H-Ras activation [70].

MPP1 interacts with different proteins

As mentioned above, MPP1 forms a tripartite complex with the 4.1R protein and glycoporphin C [71, 72]. Pro-

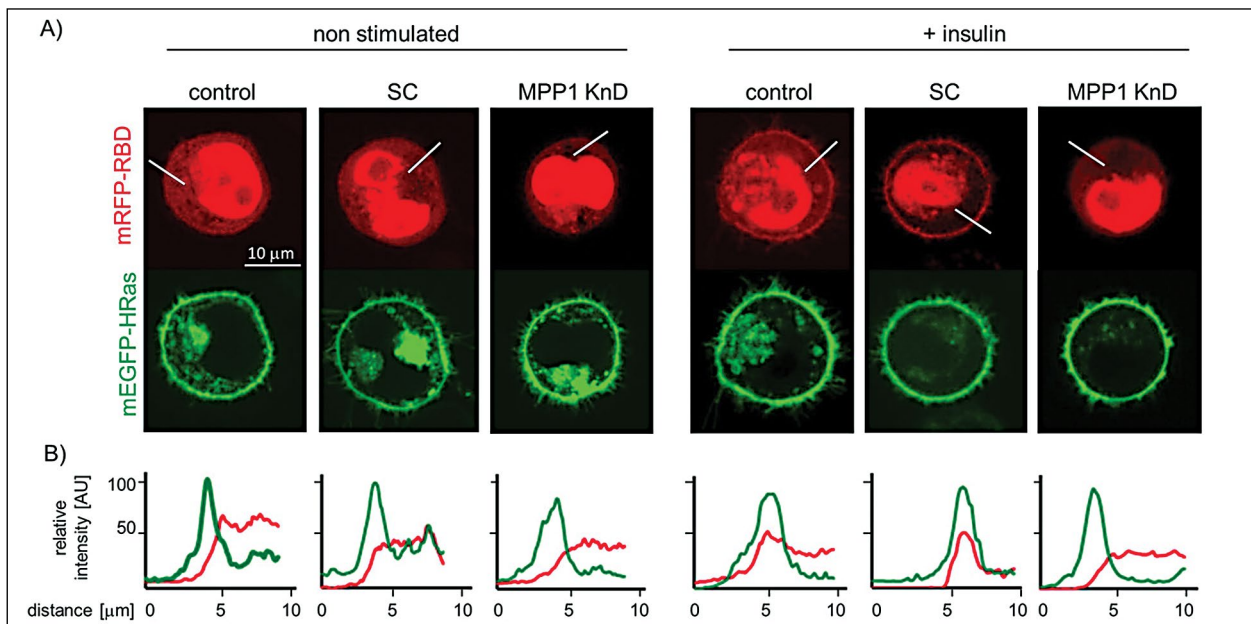


Figure 2. Localization of mEGFP-HRas and mRFP-RBD in non-stimulated and insulin-treated cells. 1×10^6 control, scramble and MPP1 KnD cells were transfected with the appropriate plasmids ($0.5 \mu\text{g}$ each) using CLB (Lonza) electroporation. After 24 hours, cells were serum-starved for 20 hours and transferred onto glass coverslips coated with 0.1 mg/ml poly-L-lysine. Cells were observed in a chamber at 37°C and $5\% \text{ CO}_2$. Photographs were taken before and after addition of insulin [$1 \mu\text{g/ml}$], 5 min after stimulation. **A.** Representative images, scale bar $10 \mu\text{m}$. **B.** Relative fluorescence intensity profiles revealed impaired recruitment of mRFP-RBD (effector molecule) to the plasma membrane by H-Ras in insulin-treated MPP1 KnD cells (+insulin) — right panel. Reproduced from ref. 70, Podkalicka *et al.* 2018 (Creative Commons Attribution 3.0 License).

tein 4.1 of red blood cells (4.1R) is a multifunctional protein that is localized in the membrane skeleton and stabilizes erythrocyte shape and membrane mechanical properties, such as deformability and stability, *via* lateral interactions with spectrin, actin, glycophorin C and protein p55 (See reviews: 1, 2, 73). Evidence that MPP1 interacts with protein 4.1 has been shown in the work of Marfatia *et al.* [72]. Patients with genetic defects resulting in the absence of protein 4.1 (4.1[-] hereditary elliptocytosis) or with defect of glycophorin C (Leach elliptocytosis) also showed absence of MPP1. It indicates that MPP1 is associated, in precise proportions, with the protein 4.1-glycophorin-C complex, linking the skeleton and the membrane. MPP1 contains a binding sequence for the FERM (4.1, ezrin, radixin, moesin) domain of protein 4.1R [74].

Further studies on molecular partners of MPP1 in the erythrocyte membrane by using different methods, such as chemical cross-linking of membrane proteins, co-immunoprecipitation, overlay and solid phase pull-down assays as well as in situ proximity assay, led to the identification of novel interactions of MPP1 and flotillin 1 and flotillin 2 (raft-marker proteins) in the erythrocyte membrane [75]. These interactions

are under further, detailed kinetic exploration in a model system and confirm high affinity of formation of these complexes (Olszewska *et al.* to be published). These interactions were shown to be separate from the above-mentioned well-known protein 4.1-dependent interactions with MPP1 membrane proteins [61]. Flo-tillins are membrane-associated proteins [76] which are functional in different cellular processes, including clustering of membrane receptors, regulation of signaling pathways [77, 78], participation in cell adhesion [79] and interactions with the cytoskeleton [79]. The mechanism underlying their clustering remains unclear.

Furthermore, it is known that MPP1 interacts with Discs large protein P-dlg (DLG5). P-dlg is a protein encoded by the *P dlg* gene and is a human homolog of the *Drosophila dlg* tumor suppressor gene. This protein has three PDZ domains in contrast to MPP1, Dlg-2 and Dlg-3, an SH3 domain and a GUK domain, which are conserved structures in some MAGUK family proteins [80]. Interaction between P-dlg and the GUK domain of MPP1 protein has been confirmed by yeast two-hybrid screening [80]. The C-terminal portion of MPP1 (289–466) has four internal T/S-X-V motifs which may be binding sites for the PDZ domain of P-dlg [80]. It is also interesting that MPP1 is highly

abundant in AML (acute myeloid leukemia) cells, and interacts with the ABC transporter, ABCC4. The studies by Pitre *et al.* [52] showed that the expression of MPP1 highly correlated with *ABCC4* expression in AML, and moreover, it was also associated with poor prognosis for AML patients. The authors carried out an assessment of all PDZ-binding domain proteins on the oligonucleotide microarray with samples from the diagnostic leukemic blasts of 130 pediatric AML patients. They found 81 single PDZ-domain proteins. Analysis (using a correlation with *ABCC4* of > 0.4 as a threshold) led to the identification of 11 single-PDZ domain proteins that fulfilled the criteria. The MPP1 gene met all requirements with both the highest correlation with *ABCC4* ($r = 0.84$) in the studied AML data sets. Further research carried out by this group also showed that the PDZ domain is necessary and sufficient to bind *ABCC4*. Furthermore, MPP1 regulates *ABCC4* plasma membrane location and affects stability of *ABCC4*. Further research of this group indicated that this protein interaction is readily disrupted by a small molecule, antimycin A [52].

The role of MPP1 in non-erythroid cells is understood rather poorly. Mburu *et al.* [81] have shown that MPP1 forms a complex with whirlin, the protein which binds the Usher protein network in the cochlea and the Crumbs network in the retina, by direct association with *USH2A* (usherin) and *VLGR1* (a member of the 7-transmembrane receptor G-protein, which binds calcium and is expressed in the central nervous system). One of the established physiological roles of MPP1 is its involvement in the regulation of neutrophil polarity. A MPP1 knockout (*p55*^{-/-}) mouse model [82] showed that, upon agonist stimulation of neutrophils, MPP1 is rapidly recruited to the leading edge. Neutrophils of knockout mouse do not migrate efficiently *in vitro* and form multiple pseudopods upon chemotactic stimulation, in contrast to normal mouse neutrophils, which form a single pseudopod at the cell front required for efficient chemotaxis. Phosphorylation of Akt is decreased in these cells upon stimulation with chemoattractant, and this appears to be mediated by a *PI3K γ* kinase-independent mechanism [82]. A similar effect was observed in flotillin-1 KO mouse [79], which showed a significant decrease in flotillin 2. Another example is interaction of MPP1 with the FERM domain of NF2 protein. NF2 is a cytoskeletal protein also called merlin, schwannomin or neurofibromin 2 [65]. Neurofibromatosis type 2 (NF2) is a tumor-prone disorder characterized by the development of multiple schwannomas and meningiomas [83]. MPP1-NF2 protein interaction may play a functional role in the regulation of apicobasal polarity and tumor suppression pathways in non-erythroid cells [65].

MPP1 interacts with cholesterol and lipids

It should be noted that there is also a possibility of MPP1-lipid, mainly cholesterol interactions. We used a simple bioinformatics approach to establish whether MPP1 is capable of binding cholesterol. Modeled and experimentally validated fragment structures were mined from online resources and searched for CRAC and CRAC-like motifs. Several of these motifs were found in the primary structure of MPP1, and these were structurally visualized to see whether they localized to the protein surface. Since all of the CRAC and CRAC-like motifs were found at the surface of MPP1 domains, *in silico* docking experiments were performed to assess the possibility of interaction between CRAC motifs and cholesterol. The obtained results show that MPP1 can bind cholesterol *via* CRAC and CRAC-like motifs with moderate to high affinity (K_d in the nano- to micro-molar range). It was also found that palmitoylation-mimicking mutations (C/F or C/M) did not affect the affinity of MPP1 towards cholesterol [84]. Further studies on recombinant MPP1 interactions in simple Langmuir monolayer technique revealed that injection of MPP1 into the subphase of an LB monolayer composed of DOPC/SM/Chol (1:1:1 molar ratio) induced an increase in surface pressure, indicating that MPP1 molecules were incorporated into the lipid monolayer. The compressibility modulus isotherms of MPP1, lipids and lipid-MPP1 films have essentially different shapes from one another. In addition, this interaction was found to be sensitive to the presence of cholesterol in the lipid monolayer, as adding MPP1 to the subphase of lipid monolayers containing cholesterol resulted in a much larger increase in surface area than when MPP1 is injected into the subphase of a lipid monolayer devoid of cholesterol [85]. Moreover, MPP1-bound cholesterol was found to competitively inhibit surface pressure changes of the phospholipid monolayer [86].

MPP1 is the resting state raft organizing protein in erythroid cells

In conclusion, we propose MPP1 to be a main component of the mechanisms responsible for lateral organization of the erythroid cell membrane. The studies presented above indicate a new role for MPP1, and present a novel linkage between membrane raft organization and their function.

The molecular mechanism underlying MPP1's function as a resting state raft organizer remains to be explored. Our hypothesis is that, upon palmitoylation, the affinity of MPP1 for binding to the pre-existing nanocluster membrane increases. As preexisting na-

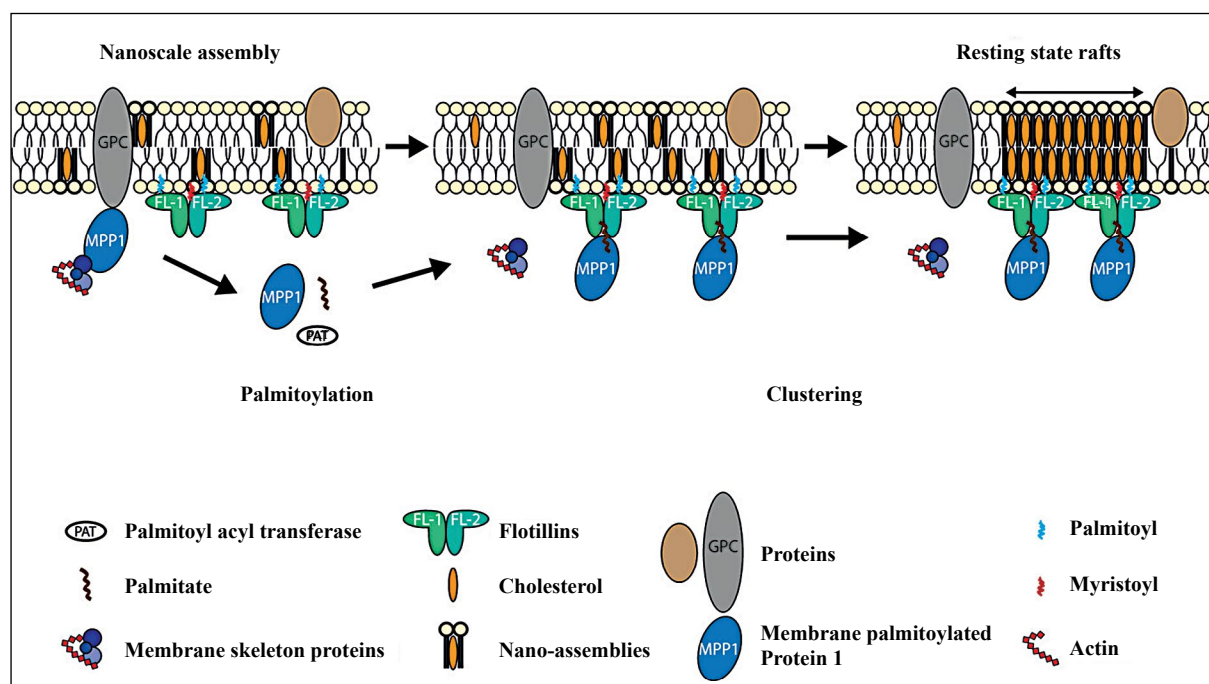


Figure 3. Schematic model of the proposed mechanism of resting state membrane raft organization in erythroid cells. Free MPP1 which is in equilibrium with membrane skeletally associated pool of this protein binds to the pre-existing short-lived flotillins-based nano-assemblies (< 10 nm in diameter, half time < 0.1 ms). This leads to oligomerization and co-assembly of flotillin-based nanoclusters into larger-scale complexes and formation of a more stable (half time ~1 s) larger (> 20 nm) structures called “resting state rafts” in erythroid cell membrane. Modified from Biernatowska *et al.* [75]) (CC BY-NC-ND 4.0).

nanoclusters we consider protein-cholesterol/lipid complexes corresponding to short-lived (half time < 0.1 ms) nanocomplexes (< 10 nm in diameter), described previously by others [87–89]. This suggestion is based on the observations that in HEL cells, upon inhibition of palmitoylation, all MPP1 remains in the high-density “skeletal” fraction within the density-gradient profile of the DRM, and also MPP1 KnD Hel cell membrane is characterized by increased membrane fluidity as measured by FLIM of the D-4 probe. We believe that flotillin-1 and -2 are important components of these nanoclusters, which was confirmed by the fact that flotillins are found in the DRM residual fraction even after treatment with beta methyl cyclodextrin. Binding of palmitoylated MPP1 to the pre-existing nanocomplexes *via* flotillins and perhaps *via* cholesterol-binding regions as was recently documented [75, 84–86] induces their fusion and stabilizes them as membrane resting-state rafts, which are larger (~20 nm) in diameter [90], more stable (~1 s), detergent-resistant, and which become functional (see Fig. 3).

MPP1 is not the raft organizer in most cells in mammalian organisms

As the data on the level of MPP1 protein in the various cell types of the human body are only

fragmentary (*e.g.* <https://www.ncbi.nlm.nih.gov/gene/4354>), we decided to test the presence of MPP1 in several human cell types. First of all we completed screening through blood cells. Cells were isolated from whole blood on the density gradient Ficoll-Paque (density 1.077 g/mL) and then further purified using MicroBeads by Miltenyi Biotec. The level of *MPP1* gene expression in the studied cells was assessed by Western blot analysis and RT-PCR (reverse transcription). Additionally, in some cases the effect of palmitoylation on the formation of DRM fractions was tested on these cells (Table 1). For this purpose, a palmitoylation inhibitor, 2-BrP, was used. The DRM fraction was isolated *via* cold 1% Triton X-100 extraction and ultracentrifugation of the extract on a sucrose step (40/30/5%) gradient. Literature data indicated the presence MPP1 in erythroid cells, mouse granulocytes and several myeloid and lymphoid cell lines. In our experience high expression of *MPP1* could be observed in most blood cells and blood cell-derived neoplastic cell lines. As could be anticipated, a relatively high level of MPP1 could be detected in the platelets as their parental cell has a common precursor with erythrocytes. In the blood cells the amount of DRM fraction protein and cholesterol and first of all the presence of MPP1 in the DRM appeared to be sensitive to inhibition

Table 1. The presence of MPP1 protein or its mRNA in different cell types

Cells/cell line	MPP1 (Western blotting)	MPP1 (rtPCR)	DRM	DRM sensitivity to 2-BrP treatment	Changes of fluorescence life-time of di-4 probe
Erythrocytes	+++	+++ ⁴	+++	+++	+++
HEL	+++	+++	+++	+++	+++
K562	+++	+++	+++	+++	nd
Thrombocytes	+++	+++	nd	nd	nd
Monocytes	+++	+++	nd	nd	nd
Neutrophils	+++	+++	nd	nd	nd
Jurkat T	+++	nd	+++	+++	+++
HL60	+/-	nd	nd	nd	nd
HEK293	++	nd	--	--	nd
MDA-MB-231	+/-	+	-	-	nd
HeLa	-	-	nd	nd	nd
A549	-	-	nd	nd	nd
A375	-	-	nd	nd	nd
SCOV3	-	-	nd	nd	nd
MCF7	-	-	nd	nd	nd
DU145	-	-	nd	nd	nd

⁴Reticulocyte +++ present; - absent; nd — not determined. The localization in DRM fractions and/or sensitivity to 2-BrP treatment are also presented. Cells or cell lines were cultured in standard conditions. For Western blot analyses, cells were dissolved in Laemmli buffer and subjected to SDS-PAGE, transferred onto nitrocellulose filter, blocked with 5% milk proteins and probed with anti-MPP1 rabbit antibodies (Aviva Systems Biology, San Diego, CA, USA) and developed with appropriate secondary antibody conjugated to horseradish peroxidase in a chemiluminescent reaction. Reverse transcriptase (RT) reaction was performed using isolated total RNA (miRNeasy kit QIAGEN, Hilden, Germany) translated into cDNA *via* RT reaction (RevertAid First Strand cDNA Synthesis Kit Thermo Fisher Scientific, Waltham, MA, USA). Primers for MPP1 (Genomed, Warsaw, Poland; FP: CCTACGAGGAAGTCGTTCCGG, RP: GGTCTGGGGCTCAATGTCAA, 340 bp, and for beta-actin Thermo Fisher Scientific; FP: TACAATGAGCTGCGTGTGGCTCCCG, RP: AATGGTATGACCTGGCCTGGCCGTCAGGC, 540 bp) were used.

of palmitoylation with 2-BrP (Table 1) as was the fluidity of the cell membrane *in vivo*, as measured *via* FLIM analysis of the di-4 probe. However, to our surprise, the *MPP1* gene was not expressed to high levels in studied cells of human tumor-derived cell lines apart from HEK293 (human embryonic kidney). In the latter cells an easily detectable signal was observed *via* either RT-PCR or Western blot, although dependence upon palmitoylation of DRM localization of MPP1 could not be observed in the applied experimental conditions. We have to keep in mind that the remaining cell lines are derived from human tumors, so we cannot anticipate with a high degree of certainty that in the case of normal tissues the results would be the same. In the case of blood cells most of the neoplastic cells expressed the *MPP1* gene at a high level, but in some of them (promyelocytic leukemia HL60 or Raji Burkitt's lymphoma) MPP1 could not be detected in Western blot.

The obtained results clearly show that MPP1 is expressed at a negligible level in many types of human cancer epithelial cells, in contrast to cells of erythroid

origin, where the level of their expression is high. The results support the hypothesis that the MPP1 protein is not responsible for the formation and maintenance of membrane rafts in epithelial cells, and this may suggest a different model of formation of these domains than in the erythroid cells.

Conclusions

The data collected by us clearly indicate that MPP1 participates in the resting state membrane rafts' organization and regulation at least in erythroid cells. Summarizing collected information about membrane raft formation and the role of MPP1, we conclude that a network of proteins involving flotillins and flotillin-binding proteins is responsible for bringing lipids closely enough to form small, relatively stable (~1 s) lo phase domains which form resting-state rafts which are functional in the sense of recruiting appropriate activated (or becoming activated after becoming a part of the raft) receptors and other elements of the signaling pathway. It may also facilitate dissociation

of certain elements of the signaling pathway from the raft domain upon their activation, *e.g.* H-Ras dissociating from the raft domain after exchange of GDP for GTP. Effects of *MPP1* knock-out on neutrophil polarization or interaction with ABBC4, which causes a significant increase in cell resistance to chemotherapy, may also be connected with *MPP1*'s resting state raft organizing role.

Our preliminary results indicate that the *MPP1* protein is abundant only in blood cells and their precursors, in other cells such as HEK293 there is a smaller amount of this protein, whereas in breast cancer cells such as MDA-MB-231 we observed only trace amounts of *MPP1*. The data collected by us may suggest that there may be more than one mechanism of the formation of membrane rafts. Our hypothesis assumes that another MAGUK protein or even proteins which do not belong to the MAGUK protein family may perform a similar function as *MPP1*. For example, a similar function was recently suggested for the palmitoylation of Rac1 in COS-7 and MEF cells [91], and these authors implicate a role for the actin cytoskeleton in the mechanism of raft clustering in these cells. Therefore, the answer to the question posed by the title at this stage of research is that the *MPP1*-based molecular mechanism of resting state raft domain organization is a mechanism limited to certain types of cells, and the question of such domain organization in other cells remains open. However, we anticipate that it could be a flotillin-binding protein based mechanism.

References

- Machnicka B, Czogalla A, Hryniewicz-Jankowska A, et al. Spectrins: a structural platform for stabilization and activation of membrane channels, receptors and transporters. *Biochim Biophys Acta*. 2014; 1838(2): 620–634, doi: [10.1016/j.bbame.2013.05.002](https://doi.org/10.1016/j.bbame.2013.05.002), indexed in Pubmed: 23673272.
- Machnicka B, Grochowalska R, Bogusławska DM, et al. Spectrin-based skeleton as an actor in cell signaling. *Cell Mol Life Sci*. 2012; 69(2): 191–201, doi: [10.1007/s00018-011-0804-5](https://doi.org/10.1007/s00018-011-0804-5), indexed in Pubmed: 21877118.
- Lux SE. Anatomy of the red cell membrane skeleton: unanswered questions. *Blood*. 2016; 127(2): 187–199, doi: [10.1182/blood-2014-12-512772](https://doi.org/10.1182/blood-2014-12-512772), indexed in Pubmed: 26537302.
- Sikorski AF, Podkalicka J, Jones W, et al. Membrane rafts in the erythrocyte membrane: a novel role of *MPP1p55*. *Adv Exp Med Biol*. 2015; 842: 61–78, doi: [10.1007/978-3-319-11280-0_5](https://doi.org/10.1007/978-3-319-11280-0_5), indexed in Pubmed: 25408337.
- Koshino I, Takakuwa Y. Disruption of lipid rafts by lidocaine inhibits erythrocyte invasion by *Plasmodium falciparum*. *Exp Parasitol*. 2009; 123(4): 381–383, doi: [10.1016/j.exppara.2009.08.019](https://doi.org/10.1016/j.exppara.2009.08.019), indexed in Pubmed: 19733566.
- Kamata K, Manno S, Ozaki M, et al. Functional evidence for presence of lipid rafts in erythrocyte membranes: Gsalpha in rafts is essential for signal transduction. *Am J Hematol*. 2008; 83(5): 371–375, doi: [10.1002/ajh.21126](https://doi.org/10.1002/ajh.21126), indexed in Pubmed: 18181202.
- Hashimoto M, Hossain S, Katakura M, et al. The binding of Aβ1-42 to lipid rafts of RBC is enhanced by dietary docosahexaenoic acid in rats: Implicates to Alzheimer's disease. *Biochim Biophys Acta*. 2015; 1848(6): 1402–1409, doi: [10.1016/j.bbame.2015.03.008](https://doi.org/10.1016/j.bbame.2015.03.008), indexed in Pubmed: 25782726.
- Leonard C, Conrard L, Guthmann M, et al. Contribution of plasma membrane lipid domains to red blood cell (re) shaping. *Sci Rep*. 2017; 7(1): 4264, doi: [10.1038/s41598-017-04388-z](https://doi.org/10.1038/s41598-017-04388-z).
- Simons K, Ikonen E. Functional rafts in cell membranes. *Nature*. 1997; 387(6633): 569–572, doi: [10.1038/42408](https://doi.org/10.1038/42408), indexed in Pubmed: 9177342.
- Raghunathan K, Kenworthy AK. Dynamic pattern generation in cell membranes: Current insights into membrane organization. *Biochim Biophys Acta Biomembr*. 2018; 1860(10): 2018–2031, doi: [10.1016/j.bbame.2018.05.002](https://doi.org/10.1016/j.bbame.2018.05.002), indexed in Pubmed: 29752898.
- Bieberich E. Sphingolipids and lipid rafts: Novel concepts and methods of analysis. *Chem Phys Lipids*. 2018; 216: 114–131, doi: [10.1016/j.chemphyslip.2018.08.003](https://doi.org/10.1016/j.chemphyslip.2018.08.003), indexed in Pubmed: 30194926.
- Kinoshita M, Suzuki KGN, Murata M, et al. Evidence of lipid rafts based on the partition and dynamic behavior of sphingomyelins. *Chem Phys Lipids*. 2018; 215: 84–95, doi: [10.1016/j.chemphyslip.2018.07.002](https://doi.org/10.1016/j.chemphyslip.2018.07.002), indexed in Pubmed: 30005889.
- Rawat SS, Zimmerman C, Johnson BT, et al. Restricted lateral mobility of plasma membrane CD4 impairs HIV-1 envelope glycoprotein mediated fusion. *Mol Membr Biol*. 2008; 25(1): 83–94, doi: [10.1080/09687680701613713](https://doi.org/10.1080/09687680701613713), indexed in Pubmed: 18097956.
- Pucadyil TJ, Chattopadhyay A. Effect of cholesterol on lateral diffusion of fluorescent lipid probes in native hippocampal membranes. *Chem Phys Lipids*. 2006; 143(1-2): 11–21, doi: [10.1016/j.chemphyslip.2006.04.003](https://doi.org/10.1016/j.chemphyslip.2006.04.003), indexed in Pubmed: 16797513.
- Simons K, Vaz WLC. Model systems, lipid rafts, and cell membranes. *Annu Rev Biophys Biomol Struct*. 2004; 33: 269–295, doi: [10.1146/annurev.biophys.32.110601.141803](https://doi.org/10.1146/annurev.biophys.32.110601.141803), indexed in Pubmed: 15139814.
- Lingwood D, Simons K. Detergent resistance as a tool in membrane research. *Nat Protoc*. 2007; 2(9): 2159–2165, doi: [10.1038/nprot.2007.294](https://doi.org/10.1038/nprot.2007.294), indexed in Pubmed: 17853872.
- Lichtenberg D, Goñi FM, Heerklotz H. Detergent-resistant membranes should not be identified with membrane rafts. *Trends Biochem Sci*. 2005; 30(8): 430–436, doi: [10.1016/j.tibs.2005.06.004](https://doi.org/10.1016/j.tibs.2005.06.004), indexed in Pubmed: 15996869.
- Pike LJ, Han X, Gross RW. Epidermal Growth Factor Receptors Are Localized to Lipid Rafts. *J Biol Chem*. 2005; 280(29): 26796–26804, doi: [10.1074/jbc.M503805200](https://doi.org/10.1074/jbc.M503805200), indexed in Pubmed: 15917253.
- Grzybek M, Kubiak J, Łach A, et al. A raft-associated species of phosphatidylethanolamine interacts with cholesterol comparably to sphingomyelin. A Langmuir-Blodgett monolayer study. *PLoS One*. 2009; 4(3): e5053, doi: [10.1371/journal.pone.0005053](https://doi.org/10.1371/journal.pone.0005053), indexed in Pubmed: 19330037.
- Brown DA, London E. Structure and function of sphingolipid- and cholesterol-rich membrane rafts. *J Biol Chem*. 2000; 275(23): 17221–17224, doi: [10.1074/jbc.R000005200](https://doi.org/10.1074/jbc.R000005200), indexed in Pubmed: 10770957.
- Browman DT, Hoegg MB, Robbins SM. The SPFH domain-containing proteins: more than lipid raft markers. *Trends Cell Biol*. 2007; 17(8): 394–402, doi: [10.1016/j.tcb.2007.06.005](https://doi.org/10.1016/j.tcb.2007.06.005), indexed in Pubmed: 17766116.
- Wang TY, Leventis R, Silvius JR. Fluorescence-based evaluation of the partitioning of lipids and lipidated peptides into

- liquid-ordered lipid microdomains: a model for molecular partitioning into. *Biophys J*. 2000; 79(2): 919–933, doi: [10.1016/S0006-3495\(00\)76347-8](https://doi.org/10.1016/S0006-3495(00)76347-8), indexed in Pubmed: [10920023](https://pubmed.ncbi.nlm.nih.gov/10920023/).
23. Fantini J, Barrantes FJ. How cholesterol interacts with membrane proteins: an exploration of cholesterol-binding sites including CRAC, CARC, and tilted domains. *Front Physiol*. 2013; 4: 31, doi: [10.3389/fphys.2013.00031](https://doi.org/10.3389/fphys.2013.00031), indexed in Pubmed: [23450735](https://pubmed.ncbi.nlm.nih.gov/23450735/).
 24. Mahfoud R, Garmy N, Maresca M, et al. Identification of a common sphingolipid-binding domain in Alzheimer, prion, and HIV-1 proteins. *J Biol Chem*. 2002; 277(13): 11292–11296, doi: [10.1074/jbc.M111679200](https://doi.org/10.1074/jbc.M111679200), indexed in Pubmed: [11792705](https://pubmed.ncbi.nlm.nih.gov/11792705/).
 25. Boggan TJ, Eck MJ. Structure and regulation of Src family kinases. *Oncogene*. 2004; 23(48): 7918–7927, doi: [10.1038/sj.onc.1208081](https://doi.org/10.1038/sj.onc.1208081), indexed in Pubmed: [15489910](https://pubmed.ncbi.nlm.nih.gov/15489910/).
 26. Pike L. Lipid rafts. *Journal of Lipid Research*. 2003; 44(4): 655–667, doi: [10.1194/jlr.r200021-jlr200](https://doi.org/10.1194/jlr.r200021-jlr200).
 27. Aydar E, Palmer CP, Djamgoz MBA. Sigma receptors and cancer: possible involvement of ion channels. *Cancer Res*. 2004; 64(15): 5029–5035, doi: [10.1158/0008-5472.CAN-03-2329](https://doi.org/10.1158/0008-5472.CAN-03-2329), indexed in Pubmed: [15289298](https://pubmed.ncbi.nlm.nih.gov/15289298/).
 28. Hryniewicz-Jankowska A, Augoff K, Biernatowska A, et al. Membrane rafts as a novel target in cancer therapy. *Biochim Biophys Acta*. 2014; 1845(2): 155–165, doi: [10.1016/j.bbcan.2014.01.006](https://doi.org/10.1016/j.bbcan.2014.01.006), indexed in Pubmed: [24480320](https://pubmed.ncbi.nlm.nih.gov/24480320/).
 29. Staubach S, Hanisch FG. Lipid rafts: signaling and sorting platforms of cells and their roles in cancer. *Expert Rev Proteomics*. 2011; 8(2): 263–277, doi: [10.1586/epr.11.2](https://doi.org/10.1586/epr.11.2), indexed in Pubmed: [21501018](https://pubmed.ncbi.nlm.nih.gov/21501018/).
 30. Field KA, Holowka D, Baird B. Fc epsilon RI-mediated recruitment of p53/56lyn to detergent-resistant membrane domains accompanies cellular signaling. *Proc Natl Acad Sci U S A*. 1995; 92(20): 9201–9205, doi: [10.1073/pnas.92.20.9201](https://doi.org/10.1073/pnas.92.20.9201), indexed in Pubmed: [7568101](https://pubmed.ncbi.nlm.nih.gov/7568101/).
 31. Varshney P, Yadav V, Saini N. Lipid rafts in immune signaling: current progress and future perspective. *Immunology*. 2016; 149(1): 13–24, doi: [10.1111/imm.12617](https://doi.org/10.1111/imm.12617), indexed in Pubmed: [27153983](https://pubmed.ncbi.nlm.nih.gov/27153983/).
 32. Dick RA, Goh SL, Feigenson GW, et al. HIV-1 Gag protein can sense the cholesterol and acyl chain environment in model membranes. *Proc Natl Acad Sci U S A*. 2012; 109(46): 18761–18766, doi: [10.1073/pnas.1209408109](https://doi.org/10.1073/pnas.1209408109), indexed in Pubmed: [23010924](https://pubmed.ncbi.nlm.nih.gov/23010924/).
 33. Chinnapen DJF, Chinnapen H, Saslowsky D, et al. Rafting with cholera toxin: endocytosis and trafficking from plasma membrane to ER. *FEMS Microbiol Lett*. 2007; 266(2): 129–137, doi: [10.1111/j.1574-6968.2006.00545.x](https://doi.org/10.1111/j.1574-6968.2006.00545.x), indexed in Pubmed: [17156122](https://pubmed.ncbi.nlm.nih.gov/17156122/).
 34. Sandvig K, Bergan J, Kavaliauskiene S, et al. Lipid requirements for entry of protein toxins into cells. *Prog Lipid Res*. 2014; 54: 1–13, doi: [10.1016/j.plipres.2014.01.001](https://doi.org/10.1016/j.plipres.2014.01.001), indexed in Pubmed: [24462587](https://pubmed.ncbi.nlm.nih.gov/24462587/).
 35. Raghunathan K, Foegeding NJ, Campbell AM, et al. Determinants of Raft Partitioning of the Helicobacter pylori Pore-Forming Toxin VacA. *Infect Immun*. 2018; 86(5), doi: [10.1128/IAI.00872-17](https://doi.org/10.1128/IAI.00872-17), indexed in Pubmed: [29531133](https://pubmed.ncbi.nlm.nih.gov/29531133/).
 36. Morey P, Pfannkuch L, Pang E, et al. Helicobacter pylori Depletes Cholesterol in Gastric Glands to Prevent Interferon Gamma Signaling and Escape the Inflammatory Response. *Gastroenterology*. 2018; 154(5): 1391–1404.e9, doi: [10.1053/j.gastro.2017.12.008](https://doi.org/10.1053/j.gastro.2017.12.008), indexed in Pubmed: [29273450](https://pubmed.ncbi.nlm.nih.gov/29273450/).
 37. Rios FJO, Ferracini M, Pecenin M, et al. Uptake of oxLDL and IL-10 production by macrophages requires PAFR and CD36 recruitment into the same lipid rafts. *PLoS One*. 2013; 8(10): e76893, doi: [10.1371/journal.pone.0076893](https://doi.org/10.1371/journal.pone.0076893), indexed in Pubmed: [24130805](https://pubmed.ncbi.nlm.nih.gov/24130805/).
 38. Rios FJ, Koga MM, Pecenin M, et al. Oxidized LDL induces alternative macrophage phenotype through activation of CD36 and PAFR. *Mediators Inflamm*. 2013; 2013: 198193, doi: [10.1155/2013/198193](https://doi.org/10.1155/2013/198193), indexed in Pubmed: [24062612](https://pubmed.ncbi.nlm.nih.gov/24062612/).
 39. Kaul S, Xu H, Zabalawi M, et al. Lipid-Free Apolipoprotein A-I Reduces Progression of Atherosclerosis by Mobilizing Microdomain Cholesterol and Attenuating the Number of CD131 Expressing Cells: Monitoring Cholesterol Homeostasis Using the Cellular Ester to Total Cholesterol Ratio. *J Am Heart Assoc*. 2016; 5(11), doi: [10.1161/JAHA.116.004401](https://doi.org/10.1161/JAHA.116.004401), indexed in Pubmed: [27821400](https://pubmed.ncbi.nlm.nih.gov/27821400/).
 40. Huang SS, Liu IH, Chen CL, et al. 7-Dehydrocholesterol (7-DHC), But Not Cholesterol, Causes Suppression of Canonical TGF- β Signaling and Is Likely Involved in the Development of Atherosclerotic Cardiovascular Disease (ASCVD). *J Cell Biochem*. 2017; 118(6): 1387–1400, doi: [10.1002/jcb.25797](https://doi.org/10.1002/jcb.25797), indexed in Pubmed: [27862220](https://pubmed.ncbi.nlm.nih.gov/27862220/).
 41. Hancock JF. Lipid rafts: contentious only from simplistic standpoints. *Nat Rev Mol Cell Biol*. 2006; 7(6): 456–462, doi: [10.1038/nrm1925](https://doi.org/10.1038/nrm1925), indexed in Pubmed: [16625153](https://pubmed.ncbi.nlm.nih.gov/16625153/).
 42. Simons K, Gerl MJ. Revitalizing membrane rafts: new tools and insights. *Nat Rev Mol Cell Biol*. 2010; 11(10): 688–699, doi: [10.1038/nrm2977](https://doi.org/10.1038/nrm2977), indexed in Pubmed: [20861879](https://pubmed.ncbi.nlm.nih.gov/20861879/).
 43. Pike LJ. Rafts defined: a report on the Keystone Symposium on Lipid Rafts and Cell Function. *J Lipid Res*. 2006; 47(7): 1597–1598, doi: [10.1194/jlr.E600002-JLR200](https://doi.org/10.1194/jlr.E600002-JLR200), indexed in Pubmed: [16645198](https://pubmed.ncbi.nlm.nih.gov/16645198/).
 44. Sezgin E, Levental I, Mayor S, et al. The mystery of membrane organization: composition, regulation and roles of lipid rafts. *Nat Rev Mol Cell Biol*. 2017; 18(6): 361–374, doi: [10.1038/nrm.2017.16](https://doi.org/10.1038/nrm.2017.16), indexed in Pubmed: [28356571](https://pubmed.ncbi.nlm.nih.gov/28356571/).
 45. Sevsik E, Schütz GJ. With or without rafts? Alternative views on cell membranes. *Bioessays*. 2016; 38(2): 129–139, doi: [10.1002/bies.201500150](https://doi.org/10.1002/bies.201500150), indexed in Pubmed: [26666984](https://pubmed.ncbi.nlm.nih.gov/26666984/).
 46. Ramstedt B, Slotte JP. Interaction of cholesterol with sphingomyelins and acyl-chain-matched phosphatidylcholines: a comparative study of the effect of the chain length. *Biophys J*. 1999; 76(2): 908–915, doi: [10.1016/S0006-3495\(99\)77254-1](https://doi.org/10.1016/S0006-3495(99)77254-1), indexed in Pubmed: [9929492](https://pubmed.ncbi.nlm.nih.gov/9929492/).
 47. Lozano MM, Hovis JS, Moss FR, et al. Dynamic Reorganization and Correlation among Lipid Raft Components. *J Am Chem Soc*. 2016; 138(31): 9996–10001, doi: [10.1021/jacs.6b05540](https://doi.org/10.1021/jacs.6b05540), indexed in Pubmed: [27447959](https://pubmed.ncbi.nlm.nih.gov/27447959/).
 48. Schwarzer R, Levental I, Gramatica A, et al. The cholesterol-binding motif of the HIV-1 glycoprotein gp41 regulates lateral sorting and oligomerization. *Cell Microbiol*. 2014; 16(10): 1565–1581, doi: [10.1111/cmi.12314](https://doi.org/10.1111/cmi.12314), indexed in Pubmed: [24844300](https://pubmed.ncbi.nlm.nih.gov/24844300/).
 49. Tuldzicka K, Diaz-Rohrer BB, Farley MM, et al. Remodeling of the postsynaptic plasma membrane during neural development. *Mol Biol Cell*. 2016; 27(22): 3480–3489, doi: [10.1091/mbc.E16-06-0420](https://doi.org/10.1091/mbc.E16-06-0420), indexed in Pubmed: [27535429](https://pubmed.ncbi.nlm.nih.gov/27535429/).
 50. Contreras FX, Ernst AM, Haberkant P, et al. Molecular recognition of a single sphingolipid species by a protein's transmembrane domain. *Nature*. 2012; 481(7382): 525–529, doi: [10.1038/nature10742](https://doi.org/10.1038/nature10742), indexed in Pubmed: [22230960](https://pubmed.ncbi.nlm.nih.gov/22230960/).
 51. Dalton G, An SW, Al-Juboori SI, et al. Soluble klotho binds monosialoganglioside to regulate membrane microdomains and growth factor signaling. *Proc Natl Acad Sci U S A*. 2017; 114(4): 752–757, doi: [10.1073/pnas.1620301114](https://doi.org/10.1073/pnas.1620301114), indexed in Pubmed: [28069944](https://pubmed.ncbi.nlm.nih.gov/28069944/).

52. Pitre A, Ge Y, Lin W, et al. An unexpected protein interaction promotes drug resistance in leukemia. *Nat Commun.* 2017; 8(1): 1547, doi: [10.1038/s41467-017-01678-y](https://doi.org/10.1038/s41467-017-01678-y), indexed in Pubmed: [29146910](https://pubmed.ncbi.nlm.nih.gov/29146910/).
53. Killian JA, von Heijne G. How proteins adapt to a membrane-water interface. *Trends Biochem Sci.* 2000; 25(9): 429–434, doi: [10.1016/S0968-0004\(00\)01626-1](https://doi.org/10.1016/S0968-0004(00)01626-1), indexed in Pubmed: [10973056](https://pubmed.ncbi.nlm.nih.gov/10973056/).
54. Köster DV, Mayor S. Cortical actin and the plasma membrane: inextricably intertwined. *Curr Opin Cell Biol.* 2016; 38: 81–89, doi: [10.1016/j.ceb.2016.02.021](https://doi.org/10.1016/j.ceb.2016.02.021), indexed in Pubmed: [26986983](https://pubmed.ncbi.nlm.nih.gov/26986983/).
55. Marguet D, Lenne PF, Rigneault H, et al. Dynamics in the plasma membrane: how to combine fluidity and order. *EMBO J.* 2006; 25(15): 3446–3457, doi: [10.1038/sj.emboj.7601204](https://doi.org/10.1038/sj.emboj.7601204), indexed in Pubmed: [16900097](https://pubmed.ncbi.nlm.nih.gov/16900097/).
56. Honigsmann A, Sadeghi S, Keller J, et al. A lipid bound actin meshwork organizes liquid phase separation in model membranes. *Elife.* 2014; 3: e01671, doi: [10.7554/eLife.01671](https://doi.org/10.7554/eLife.01671), indexed in Pubmed: [24642407](https://pubmed.ncbi.nlm.nih.gov/24642407/).
57. Ehrig J, Petrov EP, Schwille P. Near-critical fluctuations and cytoskeleton-assisted phase separation lead to subdiffusion in cell membranes. *Biophys J.* 2011; 100(1): 80–89, doi: [10.1016/j.bpj.2010.11.002](https://doi.org/10.1016/j.bpj.2010.11.002), indexed in Pubmed: [21190659](https://pubmed.ncbi.nlm.nih.gov/21190659/).
58. Levental I, Grzybek M, Simons K. Raft domains of variable properties and compositions in plasma membrane vesicles. *Proc Natl Acad Sci U S A.* 2011; 108(28): 11411–11416, doi: [10.1073/pnas.1105996108](https://doi.org/10.1073/pnas.1105996108), indexed in Pubmed: [21709267](https://pubmed.ncbi.nlm.nih.gov/21709267/).
59. Baumgart T, Hammond AT, Sengupta P, et al. Large-scale fluid/fluid phase separation of proteins and lipids in giant plasma membrane vesicles. *Proc Natl Acad Sci U S A.* 2007; 104(9): 3165–3170, doi: [10.1073/pnas.0611357104](https://doi.org/10.1073/pnas.0611357104), indexed in Pubmed: [17360623](https://pubmed.ncbi.nlm.nih.gov/17360623/).
60. Sezgin E, Kaiser HJ, Baumgart T, et al. Elucidating membrane structure and protein behavior using giant plasma membrane vesicles. *Nat Protoc.* 2012; 7(6): 1042–1051, doi: [10.1038/nprot.2012.059](https://doi.org/10.1038/nprot.2012.059), indexed in Pubmed: [22555243](https://pubmed.ncbi.nlm.nih.gov/22555243/).
61. Biernatowska A, Podkalicka J, Majkowski M, et al. The role of MPP1/p55 and its palmitoylation in resting state raft organization in HEL cells. *Biochim Biophys Acta.* 2013; 1833(8): 1876–1884, doi: [10.1016/j.bbamcr.2013.03.009](https://doi.org/10.1016/j.bbamcr.2013.03.009), indexed in Pubmed: [23507198](https://pubmed.ncbi.nlm.nih.gov/23507198/).
62. Dimitratos SD, Woods DF, Stathakis DG, et al. Signaling pathways are focused at specialized regions of the plasma membrane by scaffolding proteins of the MAGUK family. *Bioessays.* 1999; 21(11): 912–921, doi: [10.1002/\(SICI\)1521-1878\(199911\)21:11<912::AID-BIES3>3.0.CO;2-Z](https://doi.org/10.1002/(SICI)1521-1878(199911)21:11<912::AID-BIES3>3.0.CO;2-Z), indexed in Pubmed: [10517864](https://pubmed.ncbi.nlm.nih.gov/10517864/).
63. Anderson JM. Cell signalling: MAGUK magic. *Curr Biol.* 1996; 6(4): 382–384, indexed in Pubmed: [8723338](https://pubmed.ncbi.nlm.nih.gov/8723338/).
64. Ruff P, Speicher DW, Husain-Chishti A. Molecular identification of a major palmitoylated erythrocyte membrane protein containing the src homology 3 motif. *Proc Natl Acad Sci U S A.* 1991; 88(15): 6595–6599, doi: [10.1073/pnas.88.15.6595](https://doi.org/10.1073/pnas.88.15.6595), indexed in Pubmed: [1713685](https://pubmed.ncbi.nlm.nih.gov/1713685/).
65. Seo PS, Quinn BJ, Khan AA, et al. Identification of erythrocyte p55/MPP1 as a binding partner of NF2 tumor suppressor protein/Merlin. *Exp Biol Med (Maywood).* 2009; 234(3): 255–262, doi: [10.3181/0809-RM-275](https://doi.org/10.3181/0809-RM-275), indexed in Pubmed: [19144871](https://pubmed.ncbi.nlm.nih.gov/19144871/).
66. Marfatia SM, Morais-Cabral JH, Kim AC, et al. The PDZ domain of human erythrocyte p55 mediates its binding to the cytoplasmic carboxyl terminus of glycophorin C. Analysis of the binding interface by in vitro mutagenesis. *J Biol Chem.* 1997; 272(39): 24191–24197, doi: [10.1074/jbc.272.39.24191](https://doi.org/10.1074/jbc.272.39.24191), indexed in Pubmed: [9305870](https://pubmed.ncbi.nlm.nih.gov/9305870/).
67. Hemming NJ, Anstee DJ, Staricoff MA, et al. Identification of the membrane attachment sites for protein 4.1 in the human erythrocyte. *J Biol Chem.* 1995; 270(10): 5360–5366, doi: [10.1074/jbc.270.10.5360](https://doi.org/10.1074/jbc.270.10.5360), indexed in Pubmed: [7890649](https://pubmed.ncbi.nlm.nih.gov/7890649/).
68. Podkalicka J, Biernatowska A, Majkowski M, et al. MPP1 as a Factor Regulating Phase Separation in Giant Plasma Membrane-Derived Vesicles. *Biophys J.* 2015; 108(9): 2201–2211, doi: [10.1016/j.bpj.2015.03.017](https://doi.org/10.1016/j.bpj.2015.03.017), indexed in Pubmed: [25954878](https://pubmed.ncbi.nlm.nih.gov/25954878/).
69. Levental I, Lingwood D, Grzybek M, et al. Palmitoylation regulates raft affinity for the majority of integral raft proteins. *Proc Natl Acad Sci U S A.* 2010; 107(51): 22050–22054, doi: [10.1073/pnas.1016184107](https://doi.org/10.1073/pnas.1016184107), indexed in Pubmed: [21131568](https://pubmed.ncbi.nlm.nih.gov/21131568/).
70. Podkalicka J, Biernatowska A, Olszewska P, et al. The microdomain-organizing protein MPP1 is required for insulin-stimulated activation of H-Ras. *Oncotarget.* 2018; 9(26): 18410–18421, doi: [10.18632/oncotarget.24847](https://doi.org/10.18632/oncotarget.24847), indexed in Pubmed: [29719614](https://pubmed.ncbi.nlm.nih.gov/29719614/).
71. Chishti AH. Function of p55 and its nonerythroid homologues. *Curr Opin Hematol.* 1998; 5(2): 116–121, indexed in Pubmed: [9570704](https://pubmed.ncbi.nlm.nih.gov/9570704/).
72. Marfatia SM, Lue RA, Branton D, et al. In vitro binding studies suggest a membrane-associated complex between erythroid p55, protein 4.1, and glycophorin C. *J Biol Chem.* 1994; 269(12): 8631–8634, indexed in Pubmed: [8132590](https://pubmed.ncbi.nlm.nih.gov/8132590/).
73. Diakowski W, Grzybek M, Sikorski AF. Protein 4.1, a component of the erythrocyte membrane skeleton and its related homologue proteins forming the protein 4.1/FERM superfamily. *Folia Histochem Cytobiol.* 2006; 44(4): 231–248, indexed in Pubmed: [17219717](https://pubmed.ncbi.nlm.nih.gov/17219717/).
74. Ward RE, Schweizer L, Lamb RS, et al. The protein 4.1, ezrin, radixin, moesin (FERM) domain of *Drosophila* Coracle, a cytoplasmic component of the septate junction, provides functions essential for embryonic development and imaginal cell proliferation. *Genetics.* 2001; 159(1): 219–228, indexed in Pubmed: [11560899](https://pubmed.ncbi.nlm.nih.gov/11560899/).
75. Biernatowska A, Augoff K, Podkalicka J, et al. MPP1 directly interacts with flotillins in erythrocyte membrane - Possible mechanism of raft domain formation. *Biochim Biophys Acta Biomembr.* 2017; 1859(11): 2203–2212, doi: [10.1016/j.bbamem.2017.08.021](https://doi.org/10.1016/j.bbamem.2017.08.021), indexed in Pubmed: [28865798](https://pubmed.ncbi.nlm.nih.gov/28865798/).
76. Lang DM, Lommel S, Jung M, et al. Identification of reggie-1 and reggie-2 as plasmamembrane-associated proteins which cocluster with activated GPI-anchored cell adhesion molecules in non-caveolar micropatches in neurons. *J Neurobiol.* 1998; 37(4): 502–523, indexed in Pubmed: [9858255](https://pubmed.ncbi.nlm.nih.gov/9858255/).
77. Neumann-Giesen C, Fernow I, Amaddii M, et al. Role of EGF-induced tyrosine phosphorylation of reggie-1/flotillin-2 in cell spreading and signaling to the actin cytoskeleton. *J Cell Sci.* 2007; 120(Pt 3): 395–406, doi: [10.1242/jcs.03336](https://doi.org/10.1242/jcs.03336), indexed in Pubmed: [17213334](https://pubmed.ncbi.nlm.nih.gov/17213334/).
78. Amaddii M, Meister M, Banning A, et al. Flotillin-1/reggie-2 protein plays dual role in activation of receptor-tyrosine kinase/mitogen-activated protein kinase signaling. *J Biol Chem.* 2012; 287(10): 7265–7278, doi: [10.1074/jbc.M111.287599](https://doi.org/10.1074/jbc.M111.287599), indexed in Pubmed: [22232557](https://pubmed.ncbi.nlm.nih.gov/22232557/).
79. Ludwig A, Otto GP, Riento K, et al. Flotillin microdomains interact with the cortical cytoskeleton to control uropod formation and neutrophil recruitment. *J Cell Biol.* 2010; 191(4): 771–781, doi: [10.1083/jcb.201005140](https://doi.org/10.1083/jcb.201005140), indexed in Pubmed: [21059848](https://pubmed.ncbi.nlm.nih.gov/21059848/).
80. Nakamura H, Sudo T, Tsuiki H, et al. Identification of a novel human homolog of the *Drosophila* dlg, P-dlg, specifically

- expressed in the gland tissues and interacting with p55. FEBS Lett. 1998; 433(1-2): 63–67, indexed in Pubmed: [9738934](#).
81. Mburu P, Kikkawa Y, Townsend S, et al. Whirlin complexes with p55 at the stereocilia tip during hair cell development. Proc Natl Acad Sci U S A. 2006; 103(29): 10973–10978, doi: [10.1073/pnas.0600923103](#), indexed in Pubmed: [16829577](#).
 82. Quinn BJ, Welch EJ, Kim AC, et al. Erythrocyte scaffolding protein p55/MPP1 functions as an essential regulator of neutrophil polarity. Proc Natl Acad Sci U S A. 2009; 106(47): 19842–19847, doi: [10.1073/pnas.0906761106](#), indexed in Pubmed: [19897731](#).
 83. Evans DG. Neurofibromatosis type 2 (NF2): a clinical and molecular review. Orphanet J Rare Dis. 2009; 4: 16, doi: [10.1186/1750-1172-4-16](#), indexed in Pubmed: [19545378](#).
 84. Listowski MA, Leluk J, Kraszewski S, et al. Cholesterol Interaction with the MAGUK Protein Family Member, MPP1, via CRAC and CRAC-Like Motifs: An In Silico Docking Analysis. PLoS One. 2015; 10(7): e0133141, doi: [10.1371/journal.pone.0133141](#), indexed in Pubmed: [26186446](#).
 85. Elderdfi M, Zegarlińska J, Jones W, et al. MPP1 interacts with DOPC/SM/Cholesterol in an artificial membrane system using Langmuir-Blodgett monolayer. Gen Physiol Biophys. 2017; 36(4): 443–454, doi: [10.4149/gpb_2017002](#), indexed in Pubmed: [28653654](#).
 86. Elderdfi M, Sikorski AF. Interaction of membrane palmitoylated protein-1 with model lipid membranes. Gen Physiol Biophys. 2018; 37(6): 603–617, doi: [10.4149/gpb_2018029](#), indexed in Pubmed: [30547893](#).
 87. Sharma P, Varma R, Sarasij RC, et al. Nanoscale organization of multiple GPI-anchored proteins in living cell membranes. Cell. 2004; 116(4): 577–589, doi: [10.1016/S0092-8674\(04\)00167-9](#), indexed in Pubmed: [14980224](#).
 88. Mayor S, Rao M. Rafts: scale-dependent, active lipid organization at the cell surface. Traffic. 2004; 5(4): 231–240, doi: [10.1111/j.1600-0854.2004.00172.x](#), indexed in Pubmed: [15030564](#).
 89. Fujita M, Kinoshita T. Structural remodeling of GPI anchors during biosynthesis and after attachment to proteins. FEBS Lett. 2010; 584(9): 1670–1677, doi: [10.1016/j.febslet.2009.10.079](#), indexed in Pubmed: [19883648](#).
 90. Eggeling C, Ringemann C, Medda R, et al. Direct observation of the nanoscale dynamics of membrane lipids in a living cell. Nature. 2009; 457(7233): 1159–1162, doi: [10.1038/nature07596](#), indexed in Pubmed: [19098897](#).
 91. Navarro-Lérida I, Sánchez-Perales S, Calvo M, et al. A palmitoylation switch mechanism regulates Rac1 function and membrane organization. EMBO J. 2012; 31(3): 534–551, doi: [10.1038/emboj.2011.446](#), indexed in Pubmed: [22157745](#).

Submitted: 8 February, 2019

Accepted after reviews: 17 April, 2019

Available as AoP: 16 May, 2019

L1-ORF1p and Ago2 are involved in a siRNA-mediated regulation for promoter activity of L1-5'UTR

Liu Shi^{1,2}, Huanhuan Shi¹, Liangliang Lou¹, Xiaoning Yuan¹, Yunfeng Zhu¹

¹College of Life Sciences and Bio-engineering, Beijing Jiao-tong University, Beijing 100044, China

²Department of Psychiatry, University of Oxford, OX3 7JX, UK

Abstract

Introduction. Long interspersed nuclear elements-1 (L1), as the only one self-active retrotransposon of the mobile element, was found to be generally activated in tumor cells. The 5'UTR of L1 (L1-5'UTR) contains both sense and antisense bidirectional promoters, transcription products of which can generate double-strand RNA (dsRNA). In addition, L1-ORF1p, a dsRNA binding protein encoded by L1, is considered to engage in some RNA-protein (RNP) formation. Ago2, one of the RISC components, can bind to dsRNA to form RISC complex, but its role in L1 regulation still remains unclear. Due that the 5'UTR of L1 (L1-5'UTR) contains both sense and antisense bidirectional promoters, so the activities in both string were identified. A dsRNA-mediated regulation of L1-5'UTR, with the feedback regulation of L1-ORF1p as well as other key molecules engaged (Ago1–4) in this process, was also investigated.

Material and methods. Genomic DNA was extracted from HEK293 cells and subjected to L1-5'UTR preparation by PCR. Report gene system pIRESneo with SV40 promoter was employed. The promoter activities of different regions in L1-5'UTR were identified by constructing these regions into pIRESneo, which SV40 region was removed prior, to generate different recombinant plasmids. The promoter activities in recombinant plasmids were detected by the luciferase expression assay. Western blot and co-immunoprecipitation were employed to identify proteins expression and protein-protein interaction respectively.

Results. Ago2 is a member of Agos family, which usually forms a RISC complex with si/miRNA and is involved in post-transcriptional regulation of many genes. Here L1-ORF1p and Ago2 conducts a regulation as a negative feedback for L1-5'UTR sense promoter. L1-ORF1p could form the immune complexes with Ago1, Ago2 and Ago4, respectively.

Conclusions. L1-5'UTR harbors both sense and antisense promoter activity and a dsRNA-mediated regulation is responsible for L1-5'UTR regulation. Agos proteins and L1-ORF1p were engaged in this process. (*Folia Histochemica et Cytobiologica* 2019, Vol. 57, No. 2, 56–63)

Key words: L1-5'UTR; Ago2; L1-ORF1p; antisense promoter; siRNA; HEK293 cells; protein interactions

Introduction

LINE-1 (Long Interspersed Nucleotide Element, L1), an autonomous retrotransposon and a parasitic element, makes up roughly 20% of human genomic DNA. It spreads throughout human genome by a manner of “copy and paste” that propagates its DNA or other DNAs within the genome through RNA intermediate and the mechanism is termed as

target-primed reverse transcription (TPRT) [1, 2]. L1, in human genome, is thought to be activated in germ cell, embryonic cells with early stage of development [3]. Promoter hypermethylation is a common phenomenon for gene deactivation; however, its deactivation is related to promoter hypermethylation in differentiated cells by epigenetic regulation. In addition, L1 as a cis-element can also suppress adjacent gene expression due to unknown mechanism [4]. Moreover, it has been reported that the promoter of L1 provides an alternative promoter site for the expression of other nearby genes. The translocation of L1 containing the 5'UTR promoter sequence to the intron region of the *Met* gene was observed in colorec-

Correspondence address: Yunfeng Zhu
College of Life Sciences and Bio-engineering,
Beijing Jiao-tong University, Beijing, China,
e-mail: zhuyf2004@163.com

tal and liver cancer. This phenomenon has been shown to be associated with an abnormal increase in Met expression and is important for malignant proliferation of cancer cells [5]. Under stress condition, e.g.: heat shock, virus infection, treating by cycloheximide, genotoxic agents and DNA base analogs, L1 can also be activated. The hypermethylation of L1 promoter occurs early in non-small-cell lung cancer (NSCLC), which is independently associated with poor prognosis in stage I NSCLC patients [6]. Physiologically, L1 is considered to be involved in X chromosome inactivation by a Xist mechanism [7]. Activated L1 not only reshapes the genome by arising gene mutations including insertion, deletion and rearrangement, but also contributes to modulation of gene expression by epigenetic mechanism. Given that L1 can lead to deleterious effects, it is important for cell to constrain its activation; however, this gene was identified to be activated ubiquitously in malignant tumor cells [8–10]. It is reported that L1 induces hTERT and ensures telomere maintenance in tumor cell lines [11]. Decreased expression of E-Cadherin and N-Cadherin proteins were observed post L1-ORF2p (L1 encoded ORF2 protein) transfection along with up-regulation of vimentin [12]. Thus, L1 with its feature of widespread distribution in human genome and ubiquitous activation in tumor cells can act as a promising model for us to understand the mechanism of tumorigenesis.

Full-length L1, 6–7kb, is consisted of a 5' untranslated region (5'-UTR), two open reading frames (ORF1 and ORF2) and a 3'-UTR. L1-ORF1p (L1 encoded protein ORF1 protein), a RNA-binding protein facilitating retrotransposition together with L1-ORF2 p [13], was identified to co-localize with RNA-induced silencing complex (RISC) recently [14, 15]. 5'-UTR of L1 containing a sense promoter (SP) and an antisense promoter (ASP) will generate a double-strand RNA (dsRNA) after transcription [16, 17], which implicates an RNA interference mechanism for its regulation. With the constructs of full-length and 3' truncated mutants of L1-5UTR, the promoter activity of L1 was investigated. At the same time, L1-ORF1p as a RNA binding protein was also identified for its function in this process.

The regulation of siRNA trafficking in human cells is executed by RNA-induced silencing complex (RISC). Small interfering RNA molecules are bound to RISC complex followed by inference with corresponding mRNA in cytoplasm. It was previously observed, that L1-5'UTR is negatively regulated by RISC via interaction with Ago2 (ArgonAUT family protein) [18]. However, the exact role of Ago2 (and other proteins of Ago family; Ago1, 3, 4) in regula-

tion negative feedback mechanism of L1 still remains unknown. Therefore, next aim of our study was to check whether the Ago2 protein interacts with L1 particles.

Materials and methods

Cell culture. HEK293 cells were cultured with DMEM medium (Gibco-BRL, Gaithersburg, MD, USA) supplemented with 10% fetal calf serum (Hyclone, Logan, UT, USA). Cells were incubated at 37° with an atmosphere containing 5% CO₂ and saturated humidity. The medium was changed every 2–3 days.

Recombinant plasmids construction. PCR reagents were purchased from Takara Company (Beijing, China) and the approach was followed according to manufacturer's protocol. In brief, the components of PCR reaction were as follows: 2 μl DNA template, 1 μl upstream primer (10 mmol/ml) and downstream primer (10 mmol/ml) respectively, 10 μl of 2 × PCR master mixture (including: Taq, dNTP and buffer), H₂O to a 20 μl final reaction volume. PCR running parameters were as follows: 95°C for 5 min followed by 35 cycles of 94°C for 5 s, annealing at 58°C for 25 s, extension at 70°C for 25 s, and a final extension at 70°C for 10 min.

L1-ORF1p recombinant plasmid: The full-length sequence of L1-ORF1 was amplified by PCR with a template of human genome DNA and cloned into pIRESneo to generate recombinant plasmid pIRES-ORF1-Flag.

L1-5'UTR recombinant plasmids: pCBG99-5UTR-FL: Full-length L1-5'UTR was amplified by PCR with a template of human genome DNA and primers (5'-CCGCTCGAG(XhoII)GAGAGGAGCCAAGATGGC-3' and 5'-CCCAAGCTT(HindIII)CTTTGTGGTTTTATCTACTTT-3'). PCR products were cloned into pCBG99-control vector digested with XhoII/HindIII (removing SV40 promoter) prior to generate pCBG99-5UTR-FL.

pCBG99-5UTR-680 and pCBG99-5UTR-400:

For constructing 3'- truncated mutants of L1-5'UTR, 5'UTR-680 (removing ASP sequence) and 5'UTR-400 (removing ASP and partial SP sequences) of L1-5'UTR were amplified by PCR with a template of pCBG99-5UTR-FL and specific primers

(5'UTR-680: 5'-CCGCTCGAG(XhoII)GAGAGGAGCCAAGATGGC-3' and 5'-CCCAAGCTT(HindIII)GCAGTCTGCCGTTCTCAGA-3; 5'UTR-400: 5'-CCGCTCGAG(XhoII)GAGAGGAGCCAAGATGGC-3', and 5'-CCCAAGCTT(HindIII)TGCAGTTTGATCTCAGACTG-3').

PCR products were cloned into pCBG99-control vector digested by XhoII/HindIII prior to generate pCBG99-5UTR-680 and pCBG99-5UTR-400, respectively.

pCBG99-actin 680: As a negative control, the sequence of beta-actin with 680bp was prepared by PCR with a template of genomic DNA and primers (5'-CCGCTCGAG (*XhoI*) CTGTGCCCATCTACGAGG-3' and 5'-CCCAAGCTT (*HindIII*) AAAGGGTGTAACGCAACTAA-3'). PCR product was cloned into pCBG99-control digested by *XhoI*/*HindIII* prior to generate pCBG99-actin 680.

pCBG99-5UTR-aFL and pCBG99-5UTR-a680: For investigating ASP activity, antisense sequence of full-length of L1-5'UTR were prepared by PCR with the primers as follows:

5'-CCCAAGCTT (*HindIII*) GAGAGGAGCCAAGATGGC-3' and 5'-CCGCTCGAG (*XhoI*) CTTTGTGGT-TTTATCTACTTT-3'.

Antisense sequence of 3' truncated mutant of 5'UTR-680 was prepared by PCR with the primers as follows:

5'-CCCAAGCTT (*HindIII*) GAGAGGAGCCAA-GATGGC-3' and 5'-CCGCTCGAG (*XhoI*) GCAG TCTGCCCGTTCTCAGA-3'.

PCR products were cloned into pCBG99-control digested by *XhoI*/*HindIII* prior to generate pCBG99-5UTR-aFL and pCBG99-5UTR-a680, respectively.

Ago2 recombinant plasmids: pSilencer-Ago2-siRNA1, pSilencer-Ago2-siRNA2, pSilencer-Ago2-Con1, pSilencer-Ago2-Con2: siRNA targeting sequences for Ago2 were designed by RNAi designer (Ambion, USA), two candidates were selected with the sequences as follows:

5'-ACCGAGTTTCGACTTCTACCTGTGTGA-3' and 5'-CAAGACTCTGCGCACCATGTACT-3'

The hairpin structure was designed with the sequences as follows:

siRNA1 gene: sense sequence, 5'-GATCCACCGAGTTCGACTTCTACCTGTGTATTCAAGAG ATACA-CAGGTAGAAGTCGAACTCGGTTTTTTTGAAA-3'; anti-sense sequence:

5'-AGCTTTTCCAAAAAACCAGAGTTCGACTTCTACCTGTGTATCTCTTGAATACACAGGTAGAA-GTCGA ACTCGGTG-3';

siRNA2 gene: sense sequence, 5'-GATCCCAAGCACTCTGCGCACCATGTACTTTCAAGAG AAGTACATGGTGCAGAGTGTCTTGTTTTTTTTGAAA-3'; anti-sense sequence:

5'-AGCTTTTCCAAAAACAAGACTCTGCGCAC-CATGTACTTCTCTTGAAGTACATGGTGCAGAGTGTCTTGG-3'.

Double strand sequence was prepared by annealing and ligated into pSilencer2.1-U6/neo (Abcam, Cambridge, MA, USA) to generate recombinant plasmid pSilencer2.1-Ago2-siRNA1 and pSilencer2.1-Ago2-siRNA2, respectively. With same procedure, the control sequences for siRNA1 (con-siRNA1: 5'-ACCTGCTAGTCTATC-

CGTTAGGTA-3') and siRNA2 (con-siRNA2: 5'-CAACACTCTGCGCACTACTGGAAGT-3') were designed, synthesized and cloned into pSilencer2.1-U6/neo to generate pSilencer-Ago2-Con1 and pSilencer-Ago2-Con2, respectively.

Western blot analysis. The recombinant plasmids (pSilencer-Ago2-siRNA1, pSilencer-Ago2-siRNA2, pSilencer-Ago2-Con1, pSilencer-Ago2-Con2) were transfected into HEK293 cells using LipofectamineTM2000 reagent (Invitrogen, Carlsbad, CA, USA) for 48 h. Harvested cells were lysed with the lysis buffer (PBS solution including 2 μ g/ml aprotinin, 100 μ g/ml phenylmethyl-sulphonyl fluoride, 2 μ g/ml leupeptin and 1% Nonidet P-40 (Beyotime, Shanghai, China) followed by centrifugation to remove unsolved debris. After fractionating by 12.5% SDS-PAGE, the proteins were transferred into nitrocellulose membrane (Bio-Rad Laboratories, Hercules, CA, USA). The membranes were incubated with 5% non-fat milk for 1 h in room temperature and then with the primary antibody (anti-Ago2, anti-FLAG, anti-beta-actin, Abcam) for additional 1 h followed by washing with TBST (Tris Buffered Saline Tween) for three times. The membranes were incubated with horseradish peroxidase-labeled second antibody (Sigma, St Louis, MO, USA) for 1 h and washed with TBST for three times. The signals were visualized by incubating with enhanced chemiluminescence reagent (Amersham, Little Chalfont, UK) for 5 min. Triplicate experiments were conducted independently.

Luciferase expression assay. HEK293 cells were cultured with DMEM containing 0.5% calf serum for 24 hours, followed by transfection using 1 μ g pCMV- β -gal (internal reference) combining with 1 μ g different constructs. After culturing for 1 h the transfected cells were lysed and subjected to luciferase and β -Galactosidase assay respectively (Promega, Shanghai, China). The values of luciferase in different groups were normalized by β -Galactosidase to eliminate differences elicited by transfection efficiency. Triplicate experiments were conducted independently.

Co-immunoprecipitation. The cells were harvested and incubated with lysis buffer (20 mM Tris HCl pH 8, 137 mM NaCl, 10% glycerol, 1% Nonidet P-40, 2 mM EDTA) including a cocktail of protease inhibitors (Roche, Basel, Switzerland) on ice for 5 min. The supernatant solution was prepared by centrifuging with 15000 rpm for 10 min at 4°C. 200 μ l cell lysate and 20 μ l 50% bead slurry (protein-A sepharose) were mixed and incubated with gently rocking for 3–4 h at 4°C. Supernatant solution was collected and incubated with 5 μ l anti-FLAG by gently rocking for 4 h at 4°C. After spinning down and washing, the pellet was re-suspended with 20 μ l 2 \times SDS buffer, heated at 95–100°C

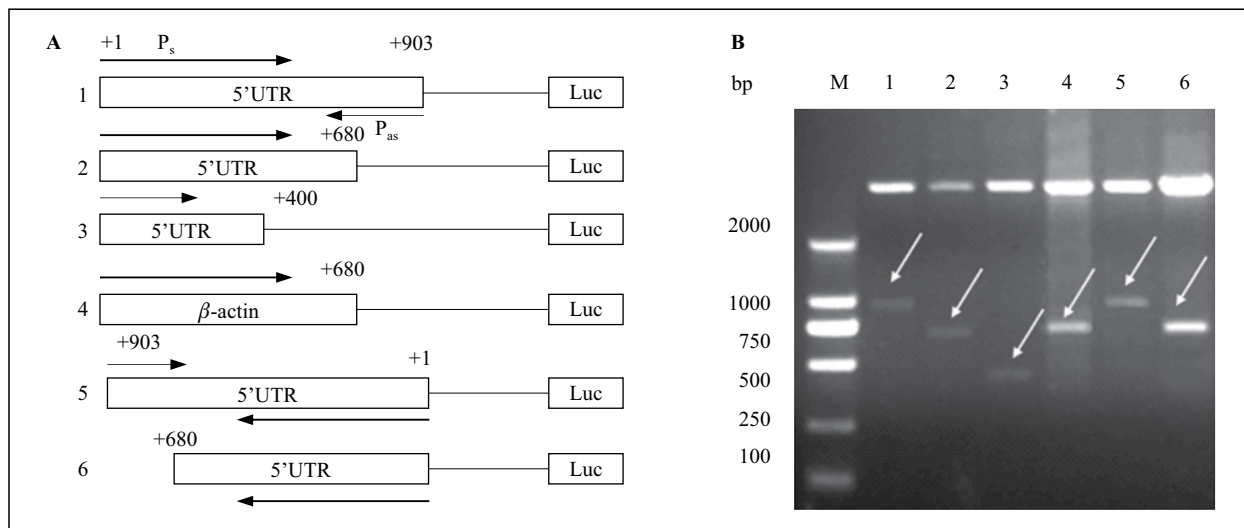


Figure 1. The constructs of full-length and truncated L1-5'UTR. **A.** A schematic map of construction of L1-5'UTR and mutants. 1: pCBG99-5UTR-FL (903bp); 2: pCBG99-5UTR-680 (680bp); 3: pCBG99-5UTR-400 (400bp); 4: pCBG99-actin 680 (680bp); 5: pCBG99-5UTR-aFL (903bp); 6: pCBG99-5UTR-a680 (680bp); **B.** The different constructs were confirmed by electrophoresis. DNA sizes of L1-5'UTR in different constructs were confirmed by digesting with restrictive enzymes as described in materials and methods. M: DNA molecular marker (2000bp, 1000bp, 750bp, 500bp, 250bp, 100bp); 1: pCBG99-5UTR-FL (903bp); 2: pCBG99-5UTR-680 (680bp); 3: pCBG99-5UTR-400 (400bp); 4: pCBG99-actin 680 (680bp); 5: pCBG99-5UTR-aFL (903bp); 6: pCBG99-5UTR-a680 (680bp). Arrows in Fig. 1B mean the different amplicons mentioned above.

for 2–5 min and then subjected to SDS-PAGE analysis. The proteins were identified by immune blot using anti-Ago1, anti-Ago2, anti-Ago3, anti-Ago4 antibodies, respectively (Abcam, Shanghai, China).

Statistical analysis. Differences between experiment groups and control were tested using SPSS software v. 11.0 (IBM, New York, NY, USA), in which $p < 0.05$ were considered as significant differences.

Results

Construction of the L1-5'UTR mutants

To elucidate the promoter activity of L1-5'UTR, the full-length and 3' mutants of L1-5'UTR were constructed with SV40-removed luciferase report system and confirmed by sequencing. The schematic map and recombinant plasmids for confirming constructs were shown in Figure 1.

The activity of SP and ASP in L1- 5'UTR were identified

With report system construct of luciferase, the promoter activities of sense and antisense in L1-5'UTR were identified quantitatively. As indicated in Figure 2, both activity of SP and ASP in L1-5'UTR were eval-

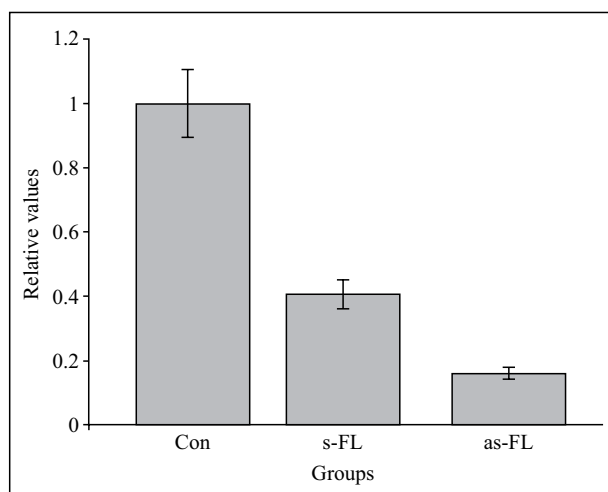


Figure 2. The identification of promoter activities of L1-5'UTR in sense and antisense sequences. The sense and antisense sequences of L1-5'UTR were constructed in immediately upstream of luciferase gene in SV40-removed pCBG99. The relative values of luciferase expressions in different groups were detected as described in Materials and methods. Con: pCBG99-Control (100%); s-FL: pCBG99-5UTR-FL (40%); as-FL: pCBG99-5UTR-aFL (16%). The percentages in parentheses are relative values of luciferase expression compared with control. The value in each group is the mean of triplicates and SEM were labeled by whiskers over the bars

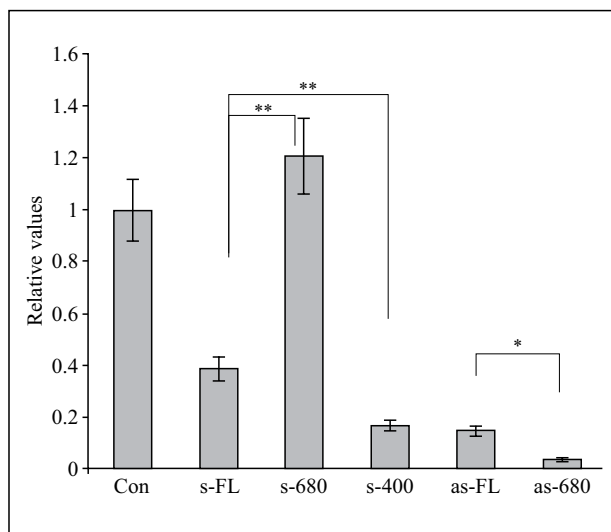


Figure 3. Antisense sequence of L1-5'UTR negatively regulates its promoter activity. Different constructs of L1-5'UTR were transfected into HEK293 cells. The expression of luciferase in different groups was detected and the relative values were calculated by normalizing with control as describing in Materials and methods. Con: pCBG99-Control (100%); s-FL: pCBG99-5'UTR-FL (40%); s-680: pCBG99-5'UTR-680 (120%); s-400: pCBG99-5'UTR-400 (18%); as-FL: pCBG99-5'UTR-aFL (16%); as-680: pCBG99-5'UTR-a680 (5%). The percentages in parentheses are relative values of luciferase expression compared with control. * $p < 0.05$; ** $p < 0.01$

uated by comparing with SV40 and indicated that SP was much stronger than ASP.

ASP can suppress SP activity

Owing to transcripts from SP and ASP in L1-5'UTR will generate a dsRNA, the effect of dsRNA on SP activity was investigated by constructing different ASP mutants. pCBG99-5UTR-680, a construct with 223bp removing in 3 terminus of 5'UTR, and pCBG99-5UTR-400, a construct with 503bp removing in 3 terminus of 5'UTR displays the strongest and weakest SP activity respectively by comparing with pCBG99-5UTR-FL, a construct with full-length of L1-5'UTR. Meanwhile, the remaining ASP activity in these truncated mutants was also determined by constructing pCBG99-5UTR-a680 and pCBG99-5UTR-a400 (data not shown) (Fig. 3). Apparently, ASP activity negatively regulates SP activity and a dsRNA-mediated regulation was responsible for this mechanism.

Argonaut 2 is involved in siRNA-mediated regulation for L1-5'UTR

To elucidate a dsRNA-mediated regulation further, Argonaut 2 (Ago2), a key component of RISC (RNA-induced Silencing Complex) playing an important role in siRNA processing was investigated. Co-transfection of constructs of Ago2-siRNA with either pCBG99-5UTR-680 or pCBG99-5UTR-400 or pCBG99-5UTR-FL was conducted. As indicated in Figure 4, luciferase expression in construct of pCBG99-5UTR-FL was increased significantly, whereas moderate and null increases were shown in constructs of pCBG99-5UTR-680 and pCBG99-

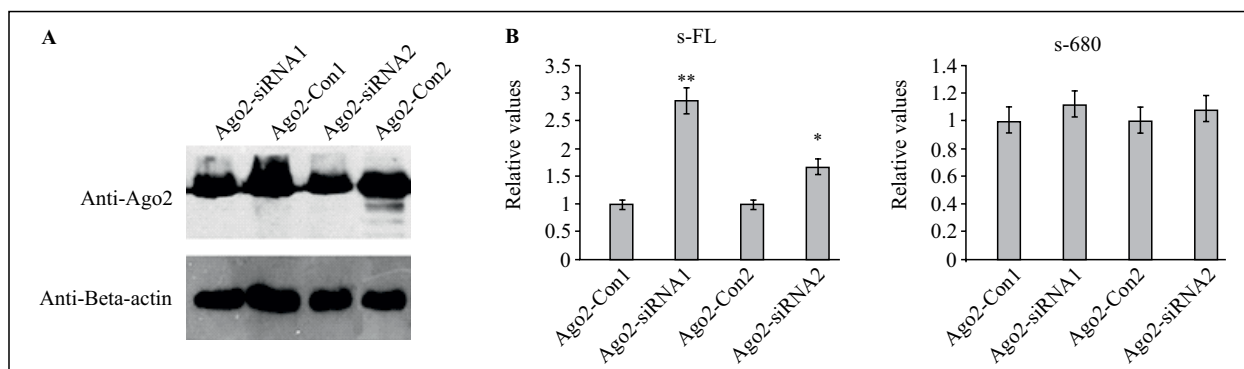


Figure 4. Ago2 is involved in the regulation of L1-5'UTR activity. HEK293 cells were transfected by either pCBG99-5UTR-FL or pCBG99-5UTR-680 combined with Ago2-siRNA constructs. The expressions of luciferase in different groups were detected by measuring the OD value at 415 nm absorbance the relative values were calculated by normalizing with respective control (transfected by either pCBG99-5UTR-FL or pCBG99-5UTR-680 only). Ago2-siRNA1: pSilencer-Ago2-siRNA1; Ago2-con1: pSilencer-Ago2-Con1; Ago2-siRNA2: pSilencer-Ago2-siRNA2; Ago2-con2: pSilencer-Ago2-Con2 s-FL: pCBG99-5'UTR-FL; s-680: pCBG99-5'UTR-680. **A.** The expressions of Ago2 in transfected HEK293 cells with different siRNA constructs where assessed by Western blot. **B.** The relative values of luciferase expressions. S-FL: Ago2-con1 (100%); Ago2-siRNA1 (280%); Ago2-con2 (100%); Ago2-siRNA2 (170%); S-680: Ago2-con1 (100%); Ago2-siRNA1 (110%); Ago2-con2 (100%); Ago2-siRNA2 (105%). The percentages in parentheses are relative values of luciferase expression compared with control. The value in each group is the mean of triplicates and SEM were labeled by whiskers over the bars * $p < 0.05$; ** $p < 0.01$

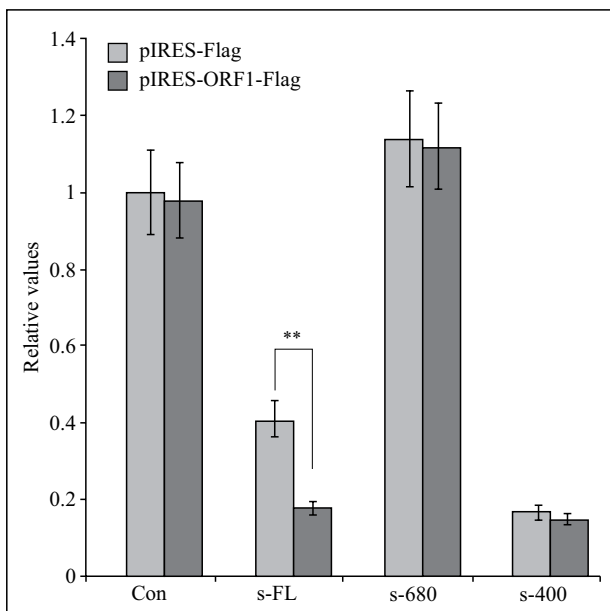


Figure 5. L1-ORF1p modulated L1-5'UTR activity. pIRES-ORF1-Flag was co-transfected with one of constructs of L1-5'UTR in HEK293 cells and the expressions of luciferase in different groups were detected by measuring the OD value at 415 nm absorbance. After normalizing with control (co-transfection of pIRES-Flag with pCBG99-Control), the relative values of expression in different groups were plotted. Con: pCBG99-Control (pIRS-FLAG: 100%, pIRS-ORF1-FLAG: 97%); s-FL: pCBG99-5UTR-FL (pIRS-FLAG: 40%, pIRS-ORF1-FLAG: 19%); s-680: pCBG99-5UTR-680 (pIRS-FLAG: 112%, pIRS-ORF1-FLAG: 110%); s-400: pCBG99-5UTR-400 (pIRS-FLAG: 19%, pIRS-ORF1-FLAG: 18%). The percentages in parentheses are relative values of luciferase expression compared with control. The value in each group is the mean of triplicates and SEM were labeled by whiskers over the bars **p < 0.01

-5UTR-400, respectively. Suggesting that Ago2 can suppress L1-5'UTR promoter activity and the mechanism by which a siRNA-mediated regulation may account for this fact.

L1-ORF1p is involved in siRNA-mediated regulation for L1-5'UTR

Given the RNA binding activity of L1-ORF1p, the effect of L1-ORF1p on siRNA-mediated regulation for L1-5'UTR was investigated. With different constructs of L1-5'UTR, the promoter activity was investigated in L1-ORF1p over-expressed HEK293 cells. As indicated in Figure 5, over-expression of L1-ORF1p resulted in decrease of luciferase expression significantly in full-length 5'UTR construct, whereas less effect on other truncated mutants. It indicates that L1-ORF1p is involved in siRNA-mediated L1-5'UTR regulation.

L1-ORF1p can form immune complex with the members of Argonaut family

Owing that both L1-ORF1p and Ago2 are RNA-binding proteins, the interaction between them was investigated with which may account for the mechanism of L1-ORF1p. As indicated in Figure 6A, a RNA-independent interaction between Ago2 and L1-ORF1p was identified by co-immunoprecipitation. Furthermore, the other members of Argonaut family in human were also investigated and indicated that Ago1, Ago2, Ago4 but not Ago3 can form immune complex with L1ORF1p, respectively (Fig. 6B). Thus, the interaction between Ago2 (or other members of Argonaut family) and L1-ORF1p may account for the mechanism of L1-ORF1p for its feedback regulation to L1-5'UTR.

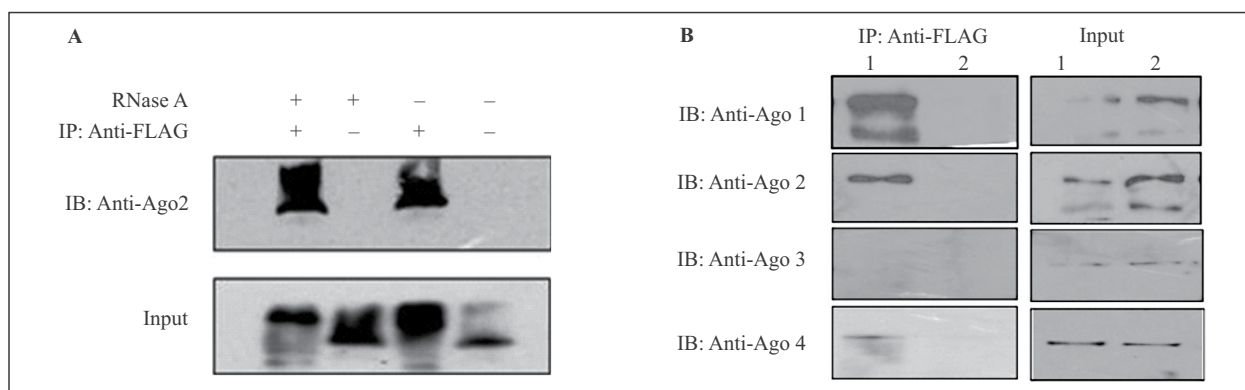


Figure 6. L1ORF1p formed a complex with the members of Argonaut family, Ago1, Ago2 and Ago4. Transfected HEK293 cells were lysed and subjected to immunoprecipitation with anti-L1ORF1p. The complexes were fractionated by SDS-PAGE and immune-blotted with anti-Ago1, anti-Ago2, anti-Ago3 and anti-Ago4, respectively. 1: pIRES-L1ORF1-Flag; 2: pIRES (control). **A.** RNA-independent interaction of L1-ORF1p and Ago2. **B.** The interactions of L1-ORF1p with other members of Argonaut family, Ago1 and Ago4.

Discussion

SP and ASP in L1-5'UTR were identified for their activities by different constructs with luciferase report system. To elucidate a dsRNA (siRNA precursor) mediated regulation for L1-5'UTR, we constructed differently truncated mutants of 3' terminus of L1-5'UTR (removing ASP sequence) and found that the activity of SP has a negative relationship with ASP. It is implicated that a siRNA mediated regulation was employed for L1-5'UTR. Furthermore, Ago2, a critical component in RISC (RNA- Induced Silencing Complex) [18] was investigated and, resultantly, a negative regulation for L1-5'UTR was identified. Our result is consistent with previous report, in which L1-5'UTR transcripts was identified as the first endo-siRNA in germ cells and L1 retrotransposition was suppressed by endogenously encoded small interfering RNAs [19] and Ago2 [14, 20]. Thus, Ago2 plays a crucial role in siRNA-mediated regulation for L1-5'UTR. Consistently, the depletion of endo-siRNA was reported in human breast cancer cells. In addition, L1-ORF1p, a RNA binding protein and co-localizing with RISC [14], is also involved in a negative feedback regulation of L1-5'UTR by siRNA-mediated mechanism. Given that both Ago2 and L1-ORF1p are RNA binding proteins, an interaction was hypothesized and as a result that L1-ORF1p can form immune complex with Ago2 with RNA independent manner even that the domains responsible for direct interaction need to be identified further. In addition, more members, but not Ago3, of Argonaut family (Ago1, Ago2, Ago4) were identified to interact with L1-ORF1p, suggesting that L1-ORF1p is involved in both siRNA and miRNA regulation based on the fact that Ago2 usually forms a complex with siRNA and Ago1/Ago4 usually forms a complex with miRNA [21]. Usually, Argonaut proteins and miRNAs/siRNAs are localized in processing bodies and, under stress conditions, re-localized to stress granules where it results in mRNA cleavage with miRNA/siRNA-dependent manner [21]. So, the interaction of L1-ORF1p with Argonauts may also account for that L1-ORF1p is involved in the process of miRNA/siRNA maturing and processing.

Taken together, both SP and ASP are identified in L1-5'UTR and a siRNA mediated regulation is identified for L1-5'UTR. L1-ORF1p, a RNA binding protein, is involved in siRNA mediated feedback regulation for L1-5'UTR by forming a complex with Ago1, Ago2 and Ago4, respectively.

Acknowledgement

This project was supported by National High Technology Research and Development Program in China (2011AA02A110).

Conflict of interest

The authors declare no conflict of interest.

References

- Baillie JK, Barnett MW, Upton KR, et al. Somatic retrotransposition alters the genetic landscape of the human brain. *Nature*. 2011; 479(7374): 534–537, doi: [10.1038/nature10531](https://doi.org/10.1038/nature10531), indexed in Pubmed: [22037309](https://pubmed.ncbi.nlm.nih.gov/22037309/).
- Denli AM, Narvaiza I, Kerman BE, et al. Primate-specific ORF0 contributes to retrotransposon-mediated diversity. *Cell*. 2015; 163(3): 583–593, doi: [10.1016/j.cell.2015.09.025](https://doi.org/10.1016/j.cell.2015.09.025), indexed in Pubmed: [26496605](https://pubmed.ncbi.nlm.nih.gov/26496605/).
- Pittoggi C, Sciamanna I, Mattei E, et al. Role of endogenous reverse transcriptase in murine early embryo development. *Mol Reprod Dev*. 2003; 66(3): 225–236, doi: [10.1002/mrd.10349](https://doi.org/10.1002/mrd.10349), indexed in Pubmed: [14502601](https://pubmed.ncbi.nlm.nih.gov/14502601/).
- Macia A, Muñoz-Lopez M, Cortes JL, et al. Epigenetic control of retrotransposon expression in human embryonic stem cells. *Mol Cell Biol*. 2011; 31(2): 300–316, doi: [10.1128/MCB.00561-10](https://doi.org/10.1128/MCB.00561-10), indexed in Pubmed: [21041477](https://pubmed.ncbi.nlm.nih.gov/21041477/).
- Wanichnopparat W, Suwanwongse K, Pin-On P, et al. Genes associated with the cis-regulatory functions of intragenic LINE-1 elements. *BMC Genomics*. 2013; 14: 205, doi: [10.1186/1471-2164-14-205](https://doi.org/10.1186/1471-2164-14-205), indexed in Pubmed: [23530910](https://pubmed.ncbi.nlm.nih.gov/23530910/).
- Morales JF, Snow ET, Murnane JP. Environmental factors affecting transcription of the human L1 retrotransposon. II. Stressors. *Mutagenesis*. 2003; 18(2): 151–158, doi: [10.1093/mutage/18.2.151](https://doi.org/10.1093/mutage/18.2.151).
- Hansen RS. X inactivation-specific methylation of LINE-1 elements by DNMT3B: implications for the Lyon repeat hypothesis. *Hum Mol Genet*. 2003; 12(19): 2559–2567, doi: [10.1093/hmg/ddg268](https://doi.org/10.1093/hmg/ddg268), indexed in Pubmed: [12925568](https://pubmed.ncbi.nlm.nih.gov/12925568/).
- Takai D, Yagi Y, Habib N, et al. Hypomethylation of LINE1 retrotransposon in human hepatocellular carcinomas, but not in surrounding liver cirrhosis. *Jpn J Clin Oncol*. 2000; 30(7): 306–309, doi: [10.1093/jjco/hyd079](https://doi.org/10.1093/jjco/hyd079), indexed in Pubmed: [11007163](https://pubmed.ncbi.nlm.nih.gov/11007163/).
- Jürgens B, Schmitz-Dräger BJ, Schulz WA. Hypomethylation of L1 LINE sequences prevailing in human urothelial carcinoma. *Cancer Res*. 1996; 56(24): 5698–5703, indexed in Pubmed: [8971178](https://pubmed.ncbi.nlm.nih.gov/8971178/).
- Kitkumthorn N, Mutirangura A. Long interspersed nuclear element-1 hypomethylation in cancer: biology and clinical applications. *Clin Epigenetics*. 2011; 2(2): 315–330, doi: [10.1007/s13148-011-0032-8](https://doi.org/10.1007/s13148-011-0032-8), indexed in Pubmed: [22704344](https://pubmed.ncbi.nlm.nih.gov/22704344/).
- Aschacher T, Wolf B, Enzmann F, et al. LINE-1 induces hTERT and ensures telomere maintenance in tumour cell lines. *Oncogene*. 2016; 35(1): 94–104, doi: [10.1038/onc.2015.65](https://doi.org/10.1038/onc.2015.65), indexed in Pubmed: [25798839](https://pubmed.ncbi.nlm.nih.gov/25798839/).
- Reyes-Reyes EM, Aispuro I, Tavera-Garcia MA, et al. LINE-1 couples EMT programming with acquisition of oncogenic phenotypes in human bronchial epithelial cells. *Oncotarget*. 2017; 8(61): 103828–103842, doi: [10.18632/oncotarget.21953](https://doi.org/10.18632/oncotarget.21953), indexed in Pubmed: [29262603](https://pubmed.ncbi.nlm.nih.gov/29262603/).
- Martin SL. The ORF1 protein encoded by LINE-1: structure and function during L1 retrotransposition. *J Biomed Biotechnol*. 2006; 2006(1): 45621, doi: [10.1155/JBB/2006/45621](https://doi.org/10.1155/JBB/2006/45621), indexed in Pubmed: [16877816](https://pubmed.ncbi.nlm.nih.gov/16877816/).
- Goodier JL, Zhang L, Vetter MR, et al. LINE-1 ORF1 protein localizes in stress granules with other RNA-binding proteins, including components of RNA interference RNA-induced silencing complex. *Mol Cell Biol*. 2007; 27(18): 6469–6483, doi: [10.1128/MCB.00332-07](https://doi.org/10.1128/MCB.00332-07), indexed in Pubmed: [17562864](https://pubmed.ncbi.nlm.nih.gov/17562864/).

15. Martin SL, Bushman FD. Nucleic acid chaperone activity of the ORF1 protein from the mouse LINE-1 retrotransposon. *Mol Cell Biol.* 2001; 21(2): 467–475, doi: [10.1128/MCB.21.2.467-475.2001](https://doi.org/10.1128/MCB.21.2.467-475.2001), indexed in Pubmed: [11134335](https://pubmed.ncbi.nlm.nih.gov/11134335/).
16. Swergold GD. Identification, characterization, and cell specificity of a human LINE-1 promoter. *Mol Cell Biol.* 1990; 10(12): 6718–6729, doi: [10.1128/mcb.10.12.6718](https://doi.org/10.1128/mcb.10.12.6718), indexed in Pubmed: [1701022](https://pubmed.ncbi.nlm.nih.gov/1701022/).
17. Mätlik K, Redik K, Speek M. L1 antisense promoter drives tissue-specific transcription of human genes. *J Biomed Biotechnol.* 2006; 2006(1): 71753, doi: [10.1155/JBB/2006/71753](https://doi.org/10.1155/JBB/2006/71753), indexed in Pubmed: [16877819](https://pubmed.ncbi.nlm.nih.gov/16877819/).
18. Deng Y, Wang CC, Choy KW, et al. Therapeutic potentials of gene silencing by RNA interference: principles, challenges, and new strategies. *Gene.* 2014; 538(2): 217–227, doi: [10.1016/j.gene.2013.12.019](https://doi.org/10.1016/j.gene.2013.12.019), indexed in Pubmed: [24406620](https://pubmed.ncbi.nlm.nih.gov/24406620/).
19. Horman SR, Svoboda P, Luning Prak ET. The potential regulation of L1 mobility by RNA interference. *J Biomed Biotechnol.* 2006; 2006(1): 32713, doi: [10.1155/JBB/2006/32713](https://doi.org/10.1155/JBB/2006/32713), indexed in Pubmed: [16877813](https://pubmed.ncbi.nlm.nih.gov/16877813/).
20. Apornthewan C, Phokaew C, Piriyaongsa J, et al. Hypomethylation of intragenic LINE-1 represses transcription in cancer cells through AGO2. *PLoS One.* 2011; 6(3): e17934, doi: [10.1371/journal.pone.0017934](https://doi.org/10.1371/journal.pone.0017934), indexed in Pubmed: [21423624](https://pubmed.ncbi.nlm.nih.gov/21423624/).
21. Sheu-Gruttadauria J, MacRae IJ. Structural Foundations of RNA Silencing by Argonaute. *J Mol Biol.* 2017; 429(17): 2619–2639, doi: [10.1016/j.jmb.2017.07.018](https://doi.org/10.1016/j.jmb.2017.07.018), indexed in Pubmed: [28757069](https://pubmed.ncbi.nlm.nih.gov/28757069/).

Submitted: 2 January, 2019

Accepted after reviews: 12 April, 2019

Available as AoP: 20 May, 2019

The miR-1204 regulates apoptosis in NSCLC cells by targeting DEK

Zhen Qian, Juan Yang, Huanhuan Liu, Yue Yin, Lingling Hou, Honggang Hu

College of Life Sciences and Bio-engineering, Beijing Jiaotong University, Beijing 100044, China

Abstract

Introduction. This study endeavors to analyze the effects of miR-1204 on the expression of DEK oncogene in non-small cell lung cancer (NSCLC) cell lines and to study the molecular mechanisms of these effects.

Material and methods. The miR-1204 mimics and inhibitors were transfected into the (A549 and SPC) NSCLC cells. Then the mRNA levels, cell viability, apoptosis rate, morphology and caspase activity were determined. The expression of apoptosis-related proteins Bcl-2 and Bax was also analyzed.

Results. In NSCLC cell lines (A549 and SPC), DEK mRNA levels were down-regulated in miR-1204 overexpression group. In miR-1204 inhibition group, the expression of DEK mRNA showed an opposite trend. The overexpression of miR-1204 increases the apoptosis rate in NSCLC cells. The Bcl-2 level in the miR-1204 overexpression group was decreased, while the Bax level was increased. In the miR-1204 inhibition group, expression of Bcl-2 and Bax showed opposite trends. Cell staining revealed cell's morphological changes; the apoptosis in the miR-1204 overexpression group revealed significant morphological features, such as brighter nuclei and nuclear condensation. Results indicated a typical characteristic of apoptosis in the miR-1204 overexpression group. Caspase-9 and Caspase-3 were involved in the apoptosis pathway, which was mediated by miR-1204 and DEK. **Conclusions.** The miR-1204 induces apoptosis of NSCLC cells by inhibiting the expression of DEK. The mechanism of apoptosis involves down-regulation of Bcl-2 and up-regulation of Bax expression. Moreover, the apoptosis was mediated by mitochondria-related caspase 9/3 pathway. (*Folia Histochemica et Cytobiologica* 2019, Vol. 57, No. 2, 64–73)

Key words: NSCLC; A549 cells; SPC cells; DEK; miR-1204; apoptosis; Bcl-2; Bax; caspase-3; caspase-9

Introduction

Lung cancer is the leading cause of cancer-related death worldwide. More than one million cases are diagnosed each year [1]. Lung cancer is morphologically divided into non-small cell lung cancer (NSCLC) and small cell lung cancer, of which NSCLC accounts for about 80% of all lung cancer cases [2]. Despite the growing number of NSCLC genomics studies and targeted therapies, the overall 5-year survival rate is only 15% [3, 4]. This highlights the need for a better understanding of NSCLC biology to improve the prevention, diagnosis and treatment of this cancer [5]. Recently, there is evidence that microRNAs

(miRNAs) may be involved in the pathogenesis of NSCLC, providing new insights into disease biology.

DEK oncogene (DEK) is a ubiquitous protein in multicellular organisms and some single-celled organisms. DEK can promote the repair of DNA damage while also participates in apoptosis [6]. DEK has been already identified as an oncogene and is overexpressed in various malignant tumors, such as colorectal, gastric, neuroendocrine, prostate, breast, and bladder cancer [7–11]. Recent studies indicate that DEK depletion induced astrocytic tumor cell apoptosis with down-regulated expression of Bcl-2 and C-myc; the caspase-3 activity in the astrocytic tumor was also significantly enhanced after the knockdown [12]. Data indicate that DEK plays multiple roles such as promotion of proliferation and migration of cancer cells and facilitation of tumor growth and its maintenance [13]. It can be used as a potential target for astrocytic tumor diagnosis and gene therapy [14].

Correspondence address: Honggang Hu
College of Life Sciences and Bio-engineering,
Beijing Jiaotong University, Beijing, China
e-mail: hg hu@bjtu.edu.cn

DEK overexpression is an important independent risk factor for overall survival in patients with NSCLC. DEK may potentially be used as an independent biomarker for NSCLC prognosis assessment [15].

MicroRNAs (miRNAs) are a class of endogenous non-coding RNAs of approximately 20–24 nucleotides. MiRNAs play important roles in a variety of cellular processes including proliferation, apoptosis, differentiation, and malignant transformation [13–18]. New evidence has revealed that miRNAs influence the initiation and progression of various malignancies, including lung cancer [19–21]. For example, it is reported that miR-145, miR-21, miR-214, and miR-29c have a crucial role in lung cancer [22–25]. miR-1204 is a member of the PVT1 region. Recent studies have found that miR-1204 may improve B cell differentiation and metastasis in breast cancer and can target PITX1 in NSCLC, which may be a poor prognostic factor and a potential therapeutic target for NSCLC [26].

The aim of this study is to find out if miR-1204 targeting DEK in A549 and SPC cells affects cell apoptosis and apoptosis-related pathways by transfecting the cells with miR-1204 or miR-1204 inhibitors. To examine the potential molecular mechanisms of miR-1204 on apoptosis, we assayed the expression of apoptosis-related proteins (Bcl-2 and Bax), activity of caspase-3, caspase-8, and caspase-9, cell morphology and other biological behaviors of NSCLC cells and explored their related mechanisms.

Materials and methods

Cell cultures. The A549 and SPC cell lines of NSCLC were purchased from the American Type Culture Collection (Manassas, VA, USA). The cells were maintained in the Dulbecco's Modified Eagle Medium (DMEM) with 10% fetal bovine serum (FBS), 100 U/ml penicillin, and 100 mg/ml streptomycin in humidified air with 5% CO₂ at 37°C.

miRNA target gene prediction databases. Three miRNA target gene prediction databases were used in research. miRanda: <http://www.microrna.org/>; TargetScan: <http://www.targetscan.org/>; miRWalk: <http://zmf.umm.uni-heidelberg.de/>

The miRNA mimics, siRNAs, cell transfection, and luciferase reporter assays. The miR-1204 mimic, miR-1204 inhibitor, control miRNA, DEK siRNA (si-DEK), and control siRNA (si-Control) were obtained from RiboBio (Guangzhou, China). The A549 and SPC cells were transfected with miR-1204 mimics, miR-1204 inhibitors, control miRNA, DEK siRNA, and control siRNA (50 nM) using riboFECT™ CP transfection (RiboBio) following the manufacturer's instructions.

The 3'-UTR of the DEK gene containing the putative binding sites for miR-1204 was infused into a pGL vector purchased from Hai Chuang Biological Technology Co. (Beijing, China). Cells were calibrated into 24-well plates and cotransfected with miR-1204 mimics, miR-1204 inhibitors, or control miRNA with 0.8 µg luciferase reporter plasmids, or control reporter vectors. Luciferase activity was measured after 48 h of transfection using a dual-luciferase assay system (#E2920; Promega, Madison, WI, USA). Results were normalized to Renilla luciferase activity.

Real-time RT-PCR. Total RNA was extracted from NSCLC cells using Trizol reagent (Invitrogen, Carlsbad, CA, USA). The expression of miR-1204 was evaluated with miDETECT, a Track TMmiRNA qRT-PCR Starter Kit (RiboBio). Real-time PCR was conducted using the GoTaq Real-Time PCR Systems (Promega) to evaluate the DEK expression. B2M level was used as a control for the real-time PCR analysis. The primers for B2M were: sense, 5'-GGCTATCCAGCGTACTCC-3'; anti-sense, 5'-ACGGCAGGCATACTCATC-3'. Primers for DEK were: sense, 5'-TGTTAAGAAAGCAGATAGCAGCACC-3'; anti-sense 5'-ATTAAAGGTTTCATCATCTGA ACTATCCTC-3'. The primers for Bcl-2 were: sense, 5'-GGCTATCCAGCGTACTCC-3'; anti-sense 5'-ACGGCAGGCATACTCATC-3'. The primers for Bax were: sense, 5'-GGAGCTGCAGAGGATGATTG-3'; anti-sense, 5'-CCTCCCAGAAAATGCCATA-3'. The results were analyzed by the following formula: $2^{-\Delta\Delta Ct}$.

Cell viability assay. The cells were seeded into 96-well plates (3×10^4 cells/well) and evaluated for 10–60 h after transfection. The process was repeated thrice in each group. The cell viability was determined by the addition of Cell Counting Kit-8 (MedChem Express, Beijing, China). The CCK-8 kit, based on the chemical reactivity of WST-8 (2-(2-methoxy-4-nitro)-3-(4-nitrophenyl)-5-(2,4-disulfophenyl)-2H-tetrazole monosodium salt), is a rapid and highly sensitive kit widely used for the assessment of cell proliferation and cytotoxicity. WST-8 belongs to the upgraded product of MTT. In the presence of electron coupling reagent WST-8 can be reduced by mitochondrial dehydrogenases to produce highly water-soluble orange-yellow formazan product. Cell proliferation is proportional and inversely proportional to cytotoxicity. The OD value was measured at a wavelength of 450 nm using a microplate reader (TECAN, Vienna, Austria), indirectly reflecting the number of viable cells.

Analysis of cell apoptosis. Annexin V-FITC/PI kit (Keygen Biotech, Jiangsu, China) was used to assay the apoptosis. The cells were collected after 48 hours of transfection in accordance with the manufacturer's instructions. Later, the cells were incubated with Annexin V — fluorescein isothiocyanate and propidium iodide for 15 min in the dark at



Figure 1. Complementarity site for miR-1204 in the 3'-UTR region of DEK

25°C to analyze the percentage of apoptotic cells. Cells were analyzed with a FACS Calibur flow cytometer (NovoCyte, Beijing, China).

Assessment of cell morphology. The cells were assayed after 48 h of transfection and stained with Hoechst 33258 (10 mg/ml) for 20 min at 37°C. Later, after washing the cells with phosphate-buffered saline (PBS), the morphology of the cells was monitored and photographed under TE-2000S fluorescence microscope (Nikon, Tokyo, Japan).

Caspase activity assay. The cells (2 ×) were seeded in 6-well plates and collected 48 h after transfection. The cells were treated according to the protocol described, with Caspase-3, -8, and -9 Fluorescence Assay Kits (Biovision, San Francisco, CA, USA). The activities of caspase-3, -8, and -9 were measured using a fluorescence spectrophotometer (BMG LABTECH, Baden, Stuttgart, Germany) with an excitation wavelength of 400 nm and emission wavelength of 505 nm.

Statistical analysis. Statistical analysis was carried out using the SPSS version 2.0 (IBM, Armonk, NY, USA). Differences between two groups were enumerated using the two-tailed Student's *t*-tests. *P* < 0.05 was considered to illustrate a statistically significant difference, and all values were expressed as mean ± SEM.

Results

The prediction of DEK as a target of miR-1204

Earlier results from the sequencing analysis had indicated that there were large numbers of differentially expressed sequences between the DEK silencing group and the DEK silencing control group in A549 lung cancer cells, especially the miRNA sequences. Hence, it was reasonably presumed that DEK might be regulated by miRNA.

Three miRNA target gene prediction databases (miRanda, TargetScan, and miRWalk) were applied to predict the potential binding sites of miR-1204, where DEK was the target gene (Fig. 1).

The miR-1204 overexpression and inhibition

The study was successful in detecting the expression level of miR-1204, 48 hours after transfection with

miR-1204 mimic, inhibitor, or corresponding control respectively in A549 or SPC cells. The level of expression of miR-1204 in the miR-1204 mimic group was significantly higher than that in the control group, while the expression level of miR-1204 in miR-1204 inhibitor group was apparently lower than that in the control group (Fig. 2A).

The miR-1204 inhibits the activity of DEK 3'-UTR

DEK 3'-UTR luciferase reporter plasmid was co-transfected with miR-1204 mimic, inhibitor, or corresponding control, respectively, into A549 or SPC cells. After transfection for 48 hours, the cells were collected and the luciferase activity was measured. The luciferase activity of A549 and SPC cells transfected with DEK 3'-UTR encoding plasmid was observed to have been decreased in miR-1204 overexpression group. Meanwhile, the luciferase activity with DEK 3'-UTR encoding plasmid was found to have been increased in the miR-1240 inhibition group (Fig. 2B).

The miR-1204 inhibits DEK expression

The miR-1204 mimic, inhibitor, and the corresponding control were transfected in A549 and SPC cells. Thereafter, the DEK mRNA level was examined through the RT-PCR analysis. The resultant data indicated a decrease of DEK expression in the miR-1204 overexpression group when compared with the control group, whereas the DEK expression in the miR-1204 inhibition group indicated an opposite trend (Fig. 2C).

The miR-1204 overexpression increases apoptosis in NSCLC cells

To substantiate the premise that miR-1204 regulates apoptosis in NSCLC cells, we transfected miR-1204 mimic, inhibitor, or the corresponding control, respectively, into A549 and SPC cells, and measured the apoptosis rate using the flow cytometer. The apoptosis rate in miR-1204 overexpression group was found to have significantly increased, while it had decreased in the miR-1204 inhibition group (Fig. 3A–D).

By using Hoechst 333258 staining technique, we observed the changes in the cell morphology with a fluorescence microscope. The miR-1204 overexpression group revealed characteristic morphological features of apoptosis such as brighter nuclei and nuclear condensation (Fig. 3E–F).

The miR-1204 inhibits proliferation of NSCLC cells

The CCK-8 assay showed that miR-1204 inhibited the proliferation of NSCLC cells. We transfected miR-1204 mimic, inhibitor, or corresponding control into A549 and SPC cells, and the cell viability was

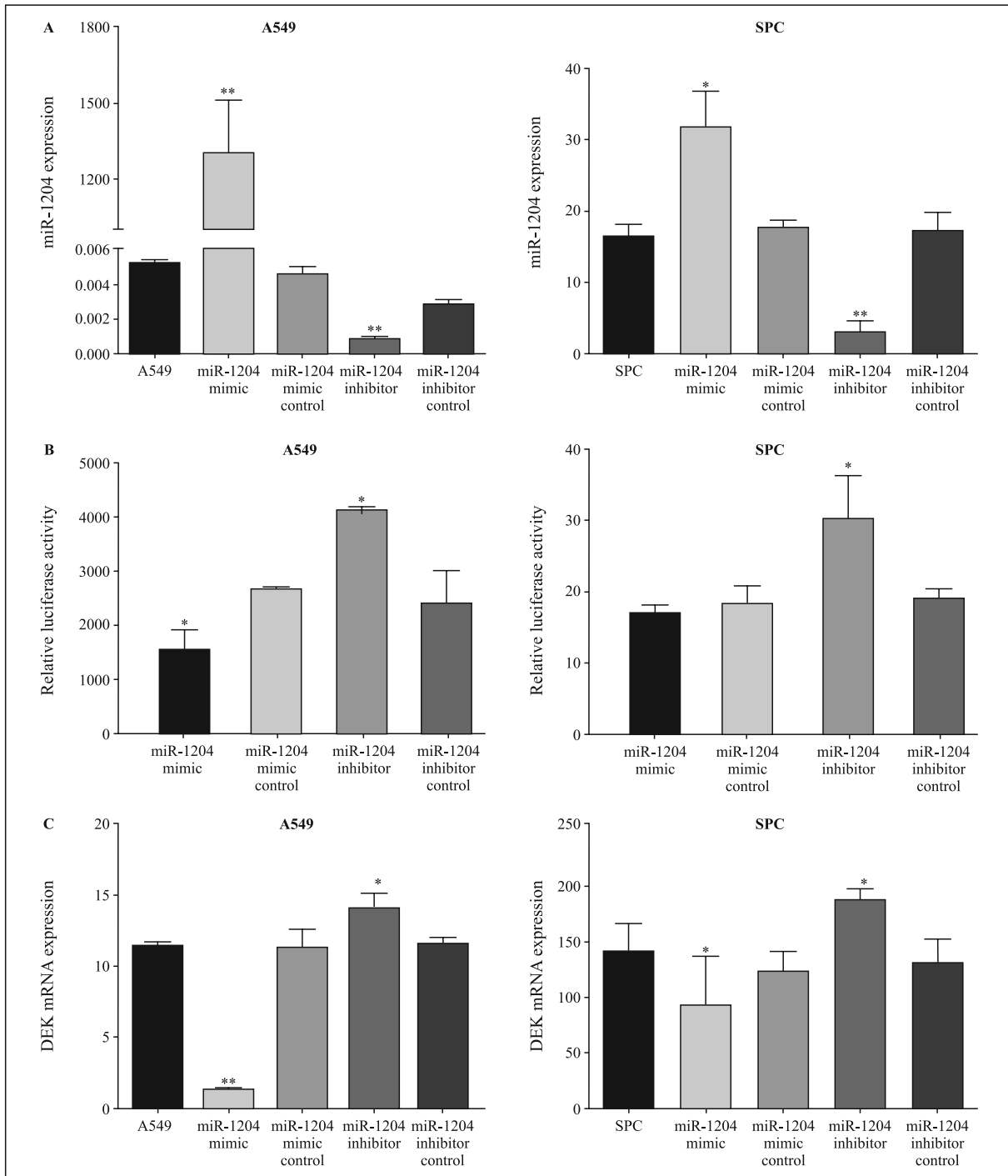


Figure 2. miR-1204 overexpression and inhibition in A549 and SPC cells. **A.** Real-time RT-PCR detection of miR-1204 expression in A549 and SPC cells transfected with miR-1204 mimic (mimic, inhibitor or corresponding controls). **B.** Luciferase activity in A549 and SPC cells transfected with DEK 3'-UTR luciferase reporter plasmid and miR-1204 mimic (mimic, inhibitor or corresponding controls). **C.** Detection of DEK mRNA expression in A549 and SPC cells transfected with miR-1204 mimic (mimic, inhibitor or corresponding controls) by real-time RT-PCR. *P < 0.05, **P < 0.01 compared with mimic or inhibitor control transfected cells. Data are presented as the mean ± SEM of three independent experiments.

determined after 10–60 h. It was found that miR-1204 significantly inhibited the proliferation of NSCLC cells and that the inhibitory effect of miR-1204 was time-dependent (Fig. 4).

Effect of siDEK on expression of Bcl-2 and Bax

We transfected A549 and SPC cells with siDEK or control, and then detected mRNA expression levels of Bcl-2 and Bax. It was demonstrated that Bcl-2

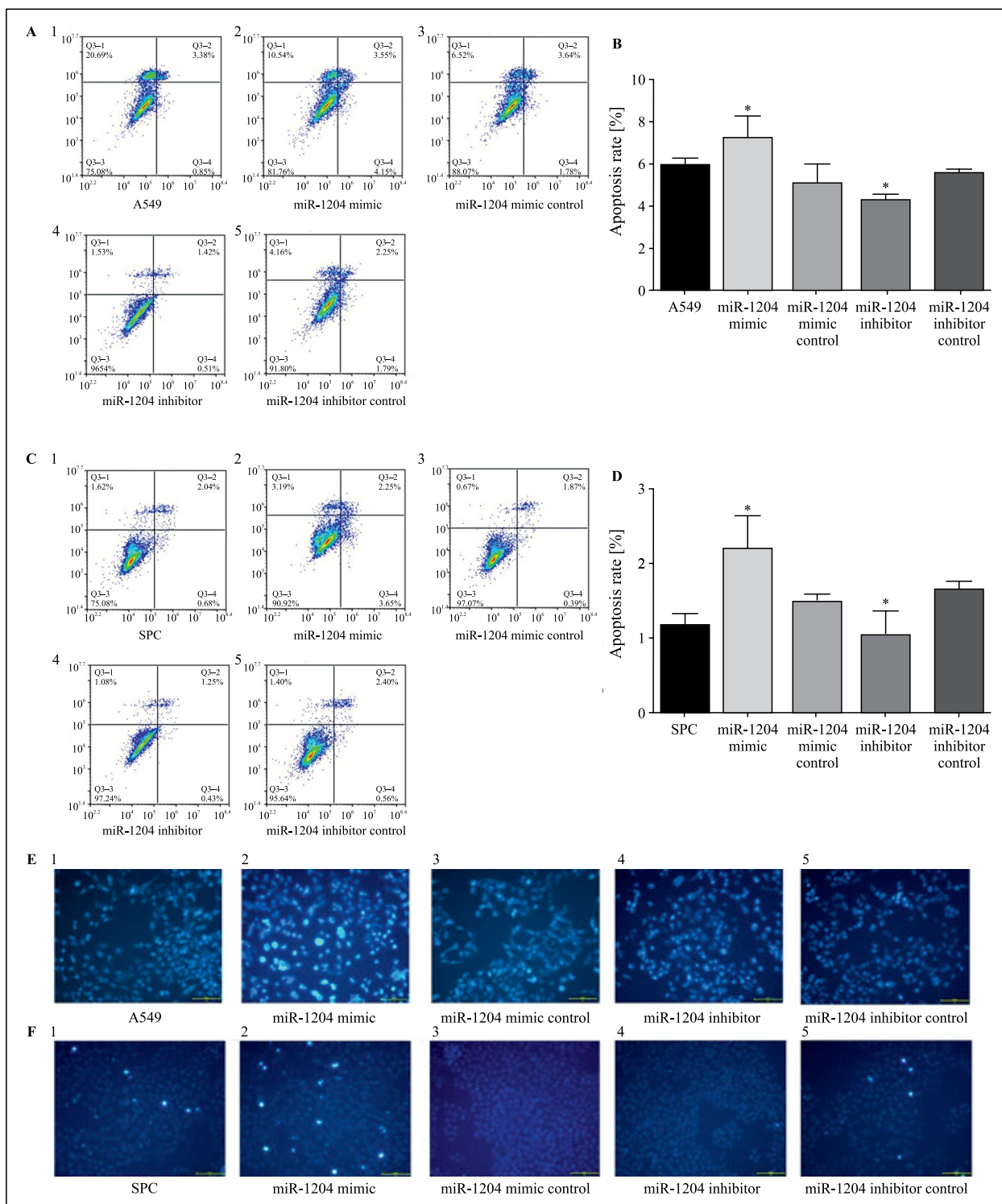


Figure 3. miR-1204 induced apoptosis in A549 and SPC cells. **A.** A549 cells apoptosis was detected by flow cytometry. Numbers 1–5 represent the A549, miR-1204 mimic, miR-1204 mimic control, miR-1204 inhibitor, miR-1204 inhibitor control. **B.** Apoptosis rate in A549 cells after transfected with miR-1204 mimic (mimic, inhibitor or corresponding controls). **C.** SPC cells apoptosis was detected by flow cytometry. Numbers 1–5 represent the SPC, miR-1204 mimic, miR-1204 mimic control, miR-1204 inhibitor, miR-1204 inhibitor control. **D.** Apoptosis rate in SPC cells after transfected with miR-1204 mimic (mimic, inhibitor or corresponding controls). * $P < 0.05$, ** $P < 0.01$ compared with mimic or inhibitor control transfected cells. Data are presented as the mean \pm SEM of three independent experiments. **E.** Nuclear morphology was observed in A549 cells by Hoechst 33258 staining. Numbers 1–5 represent the A549, miR-1204 mimic, miR-1204 mimic control, miR-1204 inhibitor, miR-1204 inhibitor control (scale bars: 100 μ m). **F.** Nuclear morphology was observed in SPC cells by Hoechst 33258 staining. Numbers 1–5 represent the SPC, miR-1204 mimic, miR-1204 mimic control, miR-1204 inhibitor, miR-1204 inhibitor control. Apoptotic cells with bright, nuclear condensation. Scale bars: 100 μ m.

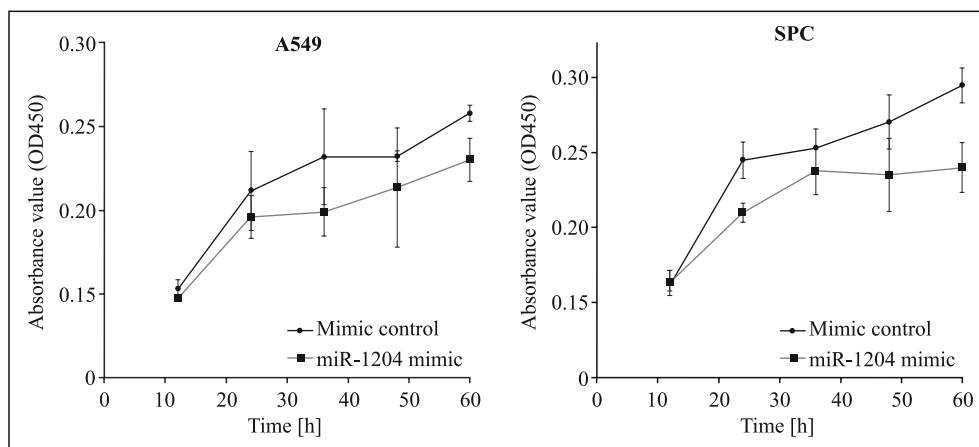


Figure 4. Cell proliferation of A549 and SPC. Cells were transfected with miR-1204 mimic or miR-1204 mimic control and measured by CCK-8 assays. The absorbance was measured at 450 nm as described in Methods.

expression was significantly decreased in siDEK group compared with the control group, while Bax expression was significantly increased (Fig. 5A–C).

Effects of miR-1204 on the expression of Bcl-2 and Bax

The miR-1204 mimic, inhibitor, or corresponding control were transfected into A549 and SPC cells and the mRNA expression levels of Bcl-2 and Bax were determined. The Bcl-2 expression was significantly decreased in the miR-1204 overexpression group compared with the control group, while the Bax expression was significantly increased. In the miR-1204 inhibition group, the opposite results were observed (Fig. 6A, B).

Activation of caspase-3, caspase-8, and caspase-9 during miR-1204-induced apoptosis

The activation of caspases in miR-1204 induced cell apoptosis were investigated sequentially. As Figure 7 shows, in the both cell lines, A549 and SPC, caspase-3 activity increased in the miR-1204 overexpression group. Caspase-9 activity was also observed to have increased. However, no change in caspase-8 activity was detected in any of the cell groups tested (Fig. 7A, B).

Discussion

miR-1204 is a member of the PVT1 region. Recent studies have found that miR-1204 may improve B cell differentiation and metastasis in breast cancer and can target PITX1 in non-small cell lung cancer, which may be a poor prognostic factor and a potential therapeutic target for NSCLC [26]. We used three miRNA target prediction databases (miRanda, TargetScan,

and miRWalk) to determine the target gene of miR-1204. It was found that one target gene of miR-1204 was DEK. The DEK overexpression is prevalent in numerous types of malignant cancers [7–8]. Recently, many studies have found DEK to be carcinogenic in lung cancer formation [9–11]. However, there is very little research on the role of microRNA in DEK. Hence, we proposed the hypothesis that the expression of DEK could be regulated by miR-1204. With an intent to confirm this hypothesis, first, we used luciferase reporter assay to confirm DEK as a target gene of miR-1204. Moreover, we also found that the mRNA levels of DEK were negatively correlated with the expression of miR-1204. The above results provided evidence to substantiate the hypothesis that the expression of DEK in NSCLC was negatively regulated by miR-1204.

Next, to reveal the effects of the miR-1204 on NSCLC cells by regulating DEK, the effect of miR-1204 on apoptosis of A549 and SPC cells were investigated. The apoptosis is a programmed cell death and an important physiological process to maintain homeostasis [27]. Alterations of the apoptosis play a significant role in the survival of abnormal cells and tumorigenesis [28, 29]. Cell apoptosis is characterized by chromatin concentration, DNA fragmentation, membrane foaming, and/or apoptotic bodies [25–30]. In our study, Annexin V FITC analysis of flow cytometry and in vitro Hoechst 33258 staining analysis indicated that the apoptosis rate of A549 and SPC cells in miR-1204 overexpression group was increased, while the apoptosis rate was found to have decreased in the miR-1204 inhibited group. The cell viability of the miR-1204 overexpression group was significantly lower than that of the control group, whereas, the

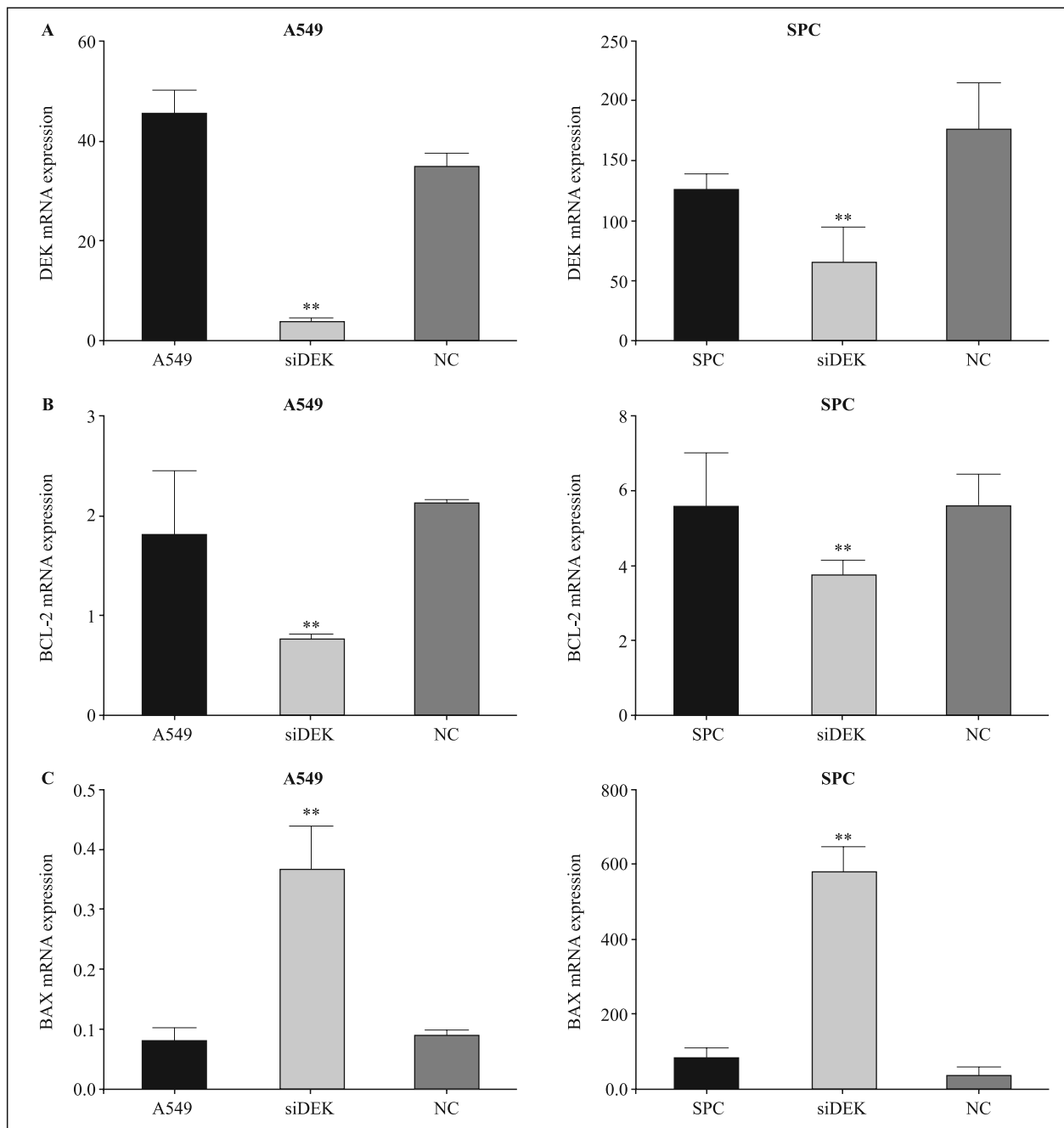


Figure 5. Expression of Bcl-2 and Bax affected by siRNA DEK. **A.** Real-time RT-PCR detection of DEK expression in A549 and SPC cells transfected with siDEK or controls. **B.** Real-time RT-PCR detection of Bcl-2 expression in A549 and SPC cells transfected with siDEK or controls. **C.** Real-time RT-PCR detection of Bax expression in A549 and SPC cells transfected with siDEK or controls. * $P < 0.05$, ** $P < 0.01$ compared with control group of transfected cells. Data are presented as the mean \pm SEM of three independent experiments.

miR-1204 inhibited group expressed an opposite trend. These results evidenced that miR-1204 over-expression induced apoptosis in A549 and SPC cells and inhibited their growth.

Apoptosis is strictly regulated by the multiple pathways and proteins. The members of the Bcl-2

family play a crucial role in inhibiting or promoting apoptosis [31]. The Bcl-2 family consists of anti-apoptotic (Bcl-2, Bcl-w, Bcl-xl, A1) and pro-apoptotic molecules (Bax, Bcl-xs, Bad, Bak, Bid, Bim, Bik) [12, 31]. Bax protein allows some ions and small molecules such as cytochrome C to penetrate the mitochondrial

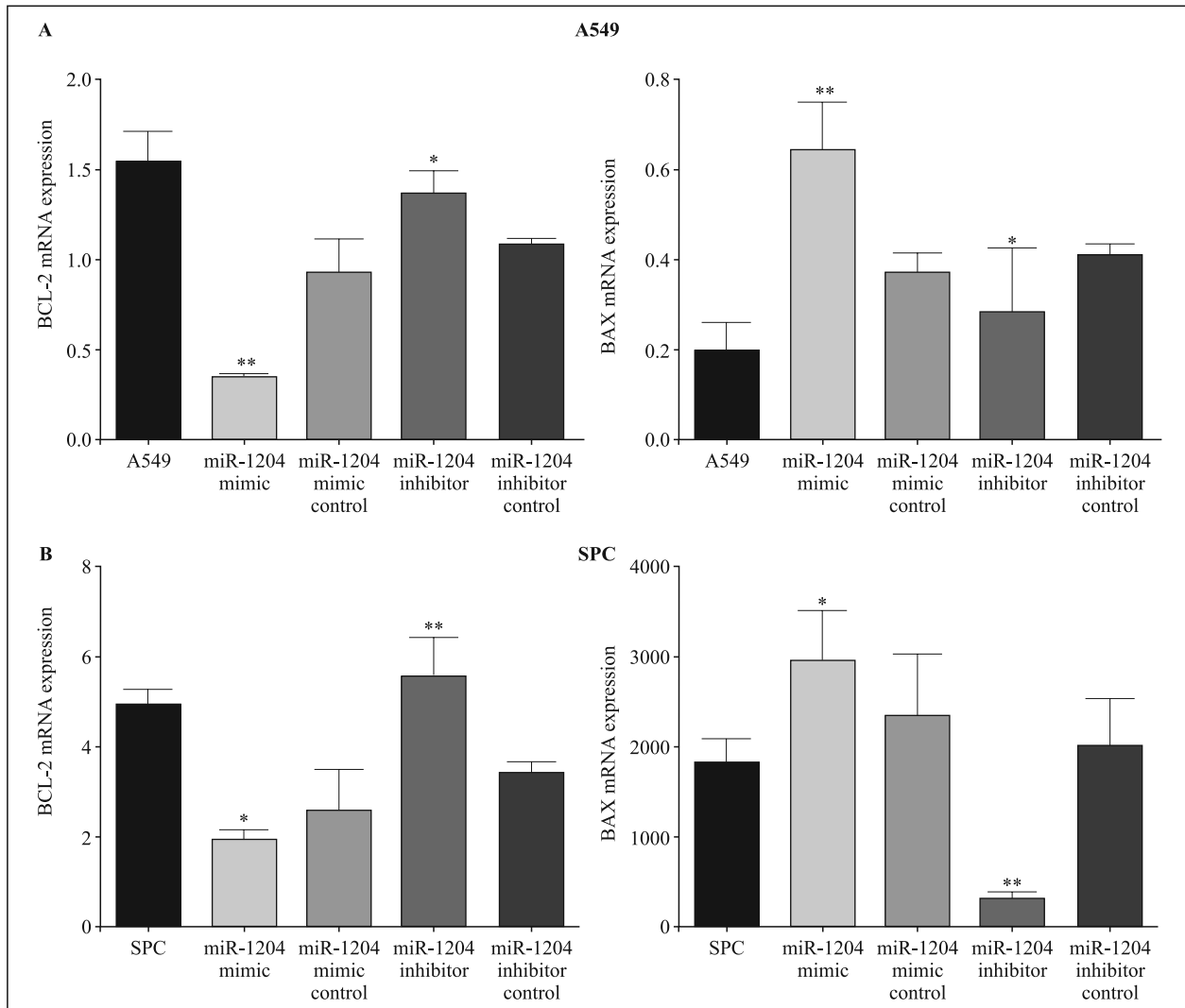


Figure 6. Expression of Bcl-2 and Bax affected by miR-1204. **A.** Bcl-2 and Bax mRNA expression in A549 cells transfected with miR-1204 mimic (mimic, inhibitor or corresponding controls) was detected by real-time PCR. **B.** Bcl-2 and Bax mRNA expression in SPC cells transfected with miR-1204 mimic (mimic, inhibitor or corresponding controls) was detected by real-time RT-PCR. Data are presented as the mean \pm SEM of three independent experiments.

membrane and enter the cytoplasm, leading to apoptosis. However, Bcl-2 has the opposite function. It can counteract the pore-forming activity of Bax and prevent the free penetration of small molecules, thus protecting the cells from imminent apoptosis [12]. This study detected the decreased Bcl-2 expression and the increased Bax expression in NSCLC cells with miR-1204 overexpression, while the miR-1204 inhibition showed opposite results in the cells. Hence, we presume that the Bcl-2 and Bax proteins were involved in the miR-1204-induced apoptosis of A549 and SPC cells.

Caspases are intracellular cysteine protease, which are capable of inducing apoptosis through

two major pathways, namely: (i) FADD-caspase-8/3 and (ii) cytochrome C (CytC)-caspase-9/3 [29]. The FADD-caspase-8/3 pathway is triggered by Fas/FasL, while the cytc-caspase-9/3 pathway is triggered by mitochondrial damage. Later, caspase-3 (an endogenous endonuclease) is activated, leading to the irreversible apoptosis [32, 33]. The activity changes of caspase-3, caspase-8, and caspase-9 by colorimetric assay in increased apoptosis group were determined. The results indicated that the activity of caspase-3 and caspase-9 were significantly increased, while the activity of caspase-8 was not affected by miR-1204. Thus, our results suggest that the main mechanism by which miR-1204 induced cell apoptosis acted *via*

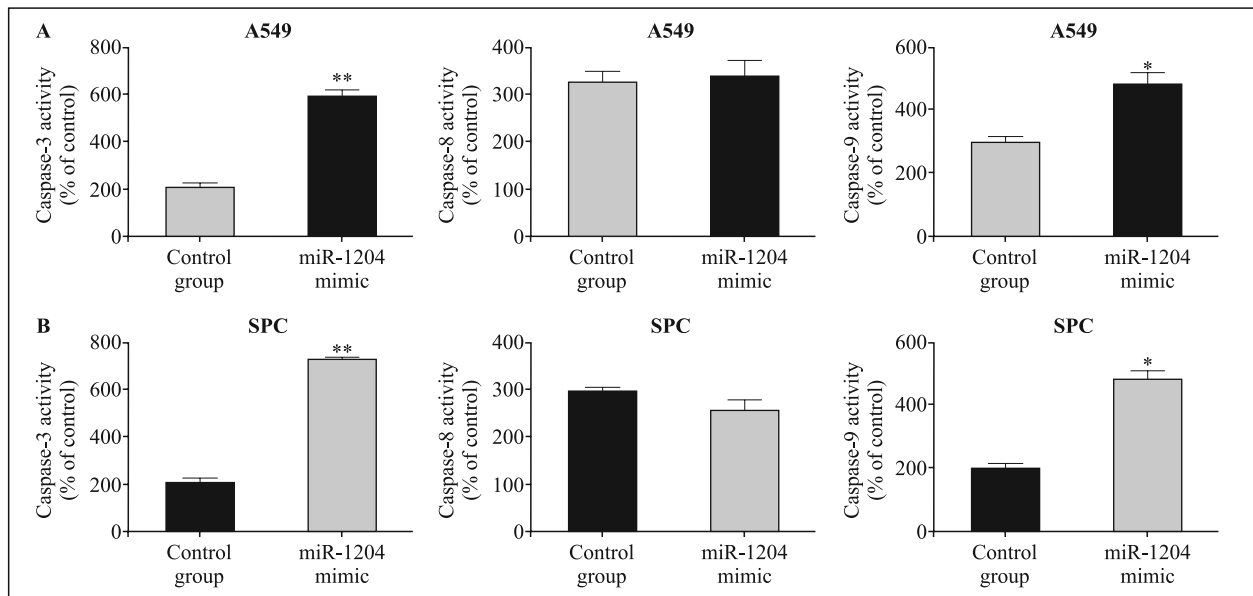


Figure 7. Caspase-3, -8 and -9 activity. Caspases' activities were detected in A549 cells (A) and SPC cells (B). * $P < 0.05$, ** $P < 0.01$ compared with control group of transfected cells. Data are presented as the mean \pm SEM of three independent experiments.

mitochondria-related CytC-caspase-9/3 pathway and not the caspase-8 pathway.

In summary, there are only a few studies related to the role of miRNA in NSCLC, while a better understanding of miRNA-mediated gene expression regulation is needed. Our study is the first to indicate that DEK is negatively regulated by miR-1204 in two NSCLC cell lines and that miR-1204 could promote apoptosis of the NSCLC cells by inhibiting the expression of DEK. The mechanism of miR-1204 induced apoptosis involves down-regulation of Bcl-2 and up-regulation of Bax expression. Besides, this apoptosis is mediated by mitochondria related caspase 9/3 pathway. However, further in-depth research is needed to elucidate the precise mechanisms of these effects.

References

1. Spiro SG, Silvestri GA. One hundred years of lung cancer. *Am J Respir Crit Care Med.* 2005; 172(5): 523–529, doi: [10.1164/rccm.200504-531OE](https://doi.org/10.1164/rccm.200504-531OE), indexed in Pubmed: 15961694.
2. Katanoda K, Yako-Suketomo H. Trends in lung cancer mortality rates in Japan, USA, UK, France and Korea based on the WHO mortality database. *Jpn J Clin Oncol.* 2012; 42(3): 239–240, doi: [10.1093/jco/hys021](https://doi.org/10.1093/jco/hys021), indexed in Pubmed: 22375029.
3. Guttman DM, Kobie J, Grover S, et al. National disparities in treatment package time for resected locally advanced head and neck cancer and impact on overall survival. *Head Neck.* 2018; 40(6): 1147–1155, doi: [10.1002/hed.25091](https://doi.org/10.1002/hed.25091), indexed in Pubmed: 29394465.
4. Fitzmaurice C, Allen C, Barber RM, et al. Global Burden of Disease Cancer Collaboration. Global, Regional, and National Cancer Incidence, Mortality, Years of Life Lost, Years Lived With Disability, and Disability-Adjusted Life-years for 32 Cancer Groups, 1990 to 2015: A Systematic Analysis for the Global Burden of Disease Study. *JAMA Oncol.* 2017; 3(4): 524–548, doi: [10.1001/jamaoncol.2016.5688](https://doi.org/10.1001/jamaoncol.2016.5688), indexed in Pubmed: 27918777.
5. Han R, Zheng R, Zhang S, et al. [Trend analyses on the differences of lung cancer incidence between gender, area and average age in China during 1989–2008]. *Zhongguo Fei Ai Za Zhi.* 2013; 16(9): 445–451, doi: [10.3779/j.issn.1009-3419.2013.09.02](https://doi.org/10.3779/j.issn.1009-3419.2013.09.02), indexed in Pubmed: 24034990.
6. Alexiadis V, Waldmann T, Andersen J, et al. The protein encoded by the proto-oncogene DEK changes the topology of chromatin and reduces the efficiency of DNA replication in a chromatin-specific manner. *Genes Dev.* 2000; 14(11): 1308–1312, indexed in Pubmed: 10837023.
7. Lin L, Piao J, Gao W, et al. DEK over expression as an independent biomarker for poor prognosis in colorectal cancer. *BMC Cancer.* 2013; 13: 366, doi: [10.1186/1471-2407-13-366](https://doi.org/10.1186/1471-2407-13-366), indexed in Pubmed: 23902796.
8. Piao J, Shang Y, Liu S, et al. High expression of DEK predicts poor prognosis of gastric adenocarcinoma. *Diagn Pathol.* 2014; 9: 67, doi: [10.1186/1746-1596-9-67](https://doi.org/10.1186/1746-1596-9-67), indexed in Pubmed: 24650035.
9. Lin D, Dong X, Wang K, et al. Identification of DEK as a potential therapeutic target for neuroendocrine prostate cancer. *Oncotarget.* 2015; 6(3): 1806–1820, doi: [10.18632/oncotarget.2809](https://doi.org/10.18632/oncotarget.2809), indexed in Pubmed: 25544761.
10. Liu S, Wang X, Sun F, et al. DEK overexpression is correlated with the clinical features of breast cancer. *Pathol Int.* 2012; 62(3): 176–181, doi: [10.1111/j.1440-1827.2011.02775.x](https://doi.org/10.1111/j.1440-1827.2011.02775.x), indexed in Pubmed: 22360505.
11. Datta A, Adelson ME, Mogilevkin Y, et al. Oncoprotein DEK as a tissue and urinary biomarker for bladder cancer. *BMC Cancer.* 2011; 11: 234, doi: [10.1186/1471-2407-11-234](https://doi.org/10.1186/1471-2407-11-234), indexed in Pubmed: 21663673.
12. Ashkenazi A, Fairbrother WJ, Levenson JD, et al. From basic apoptosis discoveries to advanced selective BCL-2 family

- inhibitors. *Nat Rev Drug Discov.* 2017; 16(4): 273–284, doi: [10.1038/nrd.2016.253](https://doi.org/10.1038/nrd.2016.253), indexed in Pubmed: 28209992.
13. Yu Le, Huang X, Zhang W, et al. Critical role of DEK and its regulation in tumorigenesis and metastasis of hepatocellular carcinoma. *Oncotarget.* 2016; 7(18): 26844–26855, doi: [10.18632/oncotarget.8565](https://doi.org/10.18632/oncotarget.8565), indexed in Pubmed: 27057626.
 14. Feng T, Liu Y, Li C, et al. DEK proto-oncogene is highly expressed in astrocytic tumors and regulates glioblastoma cell proliferation and apoptosis. *Tumour Biol.* 2017; 39(7): 1010428317716248, doi: [10.1177/1010428317716248](https://doi.org/10.1177/1010428317716248), indexed in Pubmed: 28670979.
 15. Liu X, Qi D, Qi J, et al. Significance of DEK overexpression for the prognostic evaluation of non-small cell lung carcinoma. *Oncol Rep.* 2016; 35(1): 155–162, doi: [10.3892/or.2015.4365](https://doi.org/10.3892/or.2015.4365), indexed in Pubmed: 26530274.
 16. Liu Y, Han Y, Zhang Hu, et al. Synthetic miRNA-mowers targeting miR-183-96-182 cluster or miR-210 inhibit growth and migration and induce apoptosis in bladder cancer cells. *PLoS One.* 2012; 7(12): e52280, doi: [10.1371/journal.pone.0052280](https://doi.org/10.1371/journal.pone.0052280), indexed in Pubmed: 23284967.
 17. Peck BC, Sincavage J, Feinstein S, et al. miR-30 Family Controls Proliferation and Differentiation of Intestinal Epithelial Cell Models by Directing a Broad Gene Expression Program That Includes SOX9 and the Ubiquitin Ligase Pathway. *J Biol Chem.* 2016; 291(31): 15975–15984.
 18. Nie JH, Chen ZH, Shao CL, et al. Analysis of the miRNA-mRNA networks in malignant transformation BEAS-2B cells induced by alpha-particles. *J Toxicol Environ Health A.* 2016; 79(9-10): 427–435, doi: [10.1080/15287394.2016.1176628](https://doi.org/10.1080/15287394.2016.1176628), indexed in Pubmed: 27267825.
 19. Chen Y, Zhu X, Zhang X, et al. Nanoparticles modified with tumor-targeting scFv deliver siRNA and miRNA for cancer therapy. *Mol Ther.* 2010; 18(9): 1650–1656, doi: [10.1038/mt.2010.136](https://doi.org/10.1038/mt.2010.136), indexed in Pubmed: 20606648.
 20. Wang Z, Liao H, Deng Z, et al. miRNA-205 affects infiltration and metastasis of breast cancer. *Biochem Biophys Res Commun.* 2013; 441(1): 139–143, doi: [10.1016/j.bbrc.2013.10.025](https://doi.org/10.1016/j.bbrc.2013.10.025), indexed in Pubmed: 24129185.
 21. Yao Yu, Suo AL, Li ZF, et al. MicroRNA profiling of human gastric cancer. *Mol Med Rep.* 2009; 2(6): 963–970, doi: [10.3892/mmr_00000199](https://doi.org/10.3892/mmr_00000199), indexed in Pubmed: 21475928.
 22. Chen Z, Zeng H, Guo Y, et al. miRNA-145 inhibits non-small cell lung cancer cell proliferation by targeting c-Myc. *J Exp Clin Cancer Res.* 2010; 29: 151, doi: [10.1186/1756-9966-29-151](https://doi.org/10.1186/1756-9966-29-151), indexed in Pubmed: 21092188.
 23. Wang ZX, Bian HB, Wang JR, et al. Prognostic significance of serum miRNA-21 expression in human non-small cell lung cancer. *J Surg Oncol.* 2011; 104(7): 847–851, doi: [10.1002/jso.22008](https://doi.org/10.1002/jso.22008), indexed in Pubmed: 21721011.
 24. Salim H, Akbar NS, Zong D, et al. miRNA-214 modulates radiotherapy response of non-small cell lung cancer cells through regulation of p38MAPK, apoptosis and senescence. *Br J Cancer.* 2012; 107(8): 1361–1373, doi: [10.1038/bjc.2012.382](https://doi.org/10.1038/bjc.2012.382), indexed in Pubmed: 22929890.
 25. Wang H, Zhu Y, Zhao M, et al. miRNA-29c suppresses lung cancer cell adhesion to extracellular matrix and metastasis by targeting integrin β 1 and matrix metalloproteinase2 (MMP2). *PLoS One.* 2013; 8(8): e70192, doi: [10.1371/journal.pone.0070192](https://doi.org/10.1371/journal.pone.0070192), indexed in Pubmed: 23936390.
 26. Jiang W, He Y, Shi Y, et al. MicroRNA-1204 promotes cell proliferation by regulating PITX1 in non-small-cell lung cancer. *Cell Biol Int.* 2019; 43(3): 253–264, doi: [10.1002/cbin.11083](https://doi.org/10.1002/cbin.11083), indexed in Pubmed: 30549141.
 27. Danial NN, Korsmeyer SJ. Cell death: critical control points. *Cell.* 2004; 116(2): 205–219, doi: [10.1016/S0092-8674\(04\)00046-7](https://doi.org/10.1016/S0092-8674(04)00046-7), indexed in Pubmed: 14744432.
 28. Youle RJ, Strasser A. The BCL-2 protein family: opposing activities that mediate cell death. *Nat Rev Mol Cell Biol.* 2008; 9(1): 47–59, doi: [10.1038/nrm2308](https://doi.org/10.1038/nrm2308), indexed in Pubmed: 18097445.
 29. Dejean LM, Martinez-Caballero S, Guo L, et al. Oligomeric Bax is a component of the putative cytochrome c release channel MAC, mitochondrial apoptosis-induced channel. *Mol Biol Cell.* 2005; 16(5): 2424–2432, doi: [10.1091/mbc.e04-12-1111](https://doi.org/10.1091/mbc.e04-12-1111), indexed in Pubmed: 15772159.
 30. Saba JD, Obeid LM, Hannun YA. Ceramide: an intracellular mediator of apoptosis and growth suppression. *Philos Trans R Soc Lond B Biol Sci.* 1996; 351(1336): 233–40; discussion 240, doi: [10.1098/rstb.1996.0021](https://doi.org/10.1098/rstb.1996.0021), indexed in Pubmed: 8650271.
 31. García S, Liz M, Gómez-Reino JJ, et al. Akt activity protects rheumatoid synovial fibroblasts from Fas-induced apoptosis by inhibition of Bid cleavage. *Arthritis Res Ther.* 2010; 12(1): R33, doi: [10.1186/ar2941](https://doi.org/10.1186/ar2941), indexed in Pubmed: 20187936.
 32. Rahman MdA, Kim NH, Huh SO. Cytotoxic effect of gambogic acid on SH-SY5Y neuroblastoma cells is mediated by intrinsic caspase-dependent signaling pathway. *Mol Cell Biochem.* 2013; 377(1-2): 187–196, doi: [10.1007/s11010-013-1584-z](https://doi.org/10.1007/s11010-013-1584-z), indexed in Pubmed: 23404459.
 33. Smith MA, Schnellmann RG. Calpains, mitochondria, and apoptosis. *Cardiovasc Res.* 2012; 96(1): 32–37, doi: [10.1093/cvr/cvs163](https://doi.org/10.1093/cvr/cvs163), indexed in Pubmed: 22581845.

Submitted: 31 March, 2019

Accepted after reviews: 17 May, 2019

Available as AoP: 27 June, 2019

The immunoreactivity of TGF- β 1 in non-alcoholic fatty liver disease

Radoslaw Kempinski¹, Katarzyna Neubauer¹, Elzbieta Poniewierka¹,
Maciej Kaczorowski², Agnieszka Halon²

¹Department of Gastroenterology and Hepatology, Wroclaw Medical University, Wroclaw, Poland

²Department of Pathomorphology and Oncological Cytology, Wroclaw Medical University, Wroclaw, Poland

Abstract

Introduction. Non-alcoholic fatty liver disease (NAFLD) is a common chronic liver disease which becomes a rapidly growing health problem in the Western countries. The development of the disease is most often connected to obesity. NAFLD is also considered as the hepatic manifestation of metabolic syndrome. Transforming growth factor β 1 (TGF- β 1) plays an important role in the pathogenesis of liver fibrosis, being involved in activation of hepatic stellate cells, stimulation of collagen gene transcription, and suppression of matrix metalloproteinase expression. The objective of the study was to evaluate by immunohistochemistry the expression of TGF- β 1 in the liver tissue of NAFLD patients and correlate it with anthropometric, biochemical and routine histological parameters.

Material and methods. The study group consisted of 48 patients with diagnosed NAFLD. Liver steatosis, NAFLD Activity Score (NAS) and METAVIR score of fibrosis were evaluated in liver biopsies. The immunoreactivity of TGF- β 1 was evaluated semi-quantitatively separately in portal, septal, lobular hepatocytic and lobular sinusoidal liver compartments. The results were analyzed in regard to patients' clinical and biochemical parameters.

Results. Neither steatosis nor NAS correlated with TGF- β 1 expression in any liver compartment, whereas METAVIR score of fibrosis was associated with increased immunoreactivity of TGF- β 1 in most of the studied liver compartments. TGF- β 1 immunoreactivity showed positive correlation with patients' age and its expression in septal compartment disclosed positive correlation with body mass index, and waist and hip circumference. Hyaluronic acid serum level was positively and iron concentration was negatively associated with TGF- β 1 expression in the selected consecutive liver compartments.

Conclusions. The immunohistochemical expression of TGF- β 1 may be complementary to routine methods of liver fibrosis evaluation. (*Folia Histochemica et Cytopathologica* 2019, Vol. 57, No. 2, 74–83)

Key words: TGF- β 1; NAFLD; liver fibrosis; liver compartments; IHC; hyaluronic acid; serum iron

Introduction

Non-alcoholic fatty liver disease (NAFLD) is a common chronic liver disease which becomes a rapidly growing health problem in developed countries affecting approximately 30% of population [1].

Its worldwide prevalence continues to increase with the growing problem of obesity [2]. NAFLD involves several liver conditions: simple steatosis, non-alcoholic liver steatohepatitis (NASH), hepatic cirrhosis and hepatocellular carcinoma (HCC). NAFLD is strongly associated with the metabolic syndrome [3]. The course of NAFLD differs between patients and most of them do not develop more advanced forms of the disease. However, 20% of patients with NAFLD progress to NASH and 30% of patients with NASH have liver fibrosis [1]. Age above 50 years and preexisting fibrosis are well established factors that increase the risk of cirrhosis in the course of NAFLD [4].

Correspondence address: Radoslaw Kempinski, MD, PhD
Department of Gastroenterology and Hepatology
Wroclaw Medical University
Borowska 213, 50–556 Wroclaw, Poland
tel. +48 71 733 2120; fax +48 71 733 2129
e-mail: radoslaw.kempinski@umed.wroc.pl

Additionally, NAFLD-associated non-cirrhotic HCC is a currently recognized problem [5].

Transforming growth factor (TGF) β 1 is one of the most important cytokines accelerating liver fibrosis [6]. TGF- β 1 promotes activation of hepatic stellate cells (HSCs), stimulates collagen gene transcription, and suppresses expression of matrix metalloproteinases. Therefore, TGF- β 1 signaling represents a potential therapeutic target in liver fibrosis treatment. Additionally, TGF- β 1 signaling pathway can interfere with hepatocyte proliferation and accelerate HCC progression. TGF- β 1 has been reported to play both tumor-suppressive and tumor-promoting roles [7–9].

Although liver biopsy is still a gold standard to estimate fibrosis stage, new techniques are now under validation for noninvasive fibrosis evaluation, *e.g.* serum marker panels [10], elastography [11], and functional breath tests [12].

The objective of this study was to evaluate the expression of TGF- β 1 in the liver tissue of patients with NAFLD and to correlate it with anthropometric, biochemical and classical histological parameters.

Material and methods

Patients. The study group consisted of 48 consecutive patients with NAFLD diagnosed in Department of Gastroenterology and Hepatology, Wrocław Medical University between 2015 and 2017. The diagnosis was made based on the American Association for the Study of Liver Diseases (AASLD) guidelines [13]. None of 48 consecutive patients with NAFLD had normal body weight index (BMI 18.5–25). Eighteen (40.9%) patients were overweight (BMI 25–30) and 26 (59.1%) were obese (BMI > 30). Mean age of the patients was 46.1 years; no significant difference in the mean age was found between sexes. Characteristics of the patients are shown in Table 1. NAFLD was confirmed by histological examination of liver biopsies (> 5% of hepatocytes containing fat droplets). Indications for liver biopsy included suspicion of steatohepatitis or liver fibrosis in the course of steatosis. Other causes of steatosis were excluded: viral hepatitis, autoimmune hepatitis, hemochromatosis, Wilson's disease, α -1 antitrypsin deficiency and drug-induced hepatic injury. Consumption of ethanol higher than 30 mg/day for men and 20 mg/day for women was also the exclusion criterion. Complete clinical examination with anthropometric measurements and laboratory sampling was performed in all subjects at the beginning of the study. The anthropometric data included body mass, height, body mass index (BMI) calculated as weight (kg) divided by height squared (m^2), waist circumference (WC), hip circumference (HC), waist-to-hip ratio and waist-to-height ratio.

Laboratory tests. Standard blood morphology, liver biochemical tests, serum lipids, fasting glucose, insulin, C-reactive protein, glycated hemoglobin (HbA_{1c}), C-peptide, iron and ferritin concentrations were measured. Additionally, serum was collected for potential markers of inflammation/fibrosis in the liver: hyaluronic acid, fibronectin, alpha-2-macroglobulin, haptoglobin, apolipoprotein A1, TGF- β 1 and TNF. Homeostasis model assessment of insulin resistance (HOMA-IR) was calculated using the following formula: HOMA-IR = fasting glucose (mg/dL) \times fasting insulin (μ U/mL)/405 [14]. History of concomitant diseases/medication was obtained. The diagnosis of metabolic syndrome was established according to Adult Treatment Panel III criteria [15]. The study protocol was approved by local ethics committee with compliance to the Helsinki Declaration. Informed written consent was obtained from each patient before enrollment to the study.

Histopathology. Histological examinations of all samples were performed by the same pathologist. All specimens were considered representative (sample length > 1.5 cm). After the percentage involvement by steatotic hepatocytes was assessed, the patients were divided into subgroups: 5–33% mild, 33–66% moderate or > 66% severe steatosis. NASH Clinical Research Network system for scoring activity and fibrosis in NAFLD was used to calculate NAFLD Activity Score (NAS) ranging 0–8 [16]. Patients with NAS score 0–2 were considered as not having NASH, patients with score 5–8 were diagnosed NASH. Activity scores 3 and 4 were noted as borderline cases (borderline NASH). The staging of fibrosis was assessed using METAVIR score [17] (F0: no fibrosis, F1: portal fibrosis without septa, F2: portal fibrosis with few septa, F3: numerous septa without cirrhosis, F4: cirrhosis).

Immunohistochemistry. From 10% formalin-fixed paraffin embedded blocks 5 μ m-thick sections were cut with microtome and mounted on sialinized slides (code number S3003; DAKO, Glostrup, Denmark). Next, they underwent automated dewaxing, rehydration and heat-induced epitope retrieval in PT Link Pre-Treatment Module for Tissue Specimens (DAKO), with EnVision Target Retrieval Solution (DAKO) used for 30 min incubation at 97°C. Immunohistochemical (IHC) reaction with TGF- β 1 rabbit polyclonal antibody (No. PA5-32628, 1:100 Thermo Scientific Pierce Products, Waltham, MA, USA) was performed in Autostainer Link 48 (DAKO) and EnVision FLEX/HRP system (DAKO) was used for detection. Positive and negative control slides were prepared. As a negative control, liver core biopsy was processed in the abovementioned sequences, but FLEX Mouse Negative Control, Ready-to-Use (DAKO) was used instead of the primary antibody. Human brain

Table 1. Selected clinical characteristics of patients with non-alcoholic fatty liver disease (n = 48)

Age (years)	46.1 ± 10.9 (M: 45.9 ± 9.9; F: 46.3 ± 11.1)
Sex (female/male)	17/31 (35.4%; 54.6%)
Weight [kg]	93.0 ± 16.7 (M: 95.6 ± 14.4; F: 90.1 ± 12.4)
BMI [kg/m ²]	30.9 ± 4.0 (M: 30.1 ± 3.6; F: 32.9 ± 4.2)
HC [cm]	107.1 ± 8.6 (M: 105 ± 7.2; F: 112.3 ± 9.5)
WC [cm]	107.6 ± 9.3 (M: 107.0 ± 9; F: 109 ± 9.7)
WHR	1.004 ± 0.09 (M: 1.02 ± 0.04; F: 0.97 ± 0.04)
WHtR	0.61 ± 0.06 (M: 0.6 ± 0.06; F: 0.61 ± 0.05)
Serum values	
Glucose (< 100 mg/dL)	112.9 ± 47.1
Insulin (μU/mL)	13.1 ± 10.2
HbA _{1c} (3–6.5%)	5.87 ± 0.9
C-peptide [ng/ml]	3.79 ± 2.4
ALT (< 35 U/I)	73.3 ± 33.6
AST (< 31 U/I)	53.0 ± 26.5
GGT (< 38 U/I)	82.8 ± 47.6
Alkaline phosphatase (30–120 U/I)	96.4 ± 37.1
TG (< 150 mg/dl)	233.2 ± 140.1
Iron (70–180 μg/dl)	103.42 ± 38.1
Hyaluronic acid [ng/ml]	29.47 ± 14.1
Haptoglobin [g/l]	1.66 ± 0.9
TGF-β1 [ng/ml]	6.42 ± 3.1
HOMA-IR	2.54 ± 2.54
Clinical status	
Hypertension	27 (56.2%)
Diabetes	14 (29.2%)
Dyslipidemia	20 (41.7%)
Metabolic syndrome	19 (39.6%)

Values represent mean ± SD or the number of patients with percentages in parentheses. Abbreviations: BMI — body mass index; HC — hip circumference; WC — waist circumference; WHR — waist to hip ratio; WHtR — waist to height ratio; ALT — alanine transaminase; AST — aspartate transaminase; GGT — gamma-glutamyl-transferase; TG — triglycerides; HOMA-IR — homeostasis model assessment of insulin resistance.

tissue was used for positive controls. Evaluation of TGF-β1 expression was performed with Olympus BX41 microscope by the same pathologist. TGF-β1 expression was evaluated in following compartments: portal (PC), septal (SC), lobular hepatocytic (LCH) and lobular sinusoidal (LCS). Compartments for the evaluation of IHC reactivity were distinguished by the authors based on the anatomical structure of the liver in attempt to diversify the significance of TGF-β1 in various histological regions of this organ.

Evaluation of the intensity of TGF-β1 immunoreactivity.

The assessment of TGF-β1 expression in each compartment was based on the intensity of the IHC reaction; specimens were given points according to the following scale: no re-

activity — 0, weak reactivity — 1, moderate reactivity — 2, strong reactivity — 3. In LCH and LCS compartments, TGF-β1 expression was also evaluated according to a modified scale of Remmele [18], in which two parameters were considered: percentage of cells with positive cytoplasmatic immunoreactivity (percentage of reactive area) and intensity of staining (Table 2). Final score (0–12 pts.), named Immunoreactive Score (IRS), was calculated by multiplication of points given for percentage of positive cells (0–4 pts.) and intensity of reaction (0–3 pts.).

Statistical analysis. Continuous, normally distributed variables were expressed as mean ± standard deviation. Student's t-test was performed to compare the means between groups

Table 2. Modified scale of Remmele used for evaluation of immunohistochemistry [18]

Percentage of cells with positive cytoplasmatic reaction	Points	Intensity of color reaction	Points
No cells with reaction	0	No reaction	0
< 25% cells with positive reaction	1	Weak reaction	1
25–50% cells with positive reaction	2	Moderate reaction	2
51–75% cells with positive reaction	3	Intensive reaction	3
> 75% with positive reaction	4		

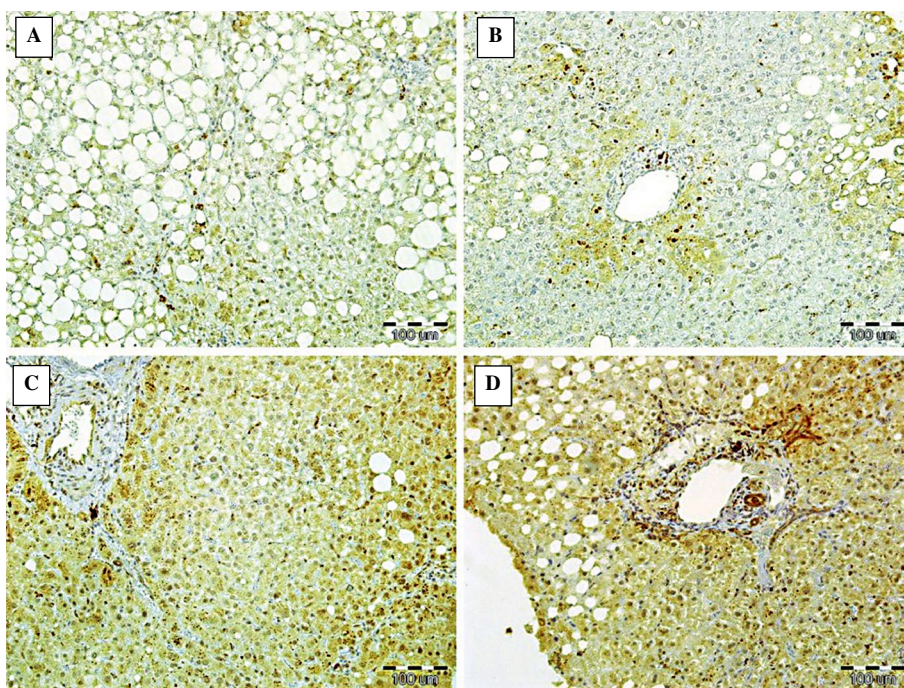


Figure 1. The immunoreactivity of TGF-β1 in liver sections. **A.** Massive hepatic steatosis; low TGF-β1 expression in lobular hepatocytic and lobular sinusoidal compartments. **B.** Centrilobular zone with mild steatosis; moderate TGF-β1 immunoreactivity in lobular hepatocytic and lobular sinusoidal compartments, mostly adjacent to the central vein. **C.** Minimal hepatic steatosis, periportal and lobular zone; high TGF-β1 expression in lobular hepatocytic compartment. **D.** Moderate hepatic steatosis, portal triad zone; high TGF-β1 expression in portal and lobular hepatocytic compartments. TGF-β1 immunoreactivity was visualized in the sections of human liver biopsies as described in Methods.

with normally distributed data. In non-parametric samples, Mann-Whitney U-test was used. Normality of distribution was evaluated with Shapiro-Wilk test. Associations between normally distributed data were analyzed using Pearson correlation coefficient and Spearman correlation was performed in non-parametric data series.

Results

The immunoreactivity of TGF-β1 in the classified liver compartments

Cytoplasmic TGF-β1 expression was observed in various cells of all analyzed liver compartments: besides expression in lobular hepatocytes, TGF-β1

reactivity was present in parasinusoidal stellate cells, sinusoidal Kupffer cells, other infiltrating immune cells as well as fibroblasts in PC and SC (Fig. 1). The distribution of TGF-β1 immunoreactivity in respective compartments, assessed as the intensity of the IHC reaction, is shown in Figure 2. The intensity of TGF-β1 immunoreactivity was compared in pairs between consecutive compartments. The intensity of TGF-β1 immunoreactivity was significantly lower in septal compartment compared with every other compartment (Mann-Whitney U-test, $p < 0.001$, Fig. 3). Additionally, the TGF-β1 immunoreactivity in lobular hepatocytic compartment was significantly lower compared to either portal compartment or lobular

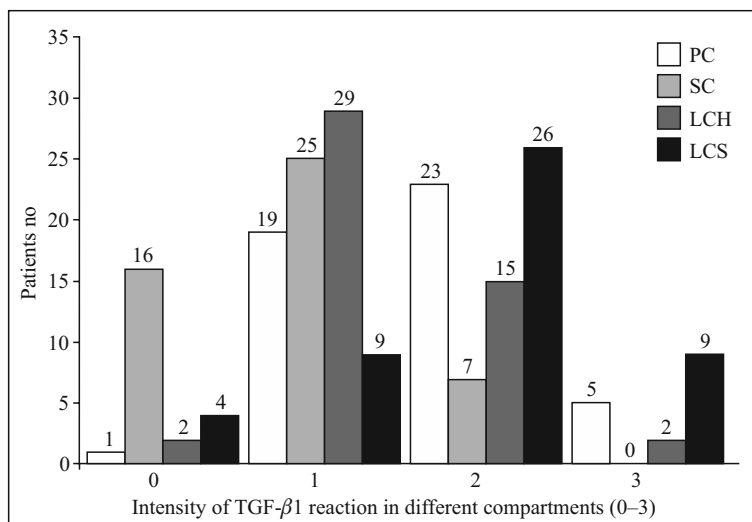


Figure 2. Distribution of the intensity of TGF- β 1 immunoreactivity in respective compartments of the human liver in patients with non-alcoholic fatty liver disease.

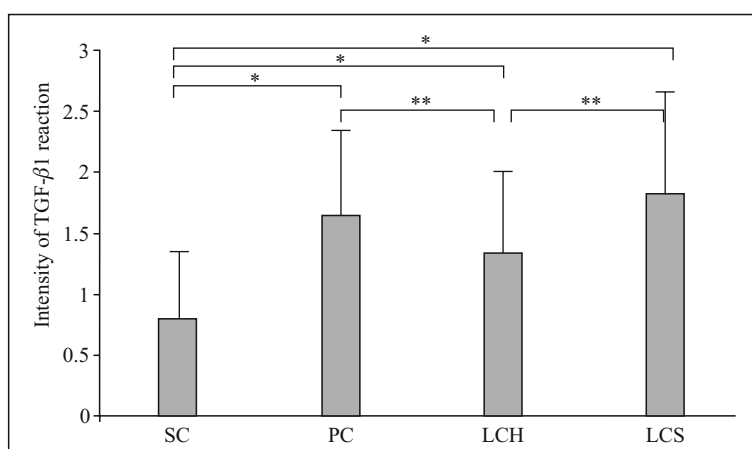


Figure 3. Mean intensity of TGF- β expression in respective compartments of the human liver in patients with non-alcoholic fatty liver disease. Abbreviations: LCH — lobular hepatocytic; LCS — lobular sinusoidal; PC — portal; SC — septal). Data are presented as mean SD. * $p < 0.001$ Septal compartment (SC) compared to PC, LCH, LCS compartments. ** $p < 0.05$ LCH compared to PC and LCS compartments.

sinusoidal compartment (Mann-Whitney U-test, $p < 0.05$, Fig. 3). The distribution of TGF- β 1 immunoreactivity in LCH and LCS, expressed by the IRS score, is shown in Figure 4.

In intercompartmental analysis of TGF- β 1 expression we observed positive correlations between intensity of staining in respective compartments (Table 3).

TGF- β 1 immunoreactivity and clinical characteristics of the NAFLD patients

Associations between TGF- β 1 expression and selected clinical parameters are shown in Table 4. Interestingly, TGF- β 1 immunoexpression correlated with

patients' age in most compartments. No significant differences between sexes were found concerning age. Natural differences in some anthropometric parameters were found between sexes (e.g. higher waist-to-hip ratio, *i.e.* WHR, in men). Moderate positive correlations were found between the intensity of reaction in septal compartment and BMI, waist and hip circumference ($p < 0.05$).

TGF- β 1 immunoexpression and laboratory findings in NAFLD patients

The analysis of TGF- β 1 expression *versus* laboratory parameters revealed moderate negative correlation

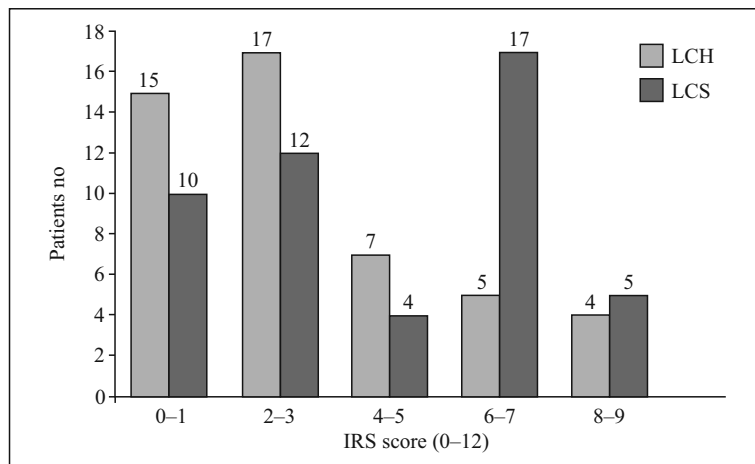


Figure 4. Immunoreactivity score (IRS) in lobular compartments of the human liver in patients with non-alcoholic fatty liver disease.

Table 3. Correlations between intensity of TGF-β1 immunoreactivity in the analyzed liver compartments of liver biopsies in patients with non-alcoholic fatty liver disease

	PC	SC	LCH	LCS
PC	1.0			
SC	0.61*	1.0		
LCH	0.45*	0.62*	1.0	
LCS	0.44*	0.46*	0.42*	1.0

Values express Spearman correlation coefficients. Abbreviations: PC — portal compartment; SC — septal compartment; LCH — lobular hepatocytic compartment; LCS — lobular sinusoidal compartment. SIMILARLY AS IN TABLE 4; *p < 0.01.

with serum iron levels. Negative correlations between iron levels and TGF-β1 immunoreactivity were observed in SC, LCH and LCS, whereas moderate positive correlations with haptoglobin, hyaluronic acid and serum TGF-β1 (Table 4). No correlations were found between TGF-β1 expression in any compartment and following parameters: components of blood morphology, alanine transaminase, aspartate transaminase, gamma-glutamyl-transferase, alkaline phosphatase, serum lipids, ferritin concentration and HOMA (data not shown). Also, no correlations between the expression of TGF-β1 in any compartment and fibronectin, alpha-2-macroglobulin, apolipoprotein A1 and TNF were found (data not shown).

TGF-β1 expression and histopathological characteristics

Neither liver steatosis nor activity of NAFLD (NAS score) were associated with TGF-β1 immunoreactivity. However, both the intensity and IRS of TGF-β1

expression in LCH were weakly, positively associated with the stage of liver fibrosis. Similar weak association was observed in PC, whereas moderate correlation with fibrosis was found in SC (Table 4).

Discussion

Liver fibrosis results from the excessive accumulation of extracellular matrix proteins including collagen that occurs in most types of chronic liver diseases [19]. Fibrosis may affect also other organs such as kidneys and heart, leading to significant changes in their structure and function [20, 21]. There is a wide range of factors causing fibrosis, such as infections, ischemia, radiation or injuries [22–24] and proinflammatory cytokines are thought to be involved in its initiation [25]. It was found that key roles in regulating promotion and acceleration of fibrosis are played by members of the TGF-β superfamily [26]. The members of the TGF-β family belong to the group of the most pleiotropic cytokines, involved in many physiological pathologic processes, e.g. inflammation, tissue repair, cell migration as well as cell differentiation and apoptosis [27]. Studies on TGF-β functions led to development of targeted therapies in kidney and lung fibrosis [28, 29] and in cancer [30]. Accordingly, fibrosis in the course of NAFLD emerges as one of the possible therapeutic targets, next to hepatic steatosis and metabolic stress, bile acid-farnesoid X receptor axis, *de novo* lipogenesis, incretins- and fibroblast growth factors-dependent pathways, inflammation and injury [31].

Furthermore, it has been recently demonstrated that fibrosis stage affects liver-related mortality in patients with NAFLD [32]. Moreover, it predicted overall- and disease-specific survival among patients with NAFLD [33].

Table 4. Correlations between the intensity of TGF- β 1 immunoreactivity in respective liver compartments, age and selected anthropometric, laboratory and histopathological parameters

	PC	SC	LCH	LCS	LCH-IRS	LCS-IRS
Age	0.29*	0.42**	0.17	0.22	0.31*	0.34*
Anthropometric parameters						
Weight	0.01	0.18	0.05	0.20	0.00	0.15
BMI	0.20	0.49**	0.10	0.24	0.14	0.25
HC	0.22	0.53**	0.25	0.16	0.23	0.21
WC	0.18	0.43**	0.07	0.23	0.13	0.24
WHR	-0.05	-0.12	-0.26	0.05	-0.13	0.07
Serum parameters						
HbA _{1c}	0.19	0.31*	0.19	-0.03	0.26	0.05
C-peptide	0.20	0.31*	0.14	0.08	0.08	0.01
Iron	-0.11	-0.37**	-0.38**	-0.32**	-0.32**	-0.31**
Hyaluronic acid	0.36*	0.37**	0.26	0.21	0.35*	0.16
Haptoglobin	0.01	0.37**	0.25	0.03	0.17	0.12
TGF- β 1-serum	0.21	0.38**	0.26	0.15	0.13	0.22
Histopathological indices						
Steatosis	0.19	0.25	0.09	0.14	0.18	0.17
NAS score	-0.18	-0.02	-0.09	-0.19	-0.13	-0.26
Fibrosis	0.32*	0.41**	0.28*	0.18	0.29*	0.16

Values represent correlation coefficients. The intensity of the TGF- β 1 immunoreactivity was assessed as described in Methods. Abbreviations: same as in the legend to Table 1 and Table 3; LCH-IRS, lobular hepatocytic compartment assessed by ImmunoReactive Score; LCS-IRS lobular sinusoidal compartment assessed by ImmunoReactive Score. *p < 0.05; **p < 0.01.

In recognition of the functional and structural heterogeneity of liver histology, we decided to evaluate TGF- β 1 expression in various compartments: periportal, septal and lobular. This division enabled characterization of the spatial distribution of TGF- β 1 in the liver tissue and more detailed analysis of possible correlations between TGF- β 1 reactivity and other clinicopathological parameters. In sinusoidal and hepatocytic compartments, TGF- β 1 staining was evaluated by two methods: intensity of immunoreactivity reaction and ImmunoReactive Score, as described in Methods). The latter technique additionally takes into account the percentage area of the reactive tissue. Overall, both methods led to similar results when TGF- β 1 expression was correlated with other clinicopathological parameters. The immunoreactivity of TGF- β 1 was found in various cells of all hepatic compartments: hepatocytes, stellate cells, Kupffer cells, infiltrating immune cells and fibroblasts. Intercompartmental correlations were strongly positive. IHC reactivity of TGF- β 1 was the strongest in LCS, which highlights the role of Kupffer cells and parasinusoidal hepatic stellate cells as a source of fibrosis-driving TGF- β 1. The intensity of the IHC

reaction was the least pronounced in SC, where the fibrosis evaluated in METAVIR scoring system is usually described. In this compartment TGF- β 1 expression showed strongest positive correlation with the stage of fibrosis (METAVIR). TGF- β 1 expression did not depend on the stage of liver steatosis. Also, the intensity of inflammation evaluated as NAS did not correlate with TGF- β 1 reactivity.

To the best of our knowledge, the distribution of TGF- β 1 has not been comprehensively studied in patients with NAFLD. However, Farrington *et al.* studied TGF- β 1 expression in fibrotic livers in patients with biliary atresia [34]. They analyzed two areas, portal and lobular, and found that TGF- β 1 was present predominantly in the latter. Consistently, we observed highest TGF- β 1 reactivity in lobular compartments. However, periportal staining for TGF- β 1 was also prominent in our study. This discrepancy may be related to the depletion of bile ducts in advanced biliary atresia. Biliary epithelium is known to be a source of TGF- β 1 and thus contributes to fibrosis [35].

In standard histological liver scoring systems most attention is paid to the periportal and septal regions. Our study showed that TGF- β 1 distribution is diffused

in liver lobules and not only limited to periportal and septal regions.

Considering anthropometrical data, we found that intensity of TGF- β 1 expression in SC correlated with BMI, waist and hip circumference, but not with absolute weight and waist-to-hip ratio. This indirectly suggests that BMI better than WHR predicts liver fibrosis. Our observation is in line with the reports of other authors. Angulo *et al.* implemented BMI in NAFLD Fibrosis Score, which is a well-established non-invasive system identifying liver fibrosis in NAFLD patients [36].

In our study we correlated selected biochemical parameters with the intensity of TGF- β 1 expression in the liver. We found positive associations with serum concentrations of HbA_{1c}, C-peptide and hyaluronic acid, haptoglobin, and TGF- β 1 in septal compartment. This is not surprising since haptoglobin in well-known marker of liver fibrosis and is incorporated in Fibrotest formula [37]. Serum concentration of hyaluronic acid seems to be biomarker of fibrosis in chronic liver diseases of different etiologies [38] such as non-alcoholic fatty liver disease [39], alcoholic fatty liver disease [40], and viral hepatitis [41].

An interesting, unexpected observation was the finding of a reverse correlation between TGF- β 1 immunoreactivity in most liver compartments and serum iron concentration. Trying to explain this phenomenon in humans we conjecture on a possible negative feedback mechanism that limits liver fibrosis. TGF- β 1 was recently recognized as an activator of hepcidin mRNA expression in isolated human hepatocytes [42]. Hepcidin maintains serum iron concentration by controlling dietary uptake of iron from duodenal enterocytes. It binds to cellular ferroportin to trigger its internalization and degradation, which blocks the transport of iron from enterocytes to portal circulation [43]. TGF- β 1 downregulates iron serum level in a hepcidin-dependent mechanism [44] which might explain the inverse correlation between iron levels and TGF- β 1 expression in our study. However, in an animal model Han *et al.* [45] showed decreased activation of hepatic stellate cells and TGF- β 1 effect by hepcidin. The authors demonstrated an inhibition of Smad3 phosphorylation in HSCs by hepcidin which may account for the anti-fibrotic effect of hepcidin. Based on this experimental study, a new model of fibrosis downregulation can be proposed: activation of HSCs results in TGF- β 1 synthesis and secretion that increases hepcidin expression. The overexpression of hepcidin, in turn, downregulates HSCs activation and thus self-limits liver fibrosis. Thus, studies of new fibrosis markers may lead not only to the improvement of the scoring systems but also to the development of

the new therapeutic strategies. It has to be noted that one of the limitations of our study is fact that majority of patients were men although this is consistent with the results of the epidemiological studies [46].

Conclusions

TGF- β 1 might be a promising immunohistochemical marker of the liver fibrosis in NAFLD patients; however, further studies on larger group of patients with NAFLD are required.

The assessment of the immunohistochemical reactivity of TGF- β 1 can be complementary to routine methods of liver fibrosis evaluation.

Acknowledgments

The study was supported by Polish National Science Center grant No NN 519463239.

Disclosure of conflict of interest

The authors declare no competing interests.

References

- Vernon G, Baranova A, Younossi ZM. Systematic review: the epidemiology and natural history of non-alcoholic fatty liver disease and non-alcoholic steatohepatitis in adults. *Aliment Pharmacol Ther.* 2011; 34(3): 274–285, doi: [10.1111/j.1365-2036.2011.04724.x](https://doi.org/10.1111/j.1365-2036.2011.04724.x), indexed in Pubmed: [21623852](https://pubmed.ncbi.nlm.nih.gov/21623852/).
- Corey KE, Kaplan LM. Obesity and liver disease: the epidemic of the twenty-first century. *Clin Liver Dis.* 2014; 18(1): 1–18, doi: [10.1016/j.cld.2013.09.019](https://doi.org/10.1016/j.cld.2013.09.019), indexed in Pubmed: [24274861](https://pubmed.ncbi.nlm.nih.gov/24274861/).
- Musso G, Gambino R, Bo S, et al. Should nonalcoholic fatty liver disease be included in the definition of metabolic syndrome? A cross-sectional comparison with Adult Treatment Panel III criteria in nonobese nondiabetic subjects. *Diabetes Care.* 2008; 31(3): 562–568, doi: [10.2337/dc07-1526](https://doi.org/10.2337/dc07-1526), indexed in Pubmed: [18056890](https://pubmed.ncbi.nlm.nih.gov/18056890/).
- Argo CK, Northup PG, Al-Osaimi AMS, et al. Systematic review of risk factors for fibrosis progression in non-alcoholic steatohepatitis. *J Hepatol.* 2009; 51(2): 371–379, doi: [10.1016/j.jhep.2009.03.019](https://doi.org/10.1016/j.jhep.2009.03.019), indexed in Pubmed: [19501928](https://pubmed.ncbi.nlm.nih.gov/19501928/).
- Perumpail RB, Liu A, Wong RJ, et al. Pathogenesis of hepatocarcinogenesis in non-cirrhotic nonalcoholic fatty liver disease: Potential mechanistic pathways. *World J Hepatol.* 2015; 7(22): 2384–2388, doi: [10.4254/wjh.v7.i22.2384](https://doi.org/10.4254/wjh.v7.i22.2384), indexed in Pubmed: [26464753](https://pubmed.ncbi.nlm.nih.gov/26464753/).
- Inagaki Y, Okazaki I. Emerging insights into Transforming growth factor beta Smad signal in hepatic fibrogenesis. *Gut.* 2007; 56(2): 284–292, doi: [10.1136/gut.2005.088690](https://doi.org/10.1136/gut.2005.088690), indexed in Pubmed: [17303605](https://pubmed.ncbi.nlm.nih.gov/17303605/).
- Seoane J, Gomis RR. TGF- Family Signaling in Tumor Suppression and Cancer Progression. *Cold Spring Harb Perspect Biol.* 2017; 9(12), doi: [10.1101/cshperspect.a022277](https://doi.org/10.1101/cshperspect.a022277), indexed in Pubmed: [28246180](https://pubmed.ncbi.nlm.nih.gov/28246180/).
- Bellam N, Pasche B. Tgf-beta signaling alterations and colon cancer. *Cancer Treat Res.* 2010; 155: 85–103, doi: [10.1007/978-1-4419-6033-7_5](https://doi.org/10.1007/978-1-4419-6033-7_5), indexed in Pubmed: [20517689](https://pubmed.ncbi.nlm.nih.gov/20517689/).
- Shi C, Chen Y, Chen Y, et al. CD4⁺ CD25⁺ regulatory T cells promote hepatocellular carcinoma invasion via TGF- β 1-in-

- duced epithelial–mesenchymal transition. *OncoTargets and Therapy*. 2018; Volume 12: 279–289, doi: [10.2147/ott.s172417](https://doi.org/10.2147/ott.s172417).
10. Zhou JH, Cai JJ, She ZG, et al. Noninvasive evaluation of nonalcoholic fatty liver disease: Current evidence and practice. *World J Gastroenterol*. 2019; 25(11): 1307–1326, doi: [10.3748/wjg.v25.i11.1307](https://doi.org/10.3748/wjg.v25.i11.1307), indexed in Pubmed: [30918425](https://pubmed.ncbi.nlm.nih.gov/30918425/).
 11. Mikolasevic I, Orlic L, Franjic N, et al. Transient elastography (FibroScan®) with controlled attenuation parameter in the assessment of liver steatosis and fibrosis in patients with nonalcoholic fatty liver disease - Where do we stand? *World J Gastroenterol*. 2016; 22(32): 7236–7251, doi: [10.3748/wjg.v22.i32.7236](https://doi.org/10.3748/wjg.v22.i32.7236), indexed in Pubmed: [27621571](https://pubmed.ncbi.nlm.nih.gov/27621571/).
 12. Kempinski R, Neubauer K, Wiczorek S, et al. 13C-Methacetin Breath Testing in Patients with Non-Alcoholic Fatty Liver Disease. *Adv Clin Exp Med*. 2016; 25(1): 77–81, doi: [10.17219/acem/60878](https://doi.org/10.17219/acem/60878), indexed in Pubmed: [26935501](https://pubmed.ncbi.nlm.nih.gov/26935501/).
 13. Chalasani N, Younossi Z, Lavine JE, et al. The diagnosis and management of non-alcoholic fatty liver disease: practice Guideline by the American Association for the Study of Liver Diseases, American College of Gastroenterology, and the American Gastroenterological Association. *Hepatology*. 2012; 55: 2005–2013, doi: [10.1053/j.gastro.2012.04.001](https://doi.org/10.1053/j.gastro.2012.04.001); indexed in Pubmed: [22488764](https://pubmed.ncbi.nlm.nih.gov/22488764/).
 14. Okita K, Iwahashi H, Kozawa J, et al. Homeostasis model assessment of insulin resistance for evaluating insulin sensitivity in patients with type 2 diabetes on insulin therapy. *Endocrine Journal*. 2013; 60(3): 283–290, doi: [10.1507/endocrj.ej12-0320](https://doi.org/10.1507/endocrj.ej12-0320).
 15. Executive Summary of the Third Report of the National Cholesterol Education Program (NCEP) Expert Panel on Detection, Evaluation, and Treatment of High Blood Cholesterol in Adults (Adult Treatment Panel III) *JAMA*. 2001; 285(19): 2486–2497, doi: [10.1001/jama.285.19.2486](https://doi.org/10.1001/jama.285.19.2486).
 16. Kleiner D, Brunt E, Natta MV, et al. Design and validation of a histological scoring system for nonalcoholic fatty liver disease. *Hepatology*. 2005; 41(6): 1313–1321, doi: [10.1002/hep.20701](https://doi.org/10.1002/hep.20701).
 17. Bedossa P, Poynard T. An algorithm for the grading of activity in chronic hepatitis C. The METAVIR Cooperative Study Group. *Hepatology*. 1996; 24(2): 289–293, doi: [10.1002/hep.510240201](https://doi.org/10.1002/hep.510240201), indexed in Pubmed: [8690394](https://pubmed.ncbi.nlm.nih.gov/8690394/).
 18. Remmele W, Schicketanz KH. Immunohistochemical determination of estrogen and progesterone receptor content in human breast cancer. Computer-assisted image analysis (QIC score) vs. subjective grading (IRS). *Pathol Res Pract*. 1993; 189(8): 862–866, doi: [10.1016/S0344-0338\(11\)81095-2](https://doi.org/10.1016/S0344-0338(11)81095-2), indexed in Pubmed: [8302707](https://pubmed.ncbi.nlm.nih.gov/8302707/).
 19. Bataller R, Brenner DA. Liver fibrosis. *J Clin Invest*. 2005; 115(2): 209–218, doi: [10.1172/JCI24282](https://doi.org/10.1172/JCI24282), indexed in Pubmed: [15690074](https://pubmed.ncbi.nlm.nih.gov/15690074/).
 20. Tanaka T. A mechanistic link between renal ischemia and fibrosis. *Med Mol Morphol*. 2017; 50(1): 1–8, doi: [10.1007/s00795-016-0146-3](https://doi.org/10.1007/s00795-016-0146-3), indexed in Pubmed: [27438710](https://pubmed.ncbi.nlm.nih.gov/27438710/).
 21. Frohlich ED. Fibrosis and ischemia: the real risks in hypertensive heart disease. *Am J Hypertens*. 2001; 14(6 Pt 2): 194S–199S, doi: [10.1016/s0895-7061\(01\)02088-x](https://doi.org/10.1016/s0895-7061(01)02088-x), indexed in Pubmed: [11411756](https://pubmed.ncbi.nlm.nih.gov/11411756/).
 22. Martin P, Nunan R. Cellular and molecular mechanisms of repair in acute and chronic wound healing. *Br J Dermatol*. 2015; 173(2): 370–378, doi: [10.1111/bjd.13954](https://doi.org/10.1111/bjd.13954), indexed in Pubmed: [26175283](https://pubmed.ncbi.nlm.nih.gov/26175283/).
 23. Stubblefield MD. Clinical Evaluation and Management of Radiation Fibrosis Syndrome. *Phys Med Rehabil Clin N Am*. 2017; 28(1): 89–100, doi: [10.1016/j.pmr.2016.08.003](https://doi.org/10.1016/j.pmr.2016.08.003), indexed in Pubmed: [27913002](https://pubmed.ncbi.nlm.nih.gov/27913002/).
 24. Bacmeister L, Schwarzl M, Warnke S, et al. Inflammation and fibrosis in murine models of heart failure. *Basic Res Cardiol*. 2019; 114(3): 19, doi: [10.1007/s00395-019-0722-5](https://doi.org/10.1007/s00395-019-0722-5), indexed in Pubmed: [30887214](https://pubmed.ncbi.nlm.nih.gov/30887214/).
 25. Pérez L, Muñoz-Durango N, Riedel CA, et al. Endothelial-to-mesenchymal transition: Cytokine-mediated pathways that determine endothelial fibrosis under inflammatory conditions. *Cytokine Growth Factor Rev*. 2017; 33: 41–54, doi: [10.1016/j.cytogfr.2016.09.002](https://doi.org/10.1016/j.cytogfr.2016.09.002), indexed in Pubmed: [27692608](https://pubmed.ncbi.nlm.nih.gov/27692608/).
 26. Walton KL, Johnson KE, Harrison CA. Targeting TGF- β Mediated SMAD Signaling for the Prevention of Fibrosis. *Front Pharmacol*. 2017; 8: 461, doi: [10.3389/fphar.2017.00461](https://doi.org/10.3389/fphar.2017.00461), indexed in Pubmed: [28769795](https://pubmed.ncbi.nlm.nih.gov/28769795/).
 27. Biernacka A, Dobaczewski M, Frangogiannis NG. TGF- β signaling in fibrosis. *Growth Factors*. 2011; 29(5): 196–202, doi: [10.3109/08977194.2011.595714](https://doi.org/10.3109/08977194.2011.595714), indexed in Pubmed: [21740331](https://pubmed.ncbi.nlm.nih.gov/21740331/).
 28. Isaka Y. Targeting TGF- β Signaling in Kidney Fibrosis. *Int J Mol Sci*. 2018; 19(9), doi: [10.3390/ijms19092532](https://doi.org/10.3390/ijms19092532), indexed in Pubmed: [30150520](https://pubmed.ncbi.nlm.nih.gov/30150520/).
 29. Fernandez IE, Eickelberg O. The impact of TGF- β on lung fibrosis: from targeting to biomarkers. *Proc Am Thorac Soc*. 2012; 9(3): 111–116, doi: [10.1513/pats.201203-023AW](https://doi.org/10.1513/pats.201203-023AW), indexed in Pubmed: [22802283](https://pubmed.ncbi.nlm.nih.gov/22802283/).
 30. Xie F, Ling Li, van Dam H, et al. TGF- β signaling in cancer metastasis. *Acta Biochim Biophys Sin (Shanghai)*. 2018; 50(1): 121–132, doi: [10.1093/abbs/gmx123](https://doi.org/10.1093/abbs/gmx123), indexed in Pubmed: [29190313](https://pubmed.ncbi.nlm.nih.gov/29190313/).
 31. Rotman Y, Sanyal AJ. Current and upcoming pharmacotherapy for non-alcoholic fatty liver disease. *Gut*. 2017; 66(1): 180–190, doi: [10.1136/gutjnl-2016-312431](https://doi.org/10.1136/gutjnl-2016-312431), indexed in Pubmed: [27646933](https://pubmed.ncbi.nlm.nih.gov/27646933/).
 32. Dulai PS, Singh S, Patel J, et al. Increased risk of mortality by fibrosis stage in nonalcoholic fatty liver disease: Systematic review and meta-analysis. *Hepatology*. 2017; 65(5): 1557–1565, doi: [10.1002/hep.29085](https://doi.org/10.1002/hep.29085), indexed in Pubmed: [28130788](https://pubmed.ncbi.nlm.nih.gov/28130788/).
 33. Ekstedt M, Hagström H, Nasr P, et al. Fibrosis stage is the strongest predictor for disease-specific mortality in NAFLD after up to 33 years of follow-up. *Hepatology*. 2015; 61(5): 1547–1554, doi: [10.1002/hep.27368](https://doi.org/10.1002/hep.27368), indexed in Pubmed: [25125077](https://pubmed.ncbi.nlm.nih.gov/25125077/).
 34. Farrington C, Novak D, Liu C, et al. Immunohistochemical localization of transforming growth factor β -1 and its relationship with collagen expression in advanced liver fibrosis due to biliary atresia. *Clin Exp Gastroenterol*. 2010; 3: 185–191, doi: [10.2147/CEG.S14220](https://doi.org/10.2147/CEG.S14220), indexed in Pubmed: [21694865](https://pubmed.ncbi.nlm.nih.gov/21694865/).
 35. Sedlacek N, Jia JD, Bauer M, et al. Proliferating bile duct epithelial cells are a major source of connective tissue growth factor in rat biliary fibrosis. *Am J Pathol*. 2001; 158(4): 1239–1244, doi: [10.1016/S0002-9440\(10\)64074-6](https://doi.org/10.1016/S0002-9440(10)64074-6), indexed in Pubmed: [11290541](https://pubmed.ncbi.nlm.nih.gov/11290541/).
 36. Angulo P, Hui JM, Marchesini G, et al. The NAFLD fibrosis score: a noninvasive system that identifies liver fibrosis in patients with NAFLD. *Hepatology*. 2007; 45(4): 846–854, doi: [10.1002/hep.21496](https://doi.org/10.1002/hep.21496), indexed in Pubmed: [17393509](https://pubmed.ncbi.nlm.nih.gov/17393509/).
 37. Vilar-Gomez E, Chalasani N. Non-invasive assessment of non-alcoholic fatty liver disease: Clinical prediction rules and blood-based biomarkers. *J Hepatol*. 2018; 68(2): 305–315, doi: [10.1016/j.jhep.2017.11.013](https://doi.org/10.1016/j.jhep.2017.11.013), indexed in Pubmed: [29154965](https://pubmed.ncbi.nlm.nih.gov/29154965/).
 38. Orasan OH, Ciulei G, Cozma A, et al. Hyaluronic acid as a biomarker of fibrosis in chronic liver diseases of different etiologies. *Clujul Med*. 2016; 89(1): 24–31, doi: [10.15386/cjmed-554](https://doi.org/10.15386/cjmed-554), indexed in Pubmed: [27004022](https://pubmed.ncbi.nlm.nih.gov/27004022/).

39. Santos VN, Leite-Mór MMB, Kondo M, et al. Serum laminin, type IV collagen and hyaluronan as fibrosis markers in non-alcoholic fatty liver disease. *Braz J Med Biol Res.* 2005; 38(5): 747–753, doi: [10.1590/s0100-879x2005000500012](https://doi.org/10.1590/s0100-879x2005000500012), indexed in Pubmed: [15917956](https://pubmed.ncbi.nlm.nih.gov/15917956/).
40. Sowa JP, Atmaca Ö, Kahraman A, et al. Non-invasive separation of alcoholic and non-alcoholic liver disease with predictive modeling. *PLoS One.* 2014; 9(7): e101444, doi: [10.1371/journal.pone.0101444](https://doi.org/10.1371/journal.pone.0101444), indexed in Pubmed: [24988316](https://pubmed.ncbi.nlm.nih.gov/24988316/).
41. Halfon P, Bourlière M, Pénaranda G, et al. Accuracy of hyaluronic acid level for predicting liver fibrosis stages in patients with hepatitis C virus. *Comp Hepatol.* 2005; 4: 6, doi: [10.1186/1476-5926-4-6](https://doi.org/10.1186/1476-5926-4-6), indexed in Pubmed: [16008833](https://pubmed.ncbi.nlm.nih.gov/16008833/).
42. Chen S, Feng T, Vujić Spasić M, et al. Transforming Growth Factor β 1 (TGF- β 1) Activates Hepcidin mRNA Expression in Hepatocytes. *J Biol Chem.* 2016; 291(25): 13160–13174, doi: [10.1074/jbc.M115.691543](https://doi.org/10.1074/jbc.M115.691543), indexed in Pubmed: [27129231](https://pubmed.ncbi.nlm.nih.gov/27129231/).
43. Ganz T, Nemeth E. Hepcidin and iron homeostasis. *Biochim Biophys Acta.* 2012; 1823(9): 1434–1443, doi: [10.1016/j.bbamcr.2012.01.014](https://doi.org/10.1016/j.bbamcr.2012.01.014), indexed in Pubmed: [22306005](https://pubmed.ncbi.nlm.nih.gov/22306005/).
44. Sangkhae V, Nemeth E. Regulation of the Iron Homeostatic Hormone Hepcidin. *Adv Nutr.* 2017; 8(1): 126–136, doi: [10.3945/an.116.013961](https://doi.org/10.3945/an.116.013961), indexed in Pubmed: [28096133](https://pubmed.ncbi.nlm.nih.gov/28096133/).
45. Han CY, Koo JaH, Kim SH, et al. Hepcidin inhibits Smad3 phosphorylation in hepatic stellate cells by impeding ferroportin-mediated regulation of Akt. *Nat Commun.* 2016; 7: 13817, doi: [10.1038/ncomms13817](https://doi.org/10.1038/ncomms13817), indexed in Pubmed: [28004654](https://pubmed.ncbi.nlm.nih.gov/28004654/).
46. Browning JD, Szczepaniak LS, Dobbins R, et al. Prevalence of hepatic steatosis in an urban population in the United States: impact of ethnicity. *Hepatology.* 2004; 40(6): 1387–1395, doi: [10.1002/hep.20466](https://doi.org/10.1002/hep.20466), indexed in Pubmed: [15565570](https://pubmed.ncbi.nlm.nih.gov/15565570/).

Submitted: 11 April, 2019

Accepted after reviews: 24 May, 2019

Available as AoP: 12 June, 2019

WNT5A gene and protein expression in endometrial cancer

Tomasz Wasniewski¹, Jacek Kiezun², Bartłomiej E. Krazinski², Anna E. Kowalczyk²,
Blazej Szostak³, Piotr M. Wierzbicki⁴, Jolanta Kiewisz²

¹Department of Obstetrics, Perinatology and Gynecology, School of Medicine, Collegium Medicum, University of Warmia and Mazury in Olsztyn, Olsztyn, Poland

²Department of Human Histology and Embryology, School of Medicine, Collegium Medicum, University of Warmia and Mazury in Olsztyn, Olsztyn, Poland

³Department of Pathomorphology, Regional Specialist Hospital, Olsztyn, Poland

⁴Department of Histology, Medical University of Gdansk, Gdansk, Poland

Abstract

Introduction. WNT5A (*Wnt family member 5A*) belongs to the WNT family of secreted signaling glycoproteins that play essential role in developmental, physiological and pathological processes. WNT5A was shown to take part in carcinogenesis process playing both oncogenic and suppressor functions in various types of human malignancies. This study aimed to assess the expression of the *WNT5A* gene at the mRNA and protein levels in the specimens derived from endometrial cancer (EC) or unchanged control endometrium. The associations between the *WNT5A* expression levels and clinicopathological characteristics and survival of EC patients were evaluated.

Materials and methods. Total RNA was isolated in order to assess the relative amounts of *WNT5A* mRNA by quantitative polymerase chain reaction (QPCR) in samples of unchanged endometrial control (n = 8) and tumor samples of EC patients (n = 28). Immunohistochemistry (IHC) was used to determine the presence of WNT5A protein in the sections of formalin-fixed, paraffin-embedded tissue specimens derived from unchanged endometrial controls (n = 6) and EC tumors (n = 19). Significance of differences in WNT5A expression levels between the studied groups of EC patients and correlations between the WNT5A and demographic data, pathological features, hematological parameters and overall survival of the patients were evaluated by statistical analysis.

Results. The level of *WNT5A* mRNA was decreased in EC in comparison to unchanged endometrium. *WNT5A* expression was associated with primary tumor invasion status exhibiting reduced level of transcripts in EC that involved organs beyond the uterus when compared to the uterus-confined cancers. WNT5A immunoreactivity was visualized in the cytoplasm and nuclei of EC cells as well as in the luminal and glandular epithelial cells of unchanged endometrium. *WNT5A* mRNA expression levels correlated negatively with cytoplasmic, and positively with nuclear immunoreactivity of the WNT5A protein in the EC cells. In addition, the relationships between blood leucocyte count (in particular granulocytes and lymphocytes) of patients with EC and their *WNT5A* mRNA and protein expression levels were established. A positive correlation between the nuclear immunoreactivity of WNT5A protein in the cancer cells in cell nuclei and mean platelet volume in blood was also found.

Conclusions. The results of the first study of *WNT5A* expression at the transcript and protein levels indicate that it could be considered as a potential marker of molecular changes that take place during EC development. (*Folia Histochemica et Cytobiologica* 2019, Vol. 57, No. 2, 84–93)

Key word: WNT5A expression; endometrial cancer; platelets volume; QPCR; IHC

Correspondence address: J. Kiewisz, PhD

Department of Human Histology and Embryology, School of Medicine, Collegium Medicum, University of Warmia and Mazury in Olsztyn, Warszawska 30, 10–082 Olsztyn, Poland; phone (+48) 89 524 53 10, e-mail: jolanta.kiewisz@uwm.edu.pl

Introduction

Endometrial cancer (EC) is the most common gynecological neoplasm diagnosed in developed countries, the fourth most common cancer in women after breast, lung, and colorectal cancer. Its incidence is increasing [1]. Exposure to endogenous and exogenous estrogens associated with obesity, diabetes, early onset of menarche, nulliparity, late onset of menopause, older age (≥ 55 years) and use of tamoxifen, are considered as the main risk factors leading to EC development [2, 3]. Patients are often diagnosed when the disease is still limited to the uterus, what results in a good prognosis. Thus, the 5-year overall survival (OS) for EC varies from 74% to 91% in non-metastatic patients [4].

Major diagnostic and prognostic problems of EC assessment are often associated with histopathological evaluation. According to WHO classification, seven subtypes of EC can be distinguished [5]. The most common subtype of EC is an endometrial endometrioid adenocarcinoma (EEAC), classified as type I or estrogen-dependent cancer [6]. Endometrial serous adenocarcinoma (ESC) and clear cell endometrial carcinoma (ccEC), aggressive neoplasia carrying a poor prognosis, are estrogen-independent and are classified as Type II [6]. Several research teams have defined immunohistochemical and/or mutation profiles to aid in distinguishing EC subtypes [7–9]. However, classification of EC by histomorphological criteria has a limited reproducibility and is not accurate or precise enough to effectively triage patients into optimal treatment groups. Thus, there is a necessity to develop better diagnostic and prognostic markers that could improve the histopathological examination [10] and would provide more biologically informative data from endometrial tumors that could assist in planning the optimal course of treatment for the affected individuals.

The WNT family consists of 19 secreted glycoproteins which participate in organogenesis during the fetal life as well as in physiological and pathological states postnatally [11]. Intracellular signal transduction pathways regulated by WNT proteins result in cell proliferation, differentiation, migration, adhesion and change of cell polarity [11]. The conservatively preserved WNT5A (*Wnt family member 5A*) protein is crucial for prenatal development, and its absence causes intrauterine fetal death associated with developmental defects [12]. Alternative splicing results in the formation of WNT5A protein isoforms [13] which can fulfill both oncogenic and suppressor functions in the process of carcinogenesis [14].

Moreover, WNT5A influences the cancer stem cell population and tumor microenvironment. It is an important molecule for the regulation of cellular senescence, epithelial-mesenchymal transition (EMT), metastasis, tumor cell metabolism and chemotherapy resistance of cancer cells in various cancer types [15]. The expression of the WNT family members, including WNT5A, in EC was evaluated by Bui *et al.* [16]; however, they analyzed only a very small group of patients with EC. Therefore, the present study was designed and performed to analyze and compare the expression of the *WNT5A* gene in unchanged endometrial control and tumor samples of EC patients at both mRNA and protein levels by the use of quantitative PCR (QPCR) and immunohistochemistry (IHC), respectively. We correlated the obtained data with clinicopathological features of the patients as well as with the OS to assess whether the evaluation of WNT5A gene or protein expression can provide a new diagnostic and/or prognostic marker in EC.

Material and methods

Patients. After receiving institutional review board approval, patients were recruited at Division of Gynecology and Obstetrics and Gynecology Oncology Center at The Regional Specialist Hospital in Olsztyn, Faculty of Medicine, University of Warmia and Mazury in Olsztyn, Poland. All participants provided written informed consent for tissue and blood sample donation. The control group ($n = 8$) included women (age: 47 ± 7.63 , mean \pm SD; BMI 18.5–25, $n = 4$; BMI 25–30, $n = 2$; BMI > 30 , $n = 2$), subjected to diagnostic curettage of the uterus and surgery, in which histopathological examination of EC and endometrial hyperplasia (hyperplasia simplex and complex, without atypia and with atypia) proved to be negative. The EC group ($n = 28$) included women (age: 66.95 ± 10.38 , mean \pm SD; BMI 18.5–25, $n = 3$; BMI 25–30, $n = 7$; BMI > 30 , $n = 18$) with histologically diagnosed EC of the uterus, detected by diagnostic curettage of the uterine cavity and treated with surgery (hysterectomy, salpingo-oophorectomy, cytological peritoneal washing and brushing, and pelvic and aortic lymph node dissection). Diagnosis of uterine cancer and its status were established by means of clinical, laboratory and histopathological evaluation. None of the patients received any anticancer therapy before the surgery. Ongoing acute illnesses (*i.e.* infection, non-infectious inflammation, cardiovascular events) or disease that had occurred within the last 30 days, known active malignancy, long-term estrogen therapy, polycystic ovarian syndrome, obesity, diabetes mellitus and hypertension as well as drug or alcohol abuse, excluded patients from the study. After the surgery, data on the OS were collected for all patients.

Material collection and clinical parameters estimation.

Blood samples were collected from the fasting patients before surgery. Blood morphology parameters and activated partial thromboplastin time (APTT) were measured using Cobas 6000 multianalyzer (Roche Diagnostics Ltd., Basel, Switzerland).

Tissue samples (5 × 5 × 5 mm) were taken from areas of endometrial tumors without blood-cysts, hemorrhage or necrosis which could disturb further molecular assays. Multiple sample blocks were taken from the same tumor-suspected area to compensate for eventual tumor heterogeneity. The samples were snap-frozen in liquid-nitrogen immediately after excision and stored at –80°C for mRNA isolation and further molecular studies. Tissue sections for routine diagnostic pathomorphological assessment and IHC were fixed in a 10% neutral-buffered formalin. After 12 h sections were dehydrated in a graded ethanol series (50–96%), cleared in xylene and embedded in paraffin for further processing.

Tumor phenotype classification. The criteria of TNM system following American Joint Committee on Cancer (AJCC) were adopted to establish primary tumor status [17]. Patients classified as T1a (n = 10) and T1b (n = 6), T2 (n = 7) and T3 (n = 5) were considered. Subsequently, the patients were grouped depending on: the depth of myometrium invasion as less or more than halfway (n = 12 and n = 16, respectively), uterine cervix infiltration as negative and positive (n = 14 and n = 14, respectively) and uterus-limited tumor growth or involvement of other organs by direct extension beyond the uterus (n = 23 and n = 5, respectively). Pathomorphological assessment was based on a routine light microscopy evaluation. Malignancy grade was assessed according to the International Federation of Gynecology and Obstetrics (FIGO) system [18], as low grade (G1; n = 2), moderate grade (G2; n = 19), and high grade (G3; n = 7). Grades 1 and 2 were grouped together (named further G2). The absence (n = 15) or presence (n = 13) of endometrial fibroids (myomas) were also recorded for each patient.

Total RNA isolation and Real time PCR. Endometrial tissues were homogenized using MagNA Lyser Instrument and MagNA Lyser Green Beads (Roche Molecular Systems, Inc., Pleasanton, CA, USA). Extraction of total RNA was conducted using mirVana Isolation Kit (Ambion; Thermo Fisher Scientific, Inc., Waltham, MA, USA), according to the protocol provided by manufacturers. The quality and quantity of isolated RNA was estimated with NanoDrop 1000 spectrophotometer (Thermo Fisher Scientific, Inc.). Obtained RNA samples were stored at –80°C until further analysis. The reverse transcription was conducted according to the protocol of HighCapacity cDNA Reverse Transcription Kit (Applied Biosystem; Thermo Fisher Scientific, Inc., Waltham, MA, USA). Quantification of *WNT5A* and peptidylprolyl isomerase A (*PPIA*) cDNA in collected samples

(Hs00998537_m1 and Hs99999904_m1) was carried out using ABI 7500 Fast Real-Time PCR System and TaqMan® Fast Advanced Master Mix (all: Applied Biosystem; Thermo Fisher Scientific, Inc.) according to the manufacturer's instructions, and using the following conditions: polymerase activation for 20 sec at 95°C, followed by 40 cycles of denaturation at 95°C for 3 sec and annealing/extension at 60°C for 30 sec. All samples were quantified in duplicate. No template control reactions were performed for each QPCR run. Standard curves consisting of serial dilutions of the appropriate cDNA were used to control the efficiency of QPCR. Relative quantification of *WNT5A* expression was evaluated using the ddCt method [19]. Quantified gene had the Ct normalized against *PPIA* expression (dCt) as the reference [20].

Immunohistochemistry. Formalin-fixed, paraffin-embedded blocks of unchanged (control) endometrium obtained from 6 patients without EC, and fragments of tumor samples from 19 patients with EC, were cut into 5 μm-thick sections, soaked in xylene and rehydrated in a series of decreasing ethanol dilutions (96–50%). Antigen retrieval was carried out using Epitope Retrieval Solution (pH 6; Dako; Agilent Technologies Inc., Santa Clara, CA, USA), microwaving for 12 min at 97°C. Endogenous peroxidase activity was blocked in a solution of 3% hydrogen peroxide in methanol for 10 min at room temperature (RT). Tissue sections were incubated with 2.5% normal horse serum (NHS; Vector Laboratories; Maravai Life Sciences, Inc., Chicago, IL, USA) in buffer containing 0.1 M PBS and 3% bovine serum albumin (BSA; Sigma-Aldrich; Merck, KGaA, Darmstadt, Germany) for 30 min at RT. Rabbit anti-human *WNT5A* (H-58) antibody (sc-30224; Santa Cruz Biotechnology Inc., Dallas, TX, USA), were diluted in NGS/PBS/BSA buffer (1:100). After overnight incubation at 4°C with primary antibody, slides were washed 3 times with PBS containing Tween20 (Sigma-Aldrich; Merck, kGa) and incubated for 30 min at RT with goat anti-rabbit antibody diluted according to the protocol provided by manufacturers (ImmPRESS Universal reagent Anti-Mouse/Rabbit Ig; Vector Laboratories; Maravai Life Sciences, Inc.). Reaction was visualized after short incubation with 3,3'-diaminobenzidine (DAB; Liquid DAB + Substrate Chromogen System; Dako; Agilent Technologies Inc.). After counterstaining in Mayer's hematoxylin (Sigma-Aldrich; Merck, KGaA), dehydration in series of alcohol dilutions (50–96%) and mounting in DPX medium (Sigma-Aldrich; Merck, KGaA) slides were viewed using XC-50 camera mounted on Olympus BX-41 (Olympus Corporation, Tokyo, Japan) light microscope by a pathologist who was blinded to the patients' clinical data. Pictures were taken with Panoramic Digital Slide Scanner MIDI (3DHitech Ltd., Budapest, Hungary). Negative controls were obtained by incubation of sections without primary antibody.

The estimation of WNT5A staining intensity and heterogeneity. The classification of intensity and heterogeneity of the staining were conducted according to the IRS (immunoreactivity score) scale as described by Remmele and Stegner [21]. Briefly, the staining intensity was estimated as 1 (the weakest), 2 (moderate), or 3 (the most intense). Heterogeneity characterized the proportion of positively stained tumor cells was evaluated as 0 points, absence of cells with positive reaction; 1 point, 1–10%; 2 points, 1–50%; 3 points, 51–80%; 4 points, > 80% cells with positive reaction by estimation on screening wide areas within each tissue section. The obtained values of intensity and heterogeneity were multiplied and scored from 0 to 12 points. All cases with negative immunoreactivity were scored as 0.

Statistical analysis. All statistical analyses were conducted using GraphPad PRISM v. 6.0 software (GraphPad Software, Inc., San Diego, CA, USA). Comparisons of *WNT5A* mRNA and immunoreactivity levels in unchanged and endometrial tumor samples were conducted with Mann-Whitney tests. Statistical differences of mRNA levels between EC tissue groups in respect to: primary tumor status, tumor myometrial invasion, infiltration of the tumor on the cervix, invasion beyond the uterus, malignancy grade and presence of endometrial fibroids (myomas) were examined using Kruskal-Wallis and Mann-Whitney tests. All correlations of *WNT5A* gene and protein expression in both studied patient groups were calculated using a Spearman test. Survival curves were plotted according to the Kaplan-Meier method and the significance of differences in OS between groups of patients was evaluated by the log-rank test. Differences were considered to be statistically significant at p value less than 0.05.

Results

Characteristics of the patients

Demographic data and blood parameters of control and EC patients included in the study are presented in Table 1.

WNT5A expression at the mRNA level in EC

In both control and EC samples, the presence of *WNT5A* mRNA was observed. Samples with *WNT5A* expression ratio below 1.0 were considered as down-regulated and those with ratio above 1.0 as up-regulated. The *WNT5A* transcript level was decreased in 24/28 (85.72%) and was elevated in 4/28 (14.28%) patients with EC. The mean *WNT5A* gene expression was reduced in EC patients compared to control group ($p < 0.0001$; Fig. 1A).

WNT5A mRNA levels were significantly lower in the group of patients characterized by tumor invasion beyond the uterus when compared to the uter-

Table 1. Demographic data and blood parameters of the studied cohort of patients

	Units	Control	Endometrial cancer
N		8	28
Age	years	47 ± 7.63	66.95 ± 10.38
BMI	kg/m	27.88 ± 5.92	31.39 ± 5.47
RBC	10 ⁶ /μl	4.57 ± 0.50	4.77 ± 0.45
Hb	g/dl	12.16 ± 1.89	13.86 ± 1.36
Ht	%	38.28 ± 4.63	41.88 ± 3.17
WBC	10 ³ /μl	7.18 ± 1.60	7.36 ± 2.14
Granulocytes	%	63.59 ± 7.10	60.32 ± 8.74
Neutrophils	%	61.34 ± 8.08	57.95 ± 9.26
Eosinophils	%	1.6 ± 0.73	1.94 ± 1.28
Basophils	%	0.52 ± 0.26	0.43 ± 0.26
Lymphocytes	%	28.46 ± 6.07	30.46 ± 7.83
Monocytes	%	5.79 ± 1.06	6.49 ± 1.81
Platelets	10 ³ /μl	296.4 ± 78.52	229.9 ± 60.26
MPV	fl	10.5 ± 0.96	10.93 ± 0.78
APTT	s	26.47 ± 1.75	27.49 ± 3.61

The results are presented as means ± SD. Abbreviations: BMI — Body Mass Index; RBC — Red Blood Cells; Hb — Hemoglobin; Ht — Hematocrit; WBC — White Blood Cells; MPV — Mean Platelet Volume; APTT — Activated Partial Thromboplastin Time

us-confined EC samples ($p < 0.05$; Fig. 1E). *WNT5A* expression also tended to correlate with the depth of myometrial invasion exhibiting lower transcript level in tumors that have grown deeper than halfway through the myometrium as compared to those which invaded less than the half of myometrium thickness, but this difference was not confirmed by the statistics ($p = 0.06$; Fig. 1C). There were no statistically significant associations between the *WNT5A* mRNA levels and primary tumor status (established as T1a, T1b, T2 and T3; Fig. 1B), infiltration of the tumor on the cervix (absent or present; Fig. 1D), malignancy grade (G2 and G3; Fig. 1F) and occurrence of uterine fibroids (absent or present; Fig. 1G).

The immunoreactivity of the WNT5A protein in control and EC tissue

Tissue samples of 6 control and 19 EC patients previously analyzed for their *WNT5A* mRNA expression levels were subjected to IHC in order to assess the immunoreactivity of *WNT5A* protein in the normal endometrium and EC cancer cells.

Representative microphotographs of IHC presenting the location of *WNT5A* protein in the control endometrium and tumor tissue of EC patients are

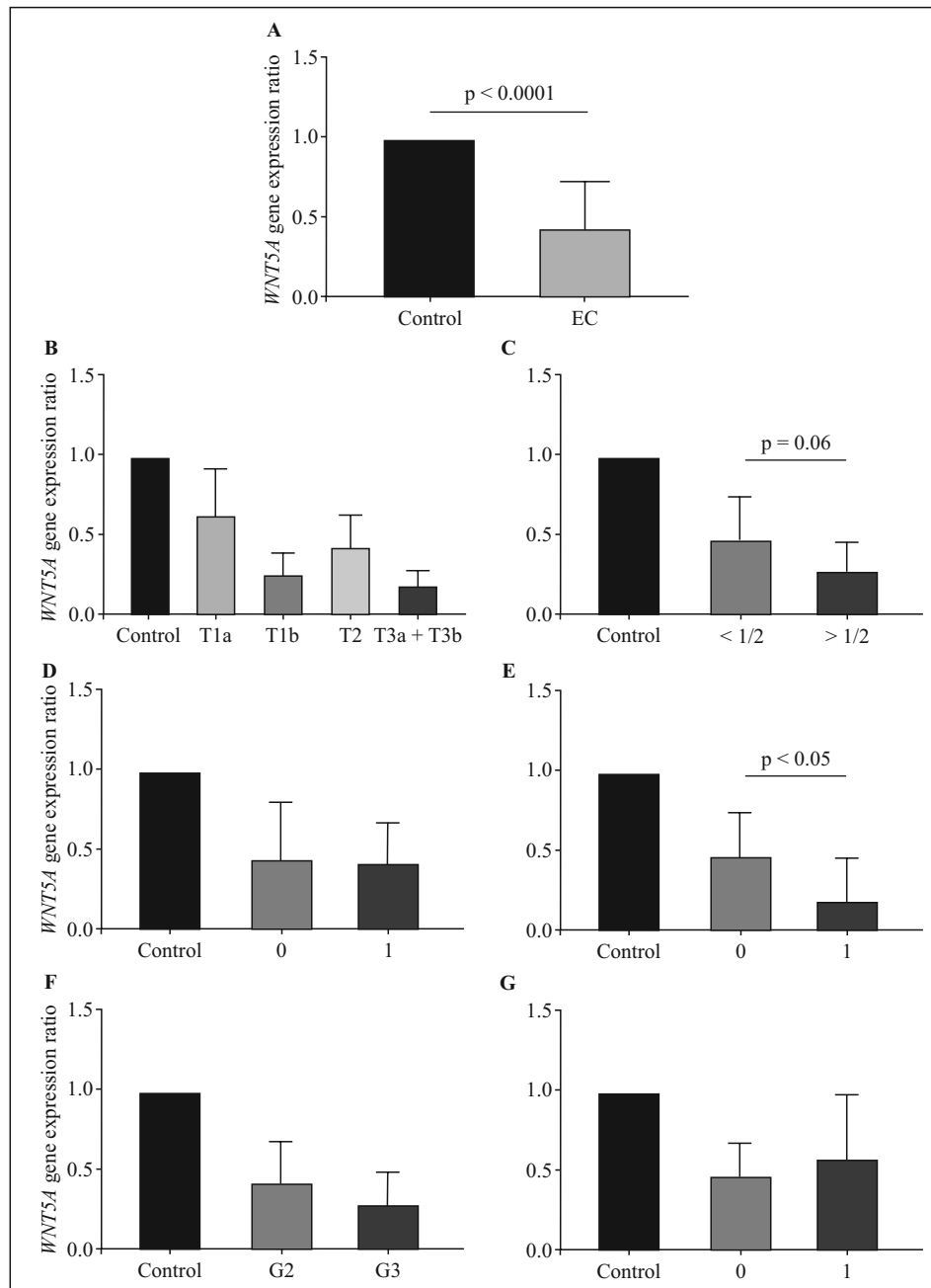


Figure 1. Quantitative Real-time PCR analysis was used to compare *WNT5A* gene expression in tumor tissue of patients with endometrial cancer (EC) and normal endometrial tissue (control). *WNT5A* mRNA levels in control endometrial samples ($n = 8$) and EC samples ($n = 28$) (A). Comparison of the *WNT5A* mRNA level in a control endometrial samples and samples of EC patients depending on the primary tumor status (B), tumor myometrial invasion (C), absence (0) or presence (1) of tumor infiltration on the cervix (D), presence at the area or beyond the uterus (E), grade (F), absence (0) or presence (1) of endometrial fibroids (G). Gene expression data were normalized against *PPLA* mRNA levels and presented as *WNT5A* gene expression ratios \pm SD as described in Methods.

shown in Figure 2. The figures presenting negative control samples were not shown.

The histologically-unchanged endometrial fragments showed dominant, strong, homogenous positive *WNT5A* immunoreactivity in the cytoplasm and, sporadically, in the nuclei of epithelial cells, whereas

in tumor tissue, *WNT5A* protein staining were mainly present in the nuclei of cancer cells. When control and EC tissue sections were compared, qualitative differences between the immunoreactivity in cytoplasmic and nuclear compartments were observed (Fig. 2). However, there were no quantitative alterations of

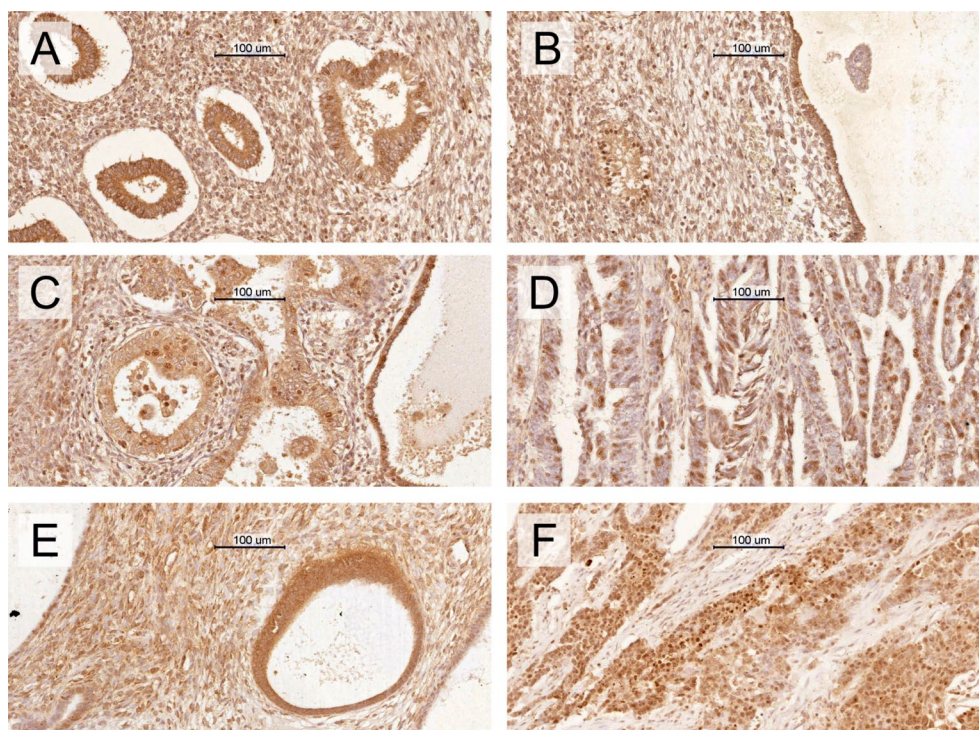


Figure 2. Representative examples of *WNT5A* protein immunoreactivity in normal endometrium (A, B) and endometrial cancer (EC) samples depending on the degree of histological differentiation; endometrium at grade 2 (C, D) and grade 3 (E, F) of EC progression. The immunohistochemical reactions were performed as described in Methods.

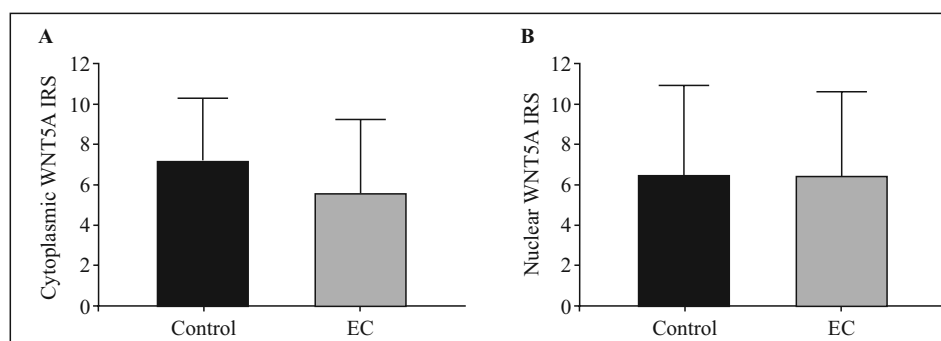


Figure 3. Quantitative analysis of the immunoreactivity of *WNT5A* protein in cytoplasmic (A) and nuclear (B) compartments of control endometrium (n = 6) and endometrial cancer (EC) samples (n = 19). The immunoreactivity score (IRS) values are shown as mean \pm SD.

WNT5A immunoreactivity in cytoplasm and nuclear compartments between the unchanged endometrium and EC samples ($p > 0.05$; Fig. 3 A and B, respectively).

WNT5A protein immunoreactivity measured on the basis of the IRS scale in the cytoplasmic and nuclear compartments of EC cells did not correlate with clinicopathological characteristics of the patients (data not showed).

Correlations between *WNT5A* mRNA levels and *WNT5A* protein immunoreactivity in the cytoplasm and nuclei of tumor cells

A negative correlation was observed between *WNT5A* mRNA expression and protein immunoreactivity in the cytoplasm of EC cells (Rho = -0.55 ; $p < 0.05$). In contrast, a positive correlation was observed between the *WNT5A* transcript levels in EC tumor samples and

WNT5A immunoreactivity in the nuclei of cancer cells (Rho = 0.60; $p < 0.01$).

Correlations between blood parameters and WNT5A mRNA expression levels and protein immunoreactivity in EC specimens

In patients with EC, *WNT5A* gene expression correlated positively with the count of leukocytes (WBCs; $p < 0.05$) and the percentage of granulocytes ($p < 0.05$), and negatively with the percentage of lymphocytes in blood ($p < 0.5$; Table 2).

In patients with EC, we observed negative correlation between the cytoplasmic immunoreactivity of the WNT5A protein and percentage of granulocytes ($p < 0.01$) or neutrophils ($p < 0.01$) in blood when the protein in the cytoplasm of EC cells was concerned (Table 2). The percentage of lymphocytes in blood positively correlated with the immunoreactivity of WNT5A in the cytoplasm of EC cells ($p < 0.01$; Table 2). Mean platelet volume (MPV) was the only blood parameter which positively correlated with WNT5A protein immunoreactivity in the nuclei of EC cells ($p < 0.05$). No correlations with age, BMI as well as or other estimated blood parameters such as RBC, WBC and platelets counts, types of leukocytes, hemoglobin (Hb), hematocrit (Ht), MPV and APTT, were found when nuclear localization of WNT5A was considered in EC patients (Table 2).

Correlations between WNT5A gene and protein expression and OS of patients with EC

The evaluation of the *WNT5A* gene expression level as a prognostic factor in the studied group of the patients with EC was assessed after the follow up of patients ($n = 28$) and the median observation period was 59 months. During the observation period 25% ($n = 7$) patients died. We found a significant correlation between the tumor grade and OS of the patients ($p < 0.001$; Fig. 4A).

In order to investigate associations between OS and *WNT5A* expression EC specimens were divided into the respective cohorts. Based on the median *WNT5A* mRNA relative expression (RQ = 0.495) the patients were divided into two groups regarded as < 0.495 ($n = 14$) and > 0.495 ($n = 14$). Consequently, the patients were dichotomously divided on the basis of their median value for the cytoplasmic (IRS = 4) or nuclear (IRS = 6) WNT5A immunoreactivity score. We found that the expression level of *WNT5A* mRNA (Fig. 4B) as well as the intensity of cytoplasmic or nuclear WNT5A immunoreactivity (Fig. 4C and D, respectively) did not correlate with patients' OS.

Discussion

There is an urgent need for intense research in the field of molecular biology of endometrial tumors in or-

Table 2. Correlations between blood parameters and *WNT5A* mRNA levels and WNT5A protein immunoreactivity in cytoplasmic and nuclear compartments of endometrial cancer cells

	WNT5A mRNA	WNT5A protein	
		Cytoplasm	Nucleus
Age	-0.22	0.18	-0.16
BMI	0.31	-0.39	0.23
RBC	-0.01	-0.19	-0.08
Hb	-0.15	0.02	-0.19
Ht	0.24	0.05	-0.13
WBC	0.39*	-0.36	0.15
Granulocytes	0.42*	-0.66**	0.24
Neutrophils	0.32	-0.61**	0.30
Eosinophils	-0.03	-0.04	-0.32
Basophils	0.18	0.12	-0.35
Lymphocytes	-0.38*	0.67**	-0.20
Monocytes	-0.09	0.22	0.005
Platelets	0.10	0.006	-0.30
MPV	0.30	-0.07	0.51*
APTT	-0.09	-0.18	0.29

Abbreviations as in the legend to Table 1. Asterisks indicate statistical significance; * $p < 0.5$; ** $p < 0.01$).

der to detect the molecular markers of carcinogenesis process. The present study is the first that used both QPCR and IHC techniques to establish *WNT5A* expression at the transcript and protein levels in the EC tissue. Our study demonstrated that *WNT5A* mRNA is down-regulated in the tumor samples as compared to normal endometrial tissue fragments. These findings support the study of Bui *et al.* [16] who investigated the expression of seven genes belonging to the WNT family in neoplastically-altered and normal endometrium by ribonuclease protection assay. Their results suggested reduced level of *WNT5A* expression in EC tumor tissue and human EC cell lines [16]. Unfortunately, the study of Bui *et al.* involved only four patients with EC and 11 control cases and its findings were neither supported by statistical analysis nor the correlations between *WNT5A* expression and clinicopathological parameters [16]. Therefore, our research was carried out on a larger cohort of patients and is the first study which shows associations between the reduced *WNT5A* expression and increasing invasive properties of EC tumors.

In our cohort of the patients with EC the *WNT5A* gene expression was markedly reduced in the tumors that spread outside the uterus as compared to the organ-confined cases. Our results suggest that

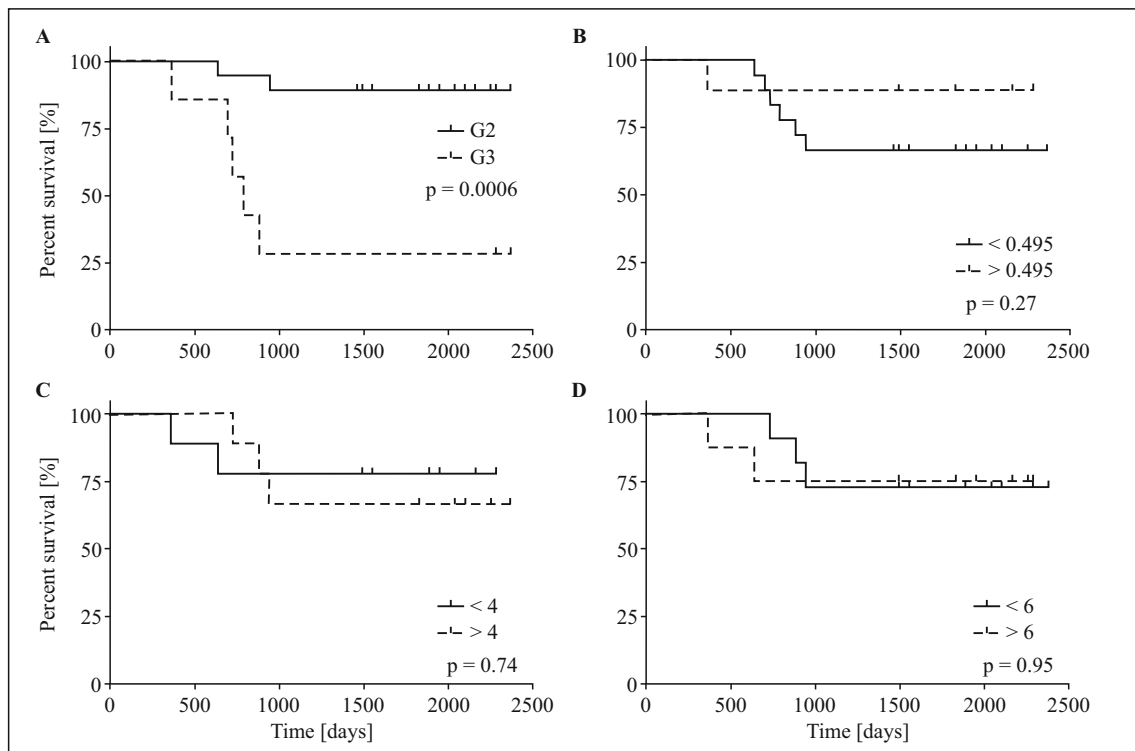


Figure 4. Analysis of the overall survival (OS) of patients with endometrial cancer (EC). Kaplan-Meier survival curves of EC patients relating to (A) the histological grade of EC tumor (n = 28), (B) levels of *WNT5A* mRNA (n = 28), (C) cytoplasmic (n = 19) and (D) nuclear (n = 19) immunoreactivity of the *WNT5A* protein. P-values of log-rank test are shown.

decreased *WNT5A* mRNA level could also correlate with the depth of invasion through myometrium. Although these findings could suggest tumor suppressor role of *WNT5A* in EC, we did not disclose any significant relationship between its expression levels and overall survival of the patients. Indeed, the precise status of the *WNT5A* gene as a factor that might have influenced cancer progression has not been established yet and the opposing observations in other human tumors imply that role of *WNT5A* protein could be tissue- and/or cancer-specific [14]. In the female reproductive system the decreased expression of *WNT5A* was documented in epithelial ovarian cancer and this reduction was attributed to the hypermethylation of the gene promoter [22]. In contrast to the latter study, Peng *et al.* found that *WNT5A* immunoreactivity was increased in the ovarian cancer cells as compared to benign tumors and normal ovarian tissue [23]. Furthermore, elevated level of *WNT5A* protein was associated with shorter overall and progression-free survival of the patients with ovarian cancer [23]. Also in patients with cervical cancer *WNT5A* expression was found to be either decreased [13] or increased [24]. Using QPCR and IHC techniques Lin *et al.* [24] showed that the expression of *WNT5A* mRNA was up-regulated in the primary

cervical tumors and *WNT5A* immunoreactivity in cancer cells correlated with the occurrence of distant metastases and worse prognosis. These discrepancies may be partially explained by the findings of Bauer *et al.* [13] who demonstrated that the tumor-promoting or tumor-suppressing role of *WNT5A* in cervical cancer can be attributed to the differential expression of two *WNT5A* isoforms that have distinct effects on cancer-relevant signaling pathways.

In our study the immunoreactivity of the *WNT5A* protein was observed not only in the cytoplasm but also in the nuclei of EC cells and, to a lesser extent, in some epithelial cells of the control endometrial tissues. Interestingly, *WNT5A* transcription can result in the synthesis of two different isoforms, long (380 amino-acids; The Consensus CDS accession number: CCDS46850) and short (365 amino-acids; CCDS58835) [25] that could be characterized by distinct biological activity [13]. The results of *in silico* analysis of their amino-acid sequences using nuclear localization signals (NLS) mapper [26] recognized a single putative NLS within the N-terminus of long *WNT5A* isoform and lack of it in the short isoform. Basing on NLS prediction it could be assumed that localization of *WNT5A* immunoreactivity within the cell may differ depending on the type of expressed

isoform, with long isoform being directed both to the cytoplasm and nucleus and short isoform expressed exclusively in the cytoplasm [26]. Therefore, we suggest that the changes in the subcellular localization of WNT5A immunoreactivity are associated with the altered expression pattern of WNT5A isoforms as it was demonstrated in other human cancers such as cervical cancer, breast cancer and neuroblastoma [13]. The QPCR assay used in our study did not discriminate between the mRNA variants encoding for long and short WNT5A isoforms. In our immunohistochemical study, we could detect both WNT5A protein isoforms, since the applied primary antibody recognizes 23–80 aa of the long isoform as well as 15–72 aa of the short WNT5A isoform, respectively. Thus, further studies aiming to determine the expression of WNT5A isoforms in EC samples could clarify whether the possible role of this protein in EC pathogenesis is isoform-specific. Furthermore, our results showed that WNT5A mRNA correlated negatively with cytoplasmic and positively with nuclear WNT5A immunoreactivity levels in EC cells. We believe that the latter observation could be, at least partially, also elucidated by the analysis of WNT5A expression with respect to the expressed variants of transcript or isoforms.

Our study revealed that *WNT5A* mRNA and immunoreactivity levels correlated with preoperative counts of white blood cells and MPV. Since the correlations with granulocytes and lymphocytes count were found for the cytoplasmic but not nuclear immunoreactivity of WNT5A, its role as secretory molecule and modulator of immune processes can be considered [15]. Other authors have shown that biomarkers of inflammation such as elevated neutrophil to lymphocyte ratio or platelet to lymphocyte ratio are significant prognostic factors in EC and correlate with worse prognosis [27]. In our study the lower cytoplasmic immunoreactivity of WNT5A was positively associated with lymphocyte and negatively with neutrophils counts. This relationships could indicate the existence of direct or indirect links between the WNT5A expressed in endometrial tumor and inflammatory processes. Indeed, WNT5A protein have been considered tumor-derived immunomodulator that has been shown to influence chemotactic cell migration in ovarian cancer cell line SKOV-3 [28] and promote differentiation of regulatory T-cells by activation of dendritic cells in melanoma [29]. Interestingly, it was demonstrated that WNT5A potentiated thromboxane A2 mimetic-induced platelet aggregation and therefore the secretion of this protein by circulating cancer cells might promote metastatic progression suggesting that WNT5A can promote tumor progression by its

interaction with the platelets [30]. It cannot be excluded that in EC, WNT5A has analogous functions to those reported in the aforementioned studies [28–30]. However, further experiments are needed to evaluate its importance in establishing of tumor microenvironment and blood-borne metastasis.

In conclusion, the investigations of the WNT5A expression in the endometrial cancer suggest that this signaling molecule could function in the development of this malignancy as tumor suppressor and/or modulator of immune response and could be considered as a potential marker in EC. However, the precise role of WNT5A in the pathogenesis of endometrial cancer must be elucidated in further experiments.

Acknowledgments

The research was financed from statutory grant (61.610.001-300) of the School of Medicine, Collegium Medicum, University of Warmia and Mazury, Olsztyn, Poland.

Disclosure Statement

The authors have no conflicts of interest to declare.

References

1. Ferlay J, Soerjomataram I, Dikshit R, et al. Cancer incidence and mortality worldwide: sources, methods and major patterns in GLOBOCAN 2012. *Int J Cancer*. 2015; 136(5): E359–E386, doi: [10.1002/ijc.29210](https://doi.org/10.1002/ijc.29210), indexed in Pubmed: [25220842](https://pubmed.ncbi.nlm.nih.gov/25220842/).
2. Kaaks R, Lukanova A, Kurzer MS. Obesity, endogenous hormones, and endometrial cancer risk: a synthetic review. *Cancer Epidemiol Biomarkers Prev* 2002;11:1531–43. PMID: 12496040.
3. Renehan AG, Tyson M, Egger M, et al. Body-mass index and incidence of cancer: a systematic review and meta-analysis of prospective observational studies. *Lancet*. 2008; 371(9612): 569–578, doi: [10.1016/S0140-6736\(08\)60269-X](https://doi.org/10.1016/S0140-6736(08)60269-X), indexed in Pubmed: [18280327](https://pubmed.ncbi.nlm.nih.gov/18280327/).
4. Siegel RL, Fedewa SA, Miller KD, et al. Cancer statistics, 2015. *CA Cancer J Clin*. 2015; 65(1): 5–29, doi: [10.3322/caac.21254](https://doi.org/10.3322/caac.21254), indexed in Pubmed: [25559415](https://pubmed.ncbi.nlm.nih.gov/25559415/).
5. Bokhman JV. Two pathogenetic types of endometrial carcinoma. *Gynecol Oncol*. 1983; 15(1): 10–17, indexed in Pubmed: [6822361](https://pubmed.ncbi.nlm.nih.gov/6822361/).
6. Ryan AJ, Susil B, Jobling TW, et al. Endometrial cancer. *Cell Tissue Res*. 2005; 322(1): 53–61, doi: [10.1007/s00441-005-1109-5](https://doi.org/10.1007/s00441-005-1109-5), indexed in Pubmed: [15947972](https://pubmed.ncbi.nlm.nih.gov/15947972/).
7. Santacana M, Maiques O, Valls J, et al. A 9-protein biomarker molecular signature for predicting histologic type in endometrial carcinoma by immunohistochemistry. *Hum Pathol*. 2014; 45(12): 2394–2403, doi: [10.1016/j.humpath.2014.06.031](https://doi.org/10.1016/j.humpath.2014.06.031), indexed in Pubmed: [25282036](https://pubmed.ncbi.nlm.nih.gov/25282036/).
8. Coenegrachts L, Garcia-Dios DA, Depreeuw J, et al. Mutation profile and clinical outcome of mixed endometrioid-serous endometrial carcinomas are different from that of pure endometrioid or serous carcinomas. *Virchows Arch*. 2015; 466(4): 415–422, doi: [10.1007/s00428-015-1728-5](https://doi.org/10.1007/s00428-015-1728-5), indexed in Pubmed: [25677978](https://pubmed.ncbi.nlm.nih.gov/25677978/).
9. Hoang LN, McConechy MK, Köbel M, et al. Histotype-genotype correlation in 36 high-grade endometrial carcinomas.

- Am J Surg Pathol. 2013; 37(9): 1421–1432, doi: [10.1097/PAS.0b013e31828c63ed](https://doi.org/10.1097/PAS.0b013e31828c63ed), indexed in Pubmed: 24076778.
10. Krejczyk K, Cymbaluk-Płoska A, Kwiatkowski S, et al. Molecular characteristics of endometrial cancer and their potential effect on clinical management. *Current Gynecologic Oncology*. 2019; 16(4): 245–250, doi: [10.15557/cgo.2018.0028](https://doi.org/10.15557/cgo.2018.0028).
 11. Nusse R, Clevers H. Wnt/ -Catenin Signaling, Disease, and Emerging Therapeutic Modalities. *Cell*. 2017; 169(6): 985–999, doi: [10.1016/j.cell.2017.05.016](https://doi.org/10.1016/j.cell.2017.05.016), indexed in Pubmed: 28575679.
 12. Yamaguchi TP, Bradley A, McMahon AP, et al. A Wnt5a pathway underlies outgrowth of multiple structures in the vertebrate embryo. *Development*. 1999; 126(6): 1211–1223, indexed in Pubmed: 10021340.
 13. Bauer M, Bénard J, Gaasterland T, et al. WNT5A encodes two isoforms with distinct functions in cancers. *PLoS One*. 2013; 8(11): e80526, doi: [10.1371/journal.pone.0080526](https://doi.org/10.1371/journal.pone.0080526), indexed in Pubmed: 24260410.
 14. McDonald SL, Silver A. The opposing roles of Wnt-5a in cancer. *Br J Cancer*. 2009; 101(2): 209–214, doi: [10.1038/sj.bjc.6605174](https://doi.org/10.1038/sj.bjc.6605174), indexed in Pubmed: 19603030.
 15. Asem MS, Buechler S, Wates RB, et al. Wnt5a Signaling in Cancer. *Cancers (Basel)*. 2016; 8(9), doi: [10.3390/cancers8090079](https://doi.org/10.3390/cancers8090079), indexed in Pubmed: 27571105.
 16. Bui TD, Zhang L, Rees MC, et al. Expression and hormone regulation of Wnt2, 3, 4, 5a, 7a, 7b and 10b in normal human endometrium and endometrial carcinoma. *Br J Cancer*. 1997; 75(8): 1131–1136, doi: [10.1038/bjc.1997.195](https://doi.org/10.1038/bjc.1997.195), indexed in Pubmed: 9099960.
 17. Greene FL, Page DL, Fleming ID, et al. Gynecological sites. In: *American Joint Committee on Cancer: AJCC Cancer Staging Manual*. 6th edition. Springer, New York, NY; 2002: 241–300.
 18. Petru E, Lück HJ, Stuart G, et al. Gynecologic Cancer Intergroup (GCIG). Gynecologic Cancer Intergroup (GCIG) proposals for changes of the current FIGO staging system. *Eur J Obstet Gynecol Reprod Biol*. 2009; 143(2): 69–74, doi: [10.1016/j.ejogrb.2008.12.015](https://doi.org/10.1016/j.ejogrb.2008.12.015), indexed in Pubmed: 19195765.
 19. Livak KJ, Schmittgen TD. Analysis of relative gene expression data using real-time quantitative PCR and the 2(-Delta Delta C(T)) Method. *Methods*. 2001; 25(4): 402–408, doi: [10.1006/meth.2001.1262](https://doi.org/10.1006/meth.2001.1262), indexed in Pubmed: 11846609.
 20. Romani C, Calza S, Todeschini P, et al. Identification of optimal reference genes for gene expression normalization in a wide cohort of endometrioid endometrial carcinoma tissues. *PLoS One*. 2014; 9(12): e113781, doi: [10.1371/journal.pone.0113781](https://doi.org/10.1371/journal.pone.0113781), indexed in Pubmed: 25473950.
 21. Remmele W, Stegner HE. [Recommendation for uniform definition of an immunoreactive score (IRS) for immunohistochemical estrogen receptor detection (ER-ICA) in breast cancer tissue]. *Pathologe*. 1987; 8(3): 138–140, indexed in Pubmed: 3303008.
 22. Bitler BG, Nicodemus JP, Li H, et al. Wnt5a suppresses epithelial ovarian cancer by promoting cellular senescence. *Cancer Res*. 2011; 71(19): 6184–6194, doi: [10.1158/0008-5472.CAN-11-1341](https://doi.org/10.1158/0008-5472.CAN-11-1341), indexed in Pubmed: 21816908.
 23. Peng C, Zhang X, Yu H, et al. Wnt5a as a predictor in poor clinical outcome of patients and a mediator in chemoresistance of ovarian cancer. *Int J Gynecol Cancer*. 2011; 21(2): 280–288, doi: [10.1097/IGC.0b013e31820aaadb](https://doi.org/10.1097/IGC.0b013e31820aaadb), indexed in Pubmed: 21270611.
 24. Lin Li, Liu Y, Zhao W, et al. Wnt5A expression is associated with the tumor metastasis and clinical survival in cervical cancer. *Int J Clin Exp Pathol*. 2014; 7(9): 6072–6078, indexed in Pubmed: 25337253.
 25. Farrell CM, O'Leary NA, Harte RA, et al. Current status and new features of the Consensus Coding Sequence database. *Nucleic Acids Res*. 2014; 42(Database issue): D865–D872, doi: [10.1093/nar/gkt1059](https://doi.org/10.1093/nar/gkt1059), indexed in Pubmed: 24217909.
 26. Kosugi S, Hasebe M, Tomita M, et al. Systematic identification of cell cycle-dependent yeast nucleocytoplasmic shuttling proteins by prediction of composite motifs. *Proc Natl Acad Sci U S A*. 2009; 106(25): 10171–10176, doi: [10.1073/pnas.0900604106](https://doi.org/10.1073/pnas.0900604106), indexed in Pubmed: 19520826.
 27. Cummings M, Merone L, Keeble C, et al. Preoperative neutrophil:lymphocyte and platelet:lymphocyte ratios predict endometrial cancer survival. *Br J Cancer*. 2015; 113(2): 311–320, doi: [10.1038/bjc.2015.200](https://doi.org/10.1038/bjc.2015.200), indexed in Pubmed: 26079303.
 28. Arabzadeh S, Hossein G, Zarnani AH. Wnt5A exerts immunomodulatory activity in the human ovarian cancer cell line SKOV-3. *Cell Biol Int*. 2016; 40(2): 177–187, doi: [10.1002/cbin.10551](https://doi.org/10.1002/cbin.10551), indexed in Pubmed: 26462870.
 29. Holtzhausen A, Zhao F, Evans KS, et al. Melanoma-Derived Wnt5a Promotes Local Dendritic-Cell Expression of IDO and Immunotolerance: Opportunities for Pharmacologic Enhancement of Immunotherapy. *Cancer Immunol Res*. 2015; 3(9): 1082–1095, doi: [10.1158/2326-6066.CIR-14-0167](https://doi.org/10.1158/2326-6066.CIR-14-0167), indexed in Pubmed: 26041736.
 30. Kim SY, Kim S, Yun-Choi HS, et al. Wnt5a potentiates U46619-induced platelet aggregation via the PI3K/Akt pathway. *Mol Cells*. 2011; 32(4): 333–336, doi: [10.1007/s10059-011-0134-3](https://doi.org/10.1007/s10059-011-0134-3), indexed in Pubmed: 21870110.

Submitted: 17 May, 2019

Accepted after reviews: 21 May, 2019

Available as AoP: 14 June, 2019

Gallbladder interstitial Cajal-like cells and gallbladder contractility in patients with cholelithiasis: a prospective study

Runyu Ding, Junmin Wei, Jingyong Xu

National Center of Gerontology, Beijing Hospital, Beijing, China

Abstract

Introduction. A reduced number of interstitial Cajal-like cells (ICLCs) in the gallbladder have been proposed to play a role in the pathogenesis of cholelithiasis. Therefore, this prospective study was conducted to investigate the relationship between gallbladder contractility and the number of gallbladder ICLCs in patients with cholelithiasis.

Material and methods. Patients admitted to the Department of Hepatobiliary Surgery for cholecystectomy were divided into the cholelithiasis ($n = 18$) and non-cholelithiasis ($n = 8$) groups based on their clinical data. Patients' clinical data were collected on admission, and B-mode ultrasonography was performed to assess their gallbladder contractility. The resected gallbladder specimens were fixed, paraffin sections mounted on slides, and the immunofluorescence staining with the anti-human CD-117 and anti-human tryptase antibodies was performed to identify ICLCs and mast cells, respectively. The number of ICLCs was counted in 10 high-power fields (HPFs) randomly.

Results. Independent sample t-tests revealed differences between the cholelithiasis and non-cholelithiasis groups in the number of ICLCs (mean \pm standard deviation: 88.61 ± 28.22 vs. 115.89 ± 27.87 per HPFs, $P = 0.032$) and gallbladder contractility ($43.94\% \pm 18.50\%$ vs. $61.00\% \pm 20.50\%$, $P = 0.046$). Pearson and Spearman correlation analyses revealed no significant correlation between the number of ICLCs and gallbladder contractility.

Conclusion. The results suggest that the number of gallbladder ICLCs in the wall of the gallbladder of patients with or without cholelithiasis is not a decisive factor affecting gallbladder contractility. (*Folia Histochemica et Cytobiologica* 2019, Vol. 57, No. 2, 94–100)

Key words: cholelithiasis; interstitial Cajal-like cells; mast cells; gallbladder contractility; immunofluorescence; ultrasonography

Introduction

Cholelithiasis combined with chronic cholecystitis is a common disease that often requires hepatobiliary surgery, and its incidence in developing countries is approximately 10–15%, with a higher prevalence in women [1]. The pathogenesis of gallstones is considered to be associated with bile cholesterol supersaturation, abnormalities in cholesterol nucleation, and impaired gallbladder function, which is believed to

be of great significance. Interstitial Cajal-like cells (ICLCs) are thought to be associated with the spontaneous rhythmic movements of the gastrointestinal tract [2], and they are considered the pacemaker cells of slow-wave potential in gastrointestinal smooth muscles. The typical ICLCs are elongated, fusiform bodies with few processes. Large ones have an oval nucleus. Numerous mitochondria can be observed in the cytoplasm under an electron microscope; they express the c-kit receptor, which can be identified by CD117 (c-kit protein) [3]. These cells also exist in the gallbladder wall in many species, including humans and guinea pigs. It was found that ICLCs are closely related to gallbladder function in guinea pigs [4]. In recent years, studies conducted in China and abroad have shown that the density of ICLCs was significantly lower in the gallbladder wall of patients with cholelith-

Correspondence address: Jingyong Xu
National Center of Gerontology,
Beijing Hospital, No. 1 Dahua Road,
Dongdan, Dongcheng District, Beijing, 100730
phone: 13810351797; fax: 85136262
e-mail: bjhxujingyong@163.com

iasis than of those without cholelithiasis [5]. Hence, it was proposed that the reduced number of ICLCs may play a role in the pathogenesis of cholelithiasis.

The aim of this prospective study was to investigate the relationship between gallbladder contractility and the number of ICLCs in the gallbladder wall of patients with cholelithiasis.

Material and methods

Ethical approval. The study was conducted in accordance with the moral, ethical, regulatory, and scientific principles governing clinical research. All surgical samples were retrieved with the approval of the Beijing Hospital ethical Committee the Declaration of Helsinki (protocol number 2016BJYYEC-057-01) and oral informed consent was obtained from the patients.

Subjects. The subjects enrolled in this study were patients admitted to the Department of Hepatobiliary Surgery in our hospital between December 2016 and March 2017, who required cholecystectomy owing to cholelithiasis combined with chronic cholecystitis or other non-cholelithiasis reasons. The patients were divided into the cholelithiasis and non-cholelithiasis groups, according to their clinical characteristics.

Inclusion and exclusion criteria. Inclusion criteria for the cholelithiasis group were as follows: 1) patients with cholelithiasis with clear indications for surgery and no obvious contraindications; and 2) patients with no history of acute cholecystitis in the past 4 weeks.

Inclusion criteria for the non-cholelithiasis group were as follows: 1) patients with no history of cholelithiasis and cholecystitis (*i.e.*, no gallstones were detected during preoperative imaging); and 2) patients who required cholecystectomy because of gallbladder polyps, gallbladder adenomyomatosis, or other reasons.

Exclusion criteria for both groups were as follows: 1) patients with acute cholecystitis or a history of acute cholecystitis in the past 4 weeks; 2) patients with a history of biliary system surgery, such as endoscopic retrograde cholangiopancreatography and endoscopic sphincterotomy; 3) patients with cholelithiasis combined with gallbladder polyps or gallbladder adenomyomatosis; 4) patients with the presence of obstructive jaundice, or intrahepatic or extrahepatic biliary stones; and 5) patients with a history of gastrointestinal anastomosis and other surgical changes to gastrointestinal continuity.

Materials and instrumentation. The following materials and instruments were used: the ProSound-Alpha 7 Color Ultrasound Diagnostic System (Hitachi Aloka Medical, Tokyo, Japan), Nikon CI-S Microscope, Nikon DS-U3 Imaging System, Image-Pro Plus 6.0 Image Analysis Software

(MediaCybernetics, Rockville, MD, USA), xylene, ethylenediamine-tetraacetic acid (EDTA) retrieval solution, rabbit anti-human CD-117 antibody (ab5505, Abcam, Cambridge, UK), mouse anti-human trypsin antibody (ab2378, Abcam), phosphate buffer solution (C1014, Jiamei Biotech, Co., Ltd, Guangzhou, China), bovine serum albumin fraction V (A8020, Solarbio, Beijing, China), Cy3-labeled goat anti-rabbit secondary antibody (ab97075, Abcam), biotin-labeled goat anti-mouse secondary antibody (ab150113, Abcam), and 4',6-diamidino-2-phenylindole (DAPI) color-developing agent (CH126, Jiamay).

Determination of gallbladder contractility. Patients' medical history was obtained on admission, and they were assigned to one of the two groups according to the aforementioned criteria. Patients underwent a fasting B-mode ultrasonography examination on the morning after admission. The examination was conducted in the supine or left lateral decubitus position. The abdominal probe was used to detect the gallbladder along the right subcostal margin. A freeze-frame image was taken at the maximum cross-section of the gallbladder, and its maximum length and width were measured. Then, the probe was rotated clockwise by 90°, and another freeze-frame image was taken to measure the height of the gallbladder. After recording the aforementioned data, the patients were instructed to quickly consume some yogurt and wait for 45 min before the length, width, and height of the gallbladder were measured again using the same methods. The fasting and post-prandial B-mode ultrasonography examinations were conducted in the same position for each patient. The volume of the gallbladder was calculated using the ellipsoid volume formula. The gallbladder contraction rate was calculated based on the following formula: $1 - (\text{45-minute gallbladder volume} / \text{fasting gallbladder volume}) \times 100\%$. The fatty-meal B-mode ultrasonography examination for all patients was conducted by the same physician.

Sample collection and immunohistochemistry. Patients underwent elective cholecystectomy after completing the preoperative preparations (including but not limited to chest radiography, electrocardiography, and routine blood tests to ensure safety). Intraoperatively, the degree of pericholecystic adhesions and the presence of abnormalities in the cystic artery and cystic duct were recorded. All resected gallbladder specimens were immersed in a 4% formaldehyde solution and sent to the pathology department. One tissue section ($0.2 \times 0.5 \times 0.8$ cm) was obtained from the neck, body, and fundus of each gallbladder specimen.

The sections were embedded in the same paraffin block by standard histological technique, and cut into slides for immunofluorescence staining. Next, the slides were immersed in xylene three times for 10 min each, followed sequentially by immersion in 100%, 95%, and 80% ethanol for 10 min each, and then rinsed thoroughly. EDTA retrieval solution was added, and the slides were heated in the microwave

(101-1BS, Bangxi Corp., Shanghai, China) at 65°C for 30 min to restore the antigenicity of the specimens. After rinsing, 3% hydrogen peroxide (prepared with deionized water) was added, and the sections were incubated at room temperature (RT) for 30 min and rinsed three times with phosphate-buffered saline (PBS) at RT for 5 min each. A working solution of bovine serum albumin fraction V was added dropwise and removed after incubation at RT for 30 min. The rabbit anti-human CD-117 antibody (1:100 dilution, ab5505, Abcam) and mouse anti-human tryptase antibody (1:100 dilution, ab2378, Abcam) were added as primary antibodies, and the slides were left at 4°C overnight. Subsequently, the slides were retrieved and washed with PBS at RT three times for 5 min each. The Cy3-labeled goat anti-rabbit secondary antibody (1:100 dilution, ab97075, Abcam) and biotin-labeled goat anti-mouse secondary antibody

(1:100 dilution, ab150113, Abcam) were added as secondary antibodies, and the slides were incubated at 37°C in the dark for 30 min. Then, the slides were retrieved, washed three times with PBS at RT, counterstained with DAPI, and washed three times again with PBS at RT. Finally, the slides were mounted and preserved using an anti-queching aqueous mounting agent.

The slides were observed and photographed under a microscope (Figs. 1–3). Ten high-power fields (final magnification 400×) were randomly photographed for each slide from the neck, body, and fundus of each gallbladder. The numbers of cells in each field that were CD117-positive (CD117⁺) and tryptase-negative (-) in the cytoplasm and located in the lamina propria or muscularis propria were counted and recorded; the number of cells that were CD117⁺ and tryptase-positive

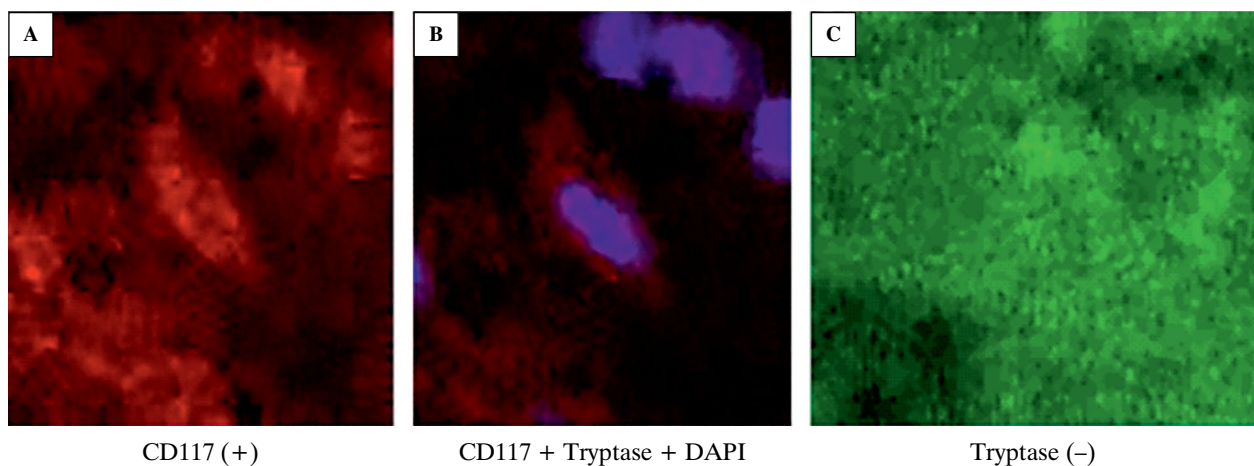


Figure 1. The interstitial Cajal-like cells that were CD117-positive and tryptase-negative in the lamina propria of a patient without cholelithiasis. **A.** c-kit (C117)-positive cells. **B.** Merged A and C. **C.** The same cells were tryptase-negative. Sections were stained by immunofluorescence as described in Methods. DAPI, 4',6-diamidino-2-phenylindole. Magnification: ×400.

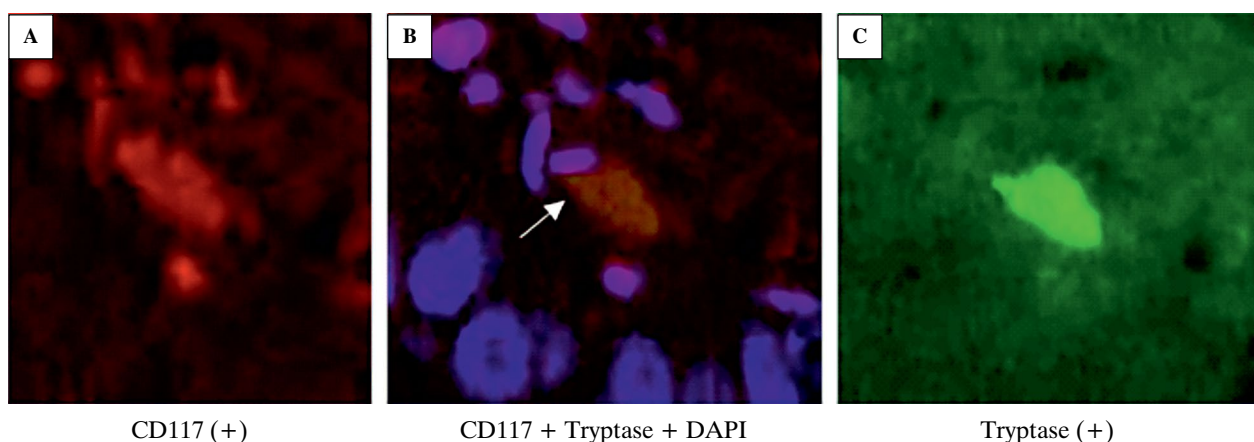


Figure 2. The interstitial Cajal-like cell that is CD117-positive and tryptase-negative in the lamina propria of a patient without cholelithiasis. **A.** c-kit (C117)-positive cell. **B.** Merging of A and C photographs reveals both C117⁺ and tryptase-positive cell (mast cell). **C.** The same cell as in (A) is also tryptase-positive. Sections were stained by immunofluorescence as described in Methods. Magnification: ×400.

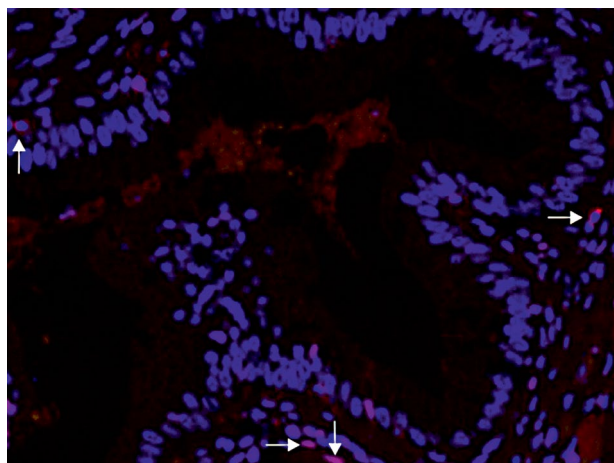


Figure 3. Cross-section of a gallbladder wall from a patient with cholelithiasis shows the presence of a few CD117-positive and tryptase-negative cells (arrows). Magnification: $\times 200$.

(+) were not counted. The recorded data were averaged for statistical analysis.

Statistical analysis. Statistical analysis was performed using SPSS 21.0 (IBM Corp., Armonk, NY, USA). The independent sample t-test was performed to compare the gallbladder contraction rate and number of ICLCs between the cholelithiasis and non-cholelithiasis groups, with $\alpha = 0.05$. A scatter plot was drawn using the number of ICLCs as the X-axis and gallbladder contraction rate as the Y-axis, and then Pearson and Spearman correlation analyses were performed. A P-value < 0.05 indicated that the difference was statistically significant for all the results.

Results

Based on the aforementioned criteria, 29 patients were screened. Of those, 3 patients were excluded because of incidental discovery of choledocholithiasis, cholelithiasis combined with gallbladder polyps, and a history of gallbladder-preserving lithotripsy. Twenty-six patients were finally included in this study, with 18 patients in the cholelithiasis group and 8 in the non-cholelithiasis group. There were 15 women and 11 men in both groups, and the range of age

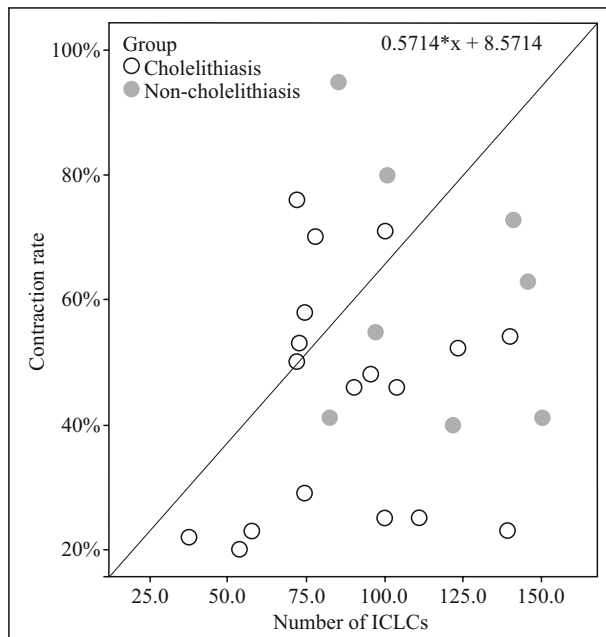


Figure 4. Scatter plot of the number of interstitial Cajal-like cells (ICLCs) and gallbladder contraction rate in patients with and without cholelithiasis.

was 28–77 years (median: both sexes, 60 years; men, 65 ys; women, 57 ys). Twenty-three patients underwent laparoscopic cholecystectomy, 1 patient underwent partial hepatectomy with cholecystectomy, and 2 patients underwent total pancreatectomy.

The independent sample t-test was performed to compare the gallbladder contraction rate between the cholelithiasis and non-cholelithiasis groups, and the difference between the two groups was statistically significant ($43.94\% \pm 18.50\%$ vs. $61.00\% \pm 20.50\%$, $P = 0.046$; Table 1). The same statistical test was performed to compare the number of ICLCs in the lamina propria between the cholelithiasis and non-cholelithiasis groups, and the difference between the two groups was statistically significant (88.61 ± 28.22 vs. 115.89 ± 27.87 , $P = 0.032$; Table 1).

Curve fitting of the scatter plot was performed (Fig. 4), and the Pearson and Spearman correlation analyses revealed no statistically significant correlations ($P > 0.05$, Table 2A, B, C).

Table 1. Comparison of gallbladder contraction rate and the number of ICLCs between patients with and without cholelithiasis

Group	N	Contraction rate, Mean \pm SD	P-value	No. of ICLCs, Mean \pm SD	P-value
Cholelithiasis	18	$43.9\% \pm 18.5\%$	0.046	88.611 ± 28.2207	0.032
Non-cholelithiasis	8	$61.0\% \pm 20.5\%$		115.888 ± 27.8715	

ICLCs — interstitial Cajal-like cells; no. — number; SD — standard deviation. Independent sample t-test.

Table 2. Pearson and Spearman correlation analyses of the number of ICLCs and gallbladder contraction rate**A) Cholelithiasis Group**

Spearman correlation coefficient				
			Contraction rate	No. of ICLCs
Spearman Rho	Contraction rate	Correlation coefficient	1.000	0.188
		Sig (two-tailed)		0.455
		N	18	18
	No. of ICLCs	Correlation coefficient	0.188	1.000
		Sig (two-tailed)	0.455	
		N	18	18

B) Non-cholelithiasis Group

Spearman correlation coefficient				
			Contraction rate	No. of ICLCs
Spearman Rho	Contraction rate	Correlation coefficient	1.000	-0.180
		Sig (two-tailed)		0.670
		N	8	8
	No. of ICLCs	Correlation coefficient	-0.180	1.000
		Sig (two-tailed)	0.670	
		N	8	8

C) Pearson correlation analysis

Pearson correlation analysis				
			Contraction rate	No. of ICLCs
Contraction rate		Pearson correlation	1	0.168
		Sig (two-tailed)		0.411
		N	26	26
No. of ICLCs		Pearson correlation	0.168	1
		Sig (two-tailed)	0.411	
		N	26	26

For abbreviations, see the legend to Table 1.

Discussion

ICLCs are a special type of interstitial cell that are widely distributed in various tissues, including the gastrointestinal tract, myocardium, and mammary glands [6–12]. The development and differentiation of these cells are related to their expression of c-kit receptors; hence, without c-kit receptors, ICLCs will degenerate to smooth muscle cells [3]. These cells are also present in biliary tissues. Lavoie *et al.* [12] showed in tissue extracts that there were synchronous rhythmic Ca^{2+} flashes in gallbladder smooth muscle cells and ICLCs. After the addition of gap junction uncouplers, the Ca^{2+} flashes in gallbladder smooth muscle decreased significantly, whereas those of ICLCs remained unchanged. However, after the ad-

dition of the c-kit tyrosine kinase inhibitor, imatinib mesylate, the synchronous rhythmic Ca^{2+} flashes in both tissues were significantly reduced [12]. Thus, the results of this study suggest that ICLCs play a crucial role in the spontaneous rhythmic contraction of gallbladder smooth muscle. Subsequently, some animal experiments have shown that cholecystokinin-A (CCK-A) receptors are expressed in the ICLCs of gallbladder in guinea pigs. Furthermore, *in vitro* experiments [13] showed that CCK-A can induce significant contractions in gallbladder muscle strips and after removing the ICLCs by exposing the methylene blue-stained muscle strips to light (532 nm, 50 mW/cm²), the gallbladder muscle strips showed significantly reduced contractions in response to CCK-A. Thus, the study concluded that the contrac-

tions induced by CCK-A in the gallbladders of guinea pigs may have been mediated by ICLCs [13]. ICLCs have also been observed in the gallbladder tissue of humans [14], and some studies have reported that the number of ICLCs found in gallbladder tissue resected from patients with cholelithiasis was significantly lower than that of patients without cholelithiasis [5]. In another study [2], it was found that gallbladder contractility, the number of gallbladder ICLCs, and SCF/c-kit expression level were all significantly lower in patients with cholelithiasis than in those without cholelithiasis. These results imply that the decrease in gallbladder contractility may be associated with the reduced number of gallbladder ICLCs, which in turn may have been caused by the inhibition of the SCF/c-kit pathway [2].

In the present study, significant differences were found between patients with and without cholelithiasis in terms of the gallbladder contractility assessed by ultrasonography before cholecystectomy and the number of ICLCs. Our findings of lower gallbladder contractility and number of ICLCs in the cholelithiasis group are consistent with those of previous studies [15, 16]. The scatter plot showed that it was highly likely for the number of gallbladder ICLCs to be positively correlated with gallbladder contractility; however, statistical analysis did not reveal a significant correlation. The reason for this finding could be related to numerous factors. Firstly, in the human body, gallbladder contractility is affected by multiple factors. Hence, the number of gallbladder ICLCs may be related to gallbladder contractility, but it cannot determine gallbladder contractility. Possible factors that may be related to gallbladder contractility include but are not limited to the degree of pericholecystic adhesions, thickening of the gallbladder wall [17], number and volume of gallstones in the gallbladder, concentration of cholecystokinin and CCK-A receptors in patients [18], duodenal pH value, and effects of acupuncture [19]. Secondly, the results of gallbladder contractility based on B-mode ultrasonography may be affected by the subjective judgement of the sonographer which could lead to errors in measuring gallbladder contractility. Additionally, the fatty meal test is only an indirect measure of gallbladder contractility, and ingesting different foods may have an impact on measurements of gallbladder contractility. A previous study suggested that ice candy of the Lundh test meal is ideal for testing gallbladder contractility, and the food item we used differed from that of a common fatty meal test [20]. To avoid the aforementioned errors, it may be necessary to perform *in vitro* experiments of muscle strip contraction. Experiments of gallbladder muscle strip contraction are widely used in animal studies.

However, in humans, such experiments are subject to many limitations and variables, and they cannot be easily implemented.

Although the present study's results suggest that there is no linear correlation between the number of ICLCs and gallbladder contractility, we cannot exclude the possibility of a non-linear correlation between these two parameters. In addition, as shown by the statistical results and scatter plot, there were significant differences in the gallbladder contractility and number of ICLCs between the cholelithiasis and non-cholelithiasis groups, with the cholelithiasis group showing significantly reduced gallbladder contractility and number of ICLCs compared to the non-cholelithiasis group. These findings imply that we should still consider that gallbladder contractility may be related to the number of gallbladder ICLCs. However, the nature and extent of this relationship(s) will require future investigation, and the construction of a mathematical model may involve multiple related factors.

Our study has several limitations. First, our study included a small number of cases. If we had at least 60 cases in this study, we would have achieved a more precise result. Second, interpretation of the results of ultrasonography is subjective. Third, the *in vitro* measurements of muscle-strip contraction may have been better than the Lundh test for evaluating the contraction rate of the gallbladder. Despite these limitations, we believe that the significant differences in the *in vivo* gallbladder contractility and the number of gallbladder ICLCs between cholelithiasis and non-cholelithiasis patients suggest that factors other than solely the number of gallbladder ICLCs affect gallbladder contractility in patients with cholelithiasis.

Acknowledgments

This study was supported by Beijing Hospital, National Center of Gerontology. We also thank Jiamay Biotech, Co., Ltd. for providing the reagent and technology support.

References

1. Stinton LM, Shaffer EA. Epidemiology of gallbladder disease: cholelithiasis and cancer. *Gut Liver*. 2012; 6(2): 172–187, doi: [10.5009/gnl.2012.6.2.172](https://doi.org/10.5009/gnl.2012.6.2.172), indexed in Pubmed: [22570746](https://pubmed.ncbi.nlm.nih.gov/22570746/).
2. Tan YY, Ji ZL, Zhao G, et al. Decreased SCF/c-kit signaling pathway contributes to loss of interstitial cells of Cajal in gallstone disease. *Int J Clin Exp Med*. 2014; 7(11): 4099–4106, indexed in Pubmed: [25550919](https://pubmed.ncbi.nlm.nih.gov/25550919/).
3. Pasternak A, Szura M, Gil K, et al. Interstitial cells of Cajal - systematic review. *Folia Morphol (Warsz)*. 2016; 75(3): 281–286, doi: [10.5603/FM.a2016.0002](https://doi.org/10.5603/FM.a2016.0002), indexed in Pubmed: [26806433](https://pubmed.ncbi.nlm.nih.gov/26806433/).
4. Xu D, Yu BP, Luo HS, et al. Control of gallbladder contractions by cholecystokinin through cholecystokinin-A receptors

- on gallbladder interstitial cells of Cajal. *World J Gastroenterol.* 2008; 14(18): 2882–2887, doi: [10.3748/wjg.14.2882](https://doi.org/10.3748/wjg.14.2882), indexed in Pubmed: [18473415](https://pubmed.ncbi.nlm.nih.gov/18473415/).
5. Pasternak A, Gil K, Matyja A, et al. Loss of gallbladder interstitial Cajal-like cells in patients with cholelithiasis. *Neurogastroenterol Motil.* 2013; 25(1): e17–e24, doi: [10.1111/nmo.12037](https://doi.org/10.1111/nmo.12037), indexed in Pubmed: [23121223](https://pubmed.ncbi.nlm.nih.gov/23121223/).
 6. Komuro T. Structure and organization of interstitial cells of Cajal in the gastrointestinal tract. *J Physiol.* 2006; 576(Pt 3): 653–658, doi: [10.1113/jphysiol.2006.116624](https://doi.org/10.1113/jphysiol.2006.116624), indexed in Pubmed: [16916909](https://pubmed.ncbi.nlm.nih.gov/16916909/).
 7. Popescu LM, Hinescu ME, Ionescu N, et al. Interstitial cells of Cajal in pancreas. *J Cell Mol Med.* 2005; 9(1): 169–190, doi: [10.1111/j.1582-4934.2005.tb00347.x](https://doi.org/10.1111/j.1582-4934.2005.tb00347.x), indexed in Pubmed: [15784175](https://pubmed.ncbi.nlm.nih.gov/15784175/).
 8. Hinescu ME, Gherghiceanu M, Mandache E, et al. Interstitial Cajal-like cells (ICLC) in atrial myocardium: ultrastructural and immunohistochemical characterization. *Journal of Cellular and Molecular Medicine.* 2006; 10(1): 243–257, doi: [10.1111/j.1582-4934.2006.tb00306.x](https://doi.org/10.1111/j.1582-4934.2006.tb00306.x).
 9. Shafik A, El-Sibai O, Shafik I, et al. Immunohistochemical identification of the pacemaker cajal cells in the normal human vagina. *Arch Gynecol Obstet.* 2005; 272(1): 13–16, doi: [10.1007/s00404-005-0725-3](https://doi.org/10.1007/s00404-005-0725-3), indexed in Pubmed: [15834581](https://pubmed.ncbi.nlm.nih.gov/15834581/).
 10. Radu E, Regalia T, Ceafalan L, et al. Cajal-type cells from human mammary gland stroma: phenotype characteristics in cell culture. *J Cell Mol Med.* 2005; 9(3): 748–752, doi: [10.1111/j.1582-4934.2005.tb00509.x](https://doi.org/10.1111/j.1582-4934.2005.tb00509.x), indexed in Pubmed: [16202226](https://pubmed.ncbi.nlm.nih.gov/16202226/).
 11. van der AA F, Roskams T, Blyweert W, et al. Identification of kit positive cells in the human urinary tract. *J Urol.* 2004; 171(6 Pt 1): 2492–2496, doi: [10.1097/01.ju.0000125097.25475.17](https://doi.org/10.1097/01.ju.0000125097.25475.17), indexed in Pubmed: [15126883](https://pubmed.ncbi.nlm.nih.gov/15126883/).
 12. Lavoie B, Balemba OB, Nelson MT, et al. Morphological and physiological evidence for interstitial cell of Cajal-like cells in the guinea pig gallbladder. *J Physiol.* 2007; 579(Pt 2): 487–501, doi: [10.1113/jphysiol.2006.122861](https://doi.org/10.1113/jphysiol.2006.122861), indexed in Pubmed: [17204499](https://pubmed.ncbi.nlm.nih.gov/17204499/).
 13. Xu D, Yu BP, Luo HS, et al. Control of gallbladder contractions by cholecystokinin through cholecystokinin-A receptors on gallbladder interstitial cells of Cajal. *World J Gastroenterol.* 2008; 14(18): 2882–2887, doi: [10.3748/wjg.14.2882](https://doi.org/10.3748/wjg.14.2882), indexed in Pubmed: [18473415](https://pubmed.ncbi.nlm.nih.gov/18473415/).
 14. Hinescu ME, Ardeleanu C, Gherghiceanu M, et al. Interstitial Cajal-like cells in human gallbladder. *J Mol Histol.* 2007; 38(4): 275–284, doi: [10.1007/s10735-007-9099-0](https://doi.org/10.1007/s10735-007-9099-0), indexed in Pubmed: [17541711](https://pubmed.ncbi.nlm.nih.gov/17541711/).
 15. Runyu D, Jingyong X. The relationship between gallstone formation and the interstitial cell of Cajal like cell in gallbladder. *Chinese J Med.* 2017; 52: 25–27.
 16. Ying F, Shouhua W, Zhenhua Y, et al. The change of slow wave and tension of muscle strip from gallbladder of guinea pig after wiping off interstitial cell of Cajal like cell. *Chin J Exp.* 2012; 2: 850–850.
 17. Jing S, Weixu C, Xia W, et al. The role and mechanism of gallbladder wall thickening in gallstone formation. *J Xuzhou Med Univ.* 2017; 37: 763–765.
 18. Ruixin C, Ming Ya, Zhiwei W, et al. Relationship between CCK-AR mRNA of gallbladder wall and plasma CCK-8 level and gallbladder emptying function in gallstone patients. *Shandong Med J.* 2006; 36: 1–2.
 19. Yanbin Z, Ziyang C, Peijin L, et al. Clinical research of ultrasound in monitoring gallbladder constriction after acupuncture and lipid-food test in diagnosis of cholecystitis. *Chinese Imaging J Integr Tradit Western Med.* 2010; 8: 193–195.
 20. Tairan S, Kai Z, Yubao S, et al. The application values of real-time ultrasound and the ice candy of LUNDH test meal in checking the gallbladder contractive function. *Chin J Med Ultrasound.* 2011; 8: 2558–2563.

Submitted: 29 August, 2018

Accepted after reviews: 19 June, 2019

Available as AoP: 24 June, 2019

INSTRUCTIONS FOR AUTHORS

MANUSCRIPT SUBMISSION

Folia Histochemica et Cytobiologica accepts manuscripts (original articles, short communications, review articles) from the field of histochemistry, as well as cell and tissue biology. Each manuscript is reviewed by independent referees. Book reviews and information concerning congresses, symposia, meetings etc., are also published.

All articles should be submitted to FHC electronically online at www.fhc.viamedica.pl where detailed instruction regarding submission process will be provided.

AUTHOR'S STATEMENT

The manuscript must be accompanied by the author's statement that it has not been published (or submitted to publication) elsewhere.

GHOSTWRITING

Ghostwriting and guest-authorship are forbidden. In case of detecting ghost written manuscripts, their actions will be taking involving both the submitting authors and the participants involved.

The corresponding author must have obtained permission from all authors for the submission of each version of the paper and for any change in authorship. Submission of a paper that has not been approved by all authors may result in immediate rejection.

COST OF PUBLICATION

The cost of publication of accepted manuscript is 800 Euro.

OFFPRINTS

PDF file of each printed paper is supplied for the author free of charge. Orders for additional offprints should be sent to the Editorial Office together with galley proofs.

ORGANIZATION OF MANUSCRIPT

The first page must include: the title, name(s) of author(s), affiliation(s), short running head (no more than 60 characters incl. spaces) and detailed address for correspondence including e-mail. Organization of the manuscript: 1. Abstract (not exceeding one typed page — should consist of the following sections: Introduction, Material and methods, Results, Conclusions); 2. Key words (max. 10); Introduction; Material and methods; Results; Discussion; Acknowledgements (if any); References; Tables (with legends); Figures; Legends to figures.

In a short communication, Results and Discussion should be written jointly. Organization of a review article is free.

TECHNICAL REQUIREMENTS

Illustrations (line drawings and halftones) — either single or mounted in the form of plates, can be 85 mm, 125 mm, or 175 mm wide and cannot exceed the size of 175 × 250 mm. The authors are requested to plan their illustrations in such a way that the printed area is economically used. Numbers, inscriptions and abbreviations on the figures must be about 3 mm high. In case of micrographs, magnification (e.g. × 65 000) should be given in the legend. Calibration bars can also be used. For the best quality of illustrations please provide images in one of commonly used formats e.g. *.tiff,

*.png, *.pdf (preferred resolution 300 dpi). Color illustrations can be published only at author's cost and the cost estimate will be sent to the author after submission of the manuscript. Tables should be numbered consecutively in Arabic numerals and each table must be typed on a separate page. The authors are requested to mark the places in the text, where a given table or figure should appear in print. Legends must begin on a new page and should be as concise as necessary for a self-sufficient explanation of the illustrations. PDF file of each paper is supplied free of charge.

CITATIONS

In References section of article please use following American Medical Association 9th Ed. citation style. Note, that items are listed numerically in the order they are cited in the text, not alphabetically. If you are using a typewriter and cannot use italics, then use underlining.

Authors: use initials of first and second names with no spaces. Include up to six authors. If there are more than six, include the first three, followed by et al. If no author is given, start with the title. **Books:** include the edition statement (ex: 3rd ed. or Rev ed.) between the title and place if it is not the first edition. **Place:** use abbreviations of states, not postal codes. **Journals:** abbreviate titles as shown in *Index Medicus*. If the journal does not paginate continuously through the volume, include the month (and day). **Websites:** include the name of the webpage, the name of the entire website, the full date of the page (if available), and the date you looked at it. The rules concerning a title within a title are *not* displayed here for purposes of clarity. See the printed version of the manual for details. For documents and situations not listed here, see the printed version of the manual.

EXAMPLES

Book:

1. Okuda M, Okuda D. *Star Trek Chronology: The History of the Future*. New York: Pocket Books; 1993.

Journal or Magazine Article (with volume numbers):

2. Redon J, Cifkova R, Laurent S et al. Mechanisms of hypertension in the cardiometabolic syndrome. *J Hypertens*. 2009; 27(3):441–451. doi: 10.1097/HJH.0b013e32831e13e5.

Book Article or Chapter:

3. James NE. Two sides of paradise: the Eden myth according to Kirk and Spock. In: Palumbo D, ed. *Spectrum of the Fantastic*. Westport, Conn: Greenwood; 1988:219–223.

When the manufacturers of the reagents etc. are mentioned for the first time, town, (state in the US) and country must be provided whereas for next referral only the name of the firm should be given.

Website:

4. Lynch T. DSN trials and tribble-ations review. Psi Phi: Bradley's Science Fiction Club Web site. 1996. Available at: <http://www.bradley.edu/campusorg/psiphi/DS9/ep/503r.htm>. Accessed October 8, 1997.

Journal Article on the Internet:

5. McCoy LH. Respiratory changes in Vulcans during pon farr. *J Extr Med* [serial online]. 1999;47:237–247. Available at: http://infotrac.galegroup.com/itweb/nysl_li_liu. Accessed April 7, 1999.

